NOVEL $CuBi_2O_4/V_2O_5$ Z-SCHEME PHOTOCATALYST FOR ENHANCED PHOTOCATALYTIC DEGRADATION OF DYES UNDER VISIBLE LIGHT IRRADIATION

Thesis Submitted

By

Abhishek Kumar

Roll No.-002110402007

Examination Roll No.- M4CIV23016

Registration No.- 160029 of 2021-22

MASTER OF ENGINEERING

Under the supervision of

Dr. Ankush Majumdar

JADAVPUR UNIVERSITY

FACULTY OF ENGINERING & TECHNOLOGY

DEPARTMENT OF CIVIL ENGINERING

(ENVIRONMENTAL ENGINEERING DIVISION)

KOLKATA-700032, INDIA

2023

DECLARATION

This Thesis titled "**Novel $CuBi_2O_4/V_2O_5$ Z-scheme photocatalyst for enhanced photocatalytic degradation of dyes under visible light irradiation**" is prepared and submitted for the award of the degree of Master of Engineering in Civil Engineering course of Jadavpur University for the session of 2021-2023. I declare that the work described in this thesis is entirely my own. No portion of the work referred to in this thesis has been submitted in support of an application for another degree or qualification of this or any other university or institute. Any help or source information that has been awarded in the thesis has been duly acknowledged.

Abhishek Kumar

Date: June 15, 2023

Place: Kolkata

Abhishek Kumar
M.C.E- 2nd Yr.
Roll No.-002110402007
Exam Roll No.: M4CIV23016
Registration No.- 160029 of 2021-22
Department of Civil Engineering
Environmental Engineering Division

JADAVPUR UNIVERSITY

DEPARTMENT OF CIVIL ENGINEERING

KOLKATA-700032

Recommendation Certificate

This is to certify that the thesis entitled "**Novel $CuBi_2O_4/V_2O_5$ Z-scheme photocatalyst for enhanced photocatalytic degradation of dyes under visible light irradiation**" is prepared and submitted by **Abhishek Kumar**, be accepted in partial fulfillment of the requirements for the Degree of Master of Civil Engineering with specialization Environmental Engineering from Jadavpur university is absolutely based upon his own work under the supervision of **Dr. Ankush Majumdar** and that neither his thesis nor any part of this thesis has been submitted for any degree or any other academic award anywhere before.

Signature of the supervisor
and date with office seal

15/06/23

Dr. Ankush Majumdar
Assistant Professor
Department of Civil Engineering
Jadavpur University

Assistant Professor
Department of Civil Engineering
Jadavpur University
Kolkata-700 032

Countersigned by

15/06/23

Dean
Faculty of Engineering Technology
Jadavpur University

DEAN
Faculty of Engineering & Technology
JADAVPUR UNIVERSITY
KOLKATA-700 032

15/6/23

Head of Department
Department of Civil Engineering
Jadavpur University

Head
Department of Civil Engineering
Jadavpur University
Kolkata-700 032

JADAVPUR UNIVERSITY

DEPARTMENT OF CIVIL ENGINEERING

KOLKATA- 700032

CERTIFICATE OF APPROVAL*

This is to certify that this thesis is hereby approved as an original work conducted and presented satisfactory to warrant its acceptance as a prerequisite to the degree for which it has been submitted. It is implied that by this approval the undersigned do not necessarily endorse or approve any statement made, opinion expressed or conclusion drawn therein, but approve the thesis only for the purpose for which it is submitted.

Final Examination for evaluation of thesis

1. _____

2. _____

3. _____

(Signature of Examiners)

* Only in case the thesis is approved.

ACKNOWLEDGEMENT

It gives me great pleasure to express my deep sense of gratitude and indebtedness to all those who are responsible for the completion of my M. E. thesis. I would like to express my deep gratitude and kindest regards to **Prof. Ankush Majumdar** for his valuable guidance, constant support and encouragement throughout my thesis work. This thesis would never been completed without his blessings, guidance, constant vigil, careful supervision and inspiration throughout the session.

I am sincerely thankful and indebted to **Prof. Somnath Mukherjee, Prof. Shibnath Chakrabarty, Prof. Anupam Debsarkar, Prof. Amit Dutta, Prof. Tumpa Hazra and Prof. Abhisek Roy** for their constant encouragement and continuous valuable suggestions throughout my thesis work.

I sincerely acknowledge the help of **Mr. Pankaj Mandal, Mr. Bhoginath Roy, Mr. Mrityunjoy Banerjee and Mr. Josimuddin Bag** of Environmental Engineering Laboratory.

My heartfelt thanks to **Mr. Mainak Maiti, Mr. Debasis Sau, Mr. Aritra Majumdar, Mr. Suvendu Halder, Mrs. Nabanita Ghosh** research scholars for being with me and encouraging all the time.

I would like to express thanks to my seniors **Mr. Snehashis Roy, Mr. Vikash Kumar, Mr. Ashes Sardar, Mr. Srikanta Sau, Mr. Arunashis Mondal and Mr. Sourav Bhunia** for their encouragement and help.

I express my sincere gratitude and appreciation to my classmates **Mr. Biswajit Chakraborty, Mr. Bikul Kumar Singh, Mr. Sanjeev Kumar, Mr. Sayan Saha, Mr. Mijanur Haque and Mr. Pratik Kumar Mandal** for their help during the coursework as well as this thesis work. I am also thankful to **Mr. Santanu De, Mr. Aditya Akash and Mr. Pankaj Verma** for their wonderful company.

I further extend my thanks to **Mrs. Dimitra Das** of the School of Materials Science and Nanotechnology for helping me in UV/Vis DRS characterization. I am also thankful to **Mr. Sudhir Kumar Ghosh** and **Mr. Jayanta Bhattacharya** of Metallurgical and Material Engineering Department for helping in XRD and SEM Characterizations.

The thesis could not have been completed without the endless love and blessings from my parents and family members.

I would like to acknowledge gratefully to AICTE for providing financial assistance in form of PG Scholarship for my M. E. course.

I would like to thank each of them who directly or indirectly rendered their help to me in the completion of this work. My apologizes to all those who have helped me but are not acknowledged.

Abhishek Kumar

Date: June 15, 2023
Place: Kolkata

Abhishek Kumar
M.C.E- 2nd Yr.
Roll No.-002110402007
Exam Roll No.: M4CIV23016
Registration No.- 160029 of 2021-22
Department of Civil Engineering
Environmental Engineering Division

ABSTRACT

The advanced oxidation processes using heterogeneous semiconductor photocatalysis is an interesting technique used for dye removal in industrial wastewater. In this paper, an experimental study is being carried out by synthesizing the Copper Bismuth oxide- Vanadium pentoxide ($CuBi_2O_4/V_2O_5$) nanocomposite photocatalyst for effective dye-degradation through photocatalysis under visible light irradiation. The as-synthesized photocatalyst has been characterized using X-Ray Diffraction and scanning electron microdcopy techniques. The optical property of the synthesized photocatalysts has been analyzed by UV-Visible DRS. The removal efficiency of the has been tested on RhB, MB and MO dyes under visible LED light irradiation. The 30-$CuBi_2O_4/V_2O_5$ nanocomposite has a removal efficiency of 73.8 % on RhB (20 mg/L) solution for 60 minutes of photocatalysis while the pristine materials V_2O_5 and $CuBi_2O_4$ have a removal efficiency of 20.7 % and 7 % only under the given reactor setup condition. The effect of photocatalyst dose, initial solution pH, initial dye concentration and stirring on the photocatalytic degradation of RhB by using 30-$CuBi_2O_4/V_2O_5$ has been reported. The 30-$CuBi_2O_4/V_2O_5$ adsorbed 95 % of MB (20 mg/L) dye in 30 minutes. Based on radical scavenging experiments and energy band structures, a Z-scheme photocatalytic mechanism has been suggested. During the photocatalytic degradation of RhB, the as-prepared 30-$CuBi_2O_4/V_2O_5$ nanocomposite also displayed 79 % COD removal efficiency in 60 minutes.

TABLE OF CONTENTS

List of Tables

List of Figures

LIST OF ABBREVIATIONS

AOP	Advance Oxidation Process
BOD	Biochemical oxygen demand
BQ	Benzoquinone
CB	Conduction Band
COD	chemical oxygen demand
EDTA	Ethylenediamine tetra-acetic acid
IPA	Isopropanol
KHP	Potassium Hydrogen Phthalate
LED	Light Emitting Diode
MB	Methylene Blue
MO	Methyl Orange
NF	Nano Filtration
RhB	Rhodamine B
RO	Reverse Osmosis
ROS	Reactive Oxygen Species
TMO	Transition metal oxides
VB	Valance Band

Chapter 1

INTRODUCTION

The rate of exploitation of the natural environment has greatly been amplified by the industrial revolution, urbanization, and population growth. In future, the excellence of human life depends upon the quality of the air they breathe, land they live and water they drink. So, it is necessary to diminish the load of contaminants from air, land, and water resources on a priority basis. Water is one of the most precious substances on this earth that sustains every form of life including humans. Contaminants free clear water is essential for healthy living and proper functioning of ecological units. Human activities have made it the most threatened resource in the world. Freshwater resources are limited and their poor management and exploitation worsen the situation. The environment and biosphere are threatened by the disposal of wastewater without proper and adequate treatment.

The water pollution due to dye-contaminated wastewater is a major part of aqueous pollution. Various industries like textile dyeing, paper making, food processing, paints, and cosmetics, release their dye-contaminated effluents to the environment resulting in dye-contaminated wastewater. It is estimated that about one million tons of dyes are produced annually around the world. More than 15% of these dyes are released as pollutants in industrial effluents to the environment [1]. The dyes released in wastewater are highly toxic, carcinogenic, and xenobiotic to living organisms. The dyes present in wastewater badly affect the aqueous ecosystem because the intense color of the aqueous body imparted by dyes inhibits the access of sunlight to the interior of the aqueous body. Due to lack of sunlight photosynthesis activity gets affected which results in deficiency of oxygen causing disruption to ecosystem. This problem continuously occurs from year by year. Accumulation of dyes on a food chain will give resistant to biological degradation of decaying process from organism such as bacteria, plankton and fungi [2].

Various treatment processes have been used for the treatment of dye-contaminated wastewater. The biological treatment methods including both aerobic and anaerobic methods are popular because they offer the possibility of energy recovery and are practical and comparatively less

costly. However, these biological methods have certain limitations too. For example, they require long time for operation, and are very sensitive to experimental conditions like accumulation of ammonia, concentration of pollutants, etc. The biological treatment methods fail for the treatment of wastewater containing high dye concentration [3]. The physicochemical treatment methods such as adsorption, coagulation, precipitation, reverse osmosis, flocculation and anaerobic oxidation are not effective because these techniques generate secondary pollution due to use of chemicals. Alternately, the advanced oxidation processes (AOPs) are considered potential and promising techniques for the treatment of dye-contaminated wastewater. In AOPs pollutant molecules are mineralized to simple inorganic and non-toxic molecules rather than transforming them into another phase. This can be used for wide range of pollutants including organic molecules, inorganic molecules, and pathogens. Further it does not produce secondary pollutants as H_2O, CO_2, and small inorganic ions are produced as final products.

The AOPs include heterogeneous and homogeneous chemical and photochemical processes; electrochemical oxidations; Fenton processes; photolysis under irradiation of gamma rays; photolysis under ultraviolet rays in combination with H_2O_2, O_3, or catalyst; and various combinations thereof. Among all these techniques, heterogeneous photocatalysis have gained significant attention in recent years. The photocatalysis with semiconductor metal oxides can also be used for harvesting solar energy and the production of hydrogen fuel. It can also be used for the degradation of pollutants other than dyes like paints, phenols, antibiotics, and pesticides. Till now, a rich dictionary of photocatalytic treatment using semiconductor metal oxides as catalysts has been designed. In this technique, the dye contaminated wastewater is treated with semiconductor metal oxides catalysts under irradiation of light.

Photocatalytic activity of a photocatalysts depends on its ability of forming free radicals generated with a participation of electrons and holes. Efficient photocatalyst fulfills various requirements like well- tuned band gap, photo and chemical stability and high affinity to light. Nano sized metal oxides have been proven as good photocatalytic materials with larger surface area and efficient recyclability, some reported catalysts are Bi_2WO_6, α-Fe2O3, CuO and Cu_2O, ZnO, TiO_2, Cr_2O_3, WO_3 and V_2O_5 nano particles. V_2O_5 is a transition metal oxide (TMO) semiconductor material used in photocatalytic degradation applications due to its narrow band gap, non-toxicity, good chemical, electrical and photo stability, low cost, ease in synthesis, large abundancy and high visible light absorption [4]. However, the photocatalytic efficiency of pristine materials can be significantly improved by using various techniques like doping with metals and nonmetals, crating vacancies, depositing noble metals, formation of

heterojunctions, Z-scheme, etc. As an imitator for natural photosynthesis, Z-scheme photocatalytic systems have attracted an increasing research interest and show great potentials for putting into practical applications [5].

$CuBi_2O_4$ is a visible-light-driven semiconductor photocatalyst, which coincides well with other semiconductor photocatalysts and also displays extensive visible-light absorption competencies. However, as with other single photocatalysts, CuBi2O4 exhibits some disadvantages including mismatched band positions, excessive recombination of photogenerated charge carriers and insufficient quantum yields. The band edges of V_2O_5 matches well with $CuBi_2O_4$ to form a Z-scheme photocatalytic system.

In the present study, Z-scheme $CuBi_2O_4/V_2O_5$ was firstly prepared for effective dye degradation under visible light irradiation. The photocatalytic performance of the as synthesized photocatalyst was determined towards the degradation of Rhodamine B (RhB), Methylene blue (MB) and Methyl orange (MO) dyes under a low-intensity, energy-efficient visible 20W LED light irradiation. The photocatalytic efficiency of the Z-scheme $CuBi_2O_4$/ V_2O_5 photocatalyst was found to be significantly higher than that of pure $CuBi_2O_4$ and V_2O_5 . The effect of photocatalyst dose, initial solution pH, initial dye concentration and stirring on the photocatalytic degradation of RhB was also studied.

Chapter 2

LITERATURE REVIEW

2.1 Dyes and their classification

Dyes are the coloured organic substances that are used in solution to impart colour to various substances like fabric, paper, leather, hair, drugs, cosmetics, plastics and food material. It is a substance with a suitable colour and the ability to fix itself or be fixed to the fabric. It must be fast and resistant towards water, dilute acids, alkalis and various organic solvents. Dyes can be natural as well as synthetic. Natural dyes are obtained from natural sources like plants (including fungi and lichens), animals, invertebrates or minerals. Some of the examples of natural dyes are Indigo dyes (from stems and leaves of indigo), Alizarin dyes (from roots of madder plant), Logwoods dyes (from the trunk for black colour to silk and cotton fabrics) etc. These dyes are not that much harmful in nature. Synthetic dyes are prepared in labs/factories for dyeing purpose. The example of synthetic dyes are mordant dyes, azo dyes etc. Majority of the dyes used today are synthetic because they are easy to use, cheaper, brighter, fast, have wider range of colours. These synthetic dyes are toxic in nature. If it is present in water source, it can cause several health hazards for human beings.

A dye molecule has two main components:

(i) Chromophores, and

(ii) Auxochromes.

Chromophore is responsible for colour while auxochromes facilitate attachment towards fibers. Based on chromophores & auxochrome the dyes are nitro & nitroso dye, azo dye, triarylmethane dye, anthraquinone dye, Indigo dyes etc. In nitro and nitroso dye contain nitro group ($-NO_2$) and nitroso group (-NO) as the chromophores respectively and hydroxyl group (-OH) as auxochrome. One of the examples of nitro dye is Naphthol yellow S and nitroso dye is Gambine-Y. In azo dyes Azo group (-N=N-) is present as primary chromophore in their molecular structure which is present between two aromatic rings. Tartrazine (yellow), Methyl Orange, Congo Red, Bismarck Brown, Chrysoidine, and other azo dyes are examples. Azo dyes account for 60-70% of dyes used in food and textile production. A central carbon is bonded to three aromatic rings in triarylmethane dyes, one of which is quinoid. The examples of triarymethane dyes are Malachite Green (used as a direct dye for wool and silk), Crystal

violet, and Phenolphthalein etc. In Anthraquinone dye Anthraquinone ring is the chromophore and -OH, $-SO_3H$, $-NH_2$ as auxochrome. One of the examples of this dye is Alizarin-red textile dye. In Indigo dyes have carbonyl chromospheres and indigoid structure (-CO=C=C-CO-). These dyes are used in cotton yarn, which is primarily used to make blue jeans denim cloth.
Dyes can be classified in three broad categories: cationic (basic dyes), anionic (direct, acid and reactive dyes) and non-ionic (disperse dyes and vat dyes).

2.1.1 Cationic dyes

Cationic dyes contain a cationic functional group that may dissolve into positively charged ions in an aqueous solution. The onium group is the most common cationic functional group. Methylene Blue (MB), Rhodamine B (RhB), Rhodamine 6G (Rh6G), Safranin O (SO), Crystal Violet (CV), and Malachite Green (MG) are some examples of cationic dyes, with most cations being N+. As a result, cationic dyes are also called basic dyes. MB was used as a model pollutant for degradation. RhB is a cationic dye that is widely used in the textile, leather, and food industries. Because of its higher toxic colourants, RhB is carcinogenic and mutagenic to aquatic wildlife and humans. The photo-catalytic reaction was enhanced by anionic dyes. The chemical properties of some cationic dyes are given in Table 2.1.

Table 2.1: Chemical properties of some Cationic Dyes [6], [7]

Dyes	**Abbreviation**	**Molecular weight (in g/mol)**	**Structure**	λ_{max} **(in nm)**
Methylene Blue	MB	319.85	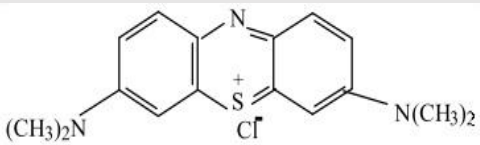	660

Dyes	Abbreviation	Molecular weight (in g/mol)	Structure	λ_{max} (in nm)
Rhodamine B	RhB	479	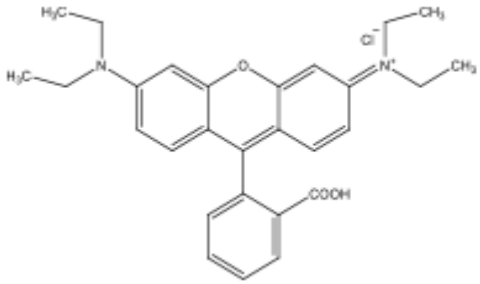	554
Safranin O	SO	350.85	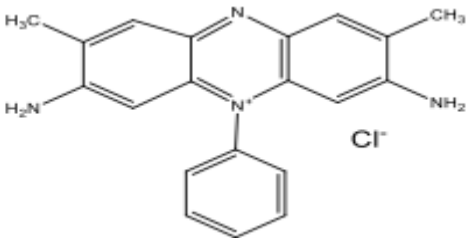	520
Crystal Violet	CV	407.98	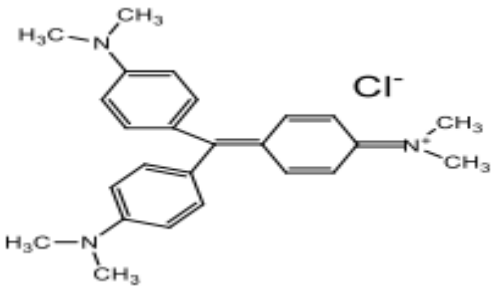	573
Victoria blue B	VBB	506.08	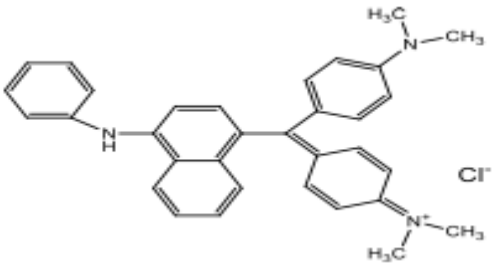	614
Auramine O	AO	303.83	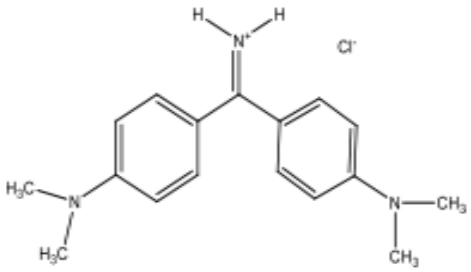	420

2.1.2 Anionic Dyes

Anionic dyes contain anionic functional groups (e.g., sulfonic or carboxylic acid groups) that are water soluble and may interact easily with photocatalysts with hydrophilic surfaces. As a result, anionic dyes are also referred as acidic dyes. Some of the anionic dyes are Acid Orange 7 (AO7), Eosin Y (EY), Methyl Orange (MO), Acid Red 14 (AR14), Alizarin Red S (ARS), Rose Bengal (RB), and Phenol Red (PR). The chemical properties of some anionic dyes are given in Table 2.2.

Table 2.2: Chemical properties of anionic dyes [6]

Dyes	**Abbreviation**	**Molecular weight (in g/mol)**	**Structure**	λ_{max} **(in nm)**
Methyl Orange	MO	327.33	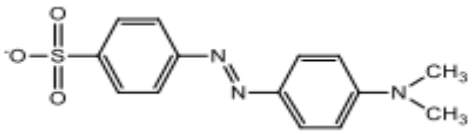	464
Alizarin Red S	ARS	240.21	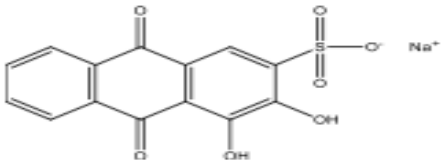	426
Acid Red14	AR14	502.43	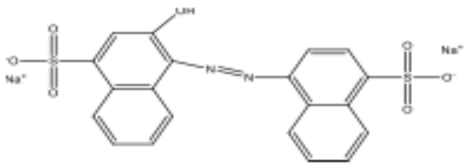	515
Congo Red	CR	696.67	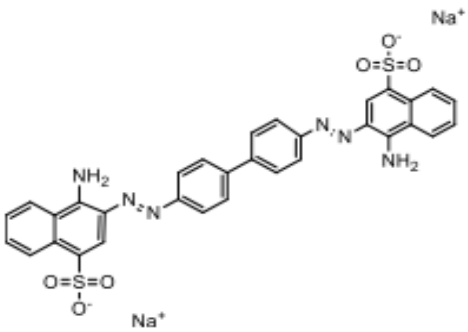	497

Dyes	**Abbreviation**	**Molecular weight (in g/mol)**	**Structure**	λ_{max} **(in nm)**
Rose Bengal	RB	937.67	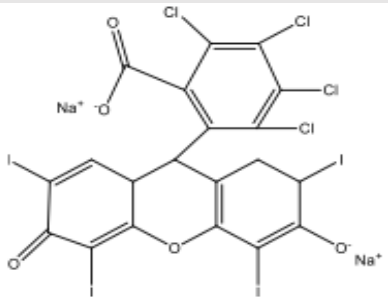	550
Eosin Y	EY	691.85	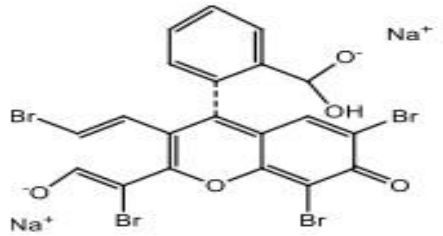	518
Acid Orange 7	AO7	350.82	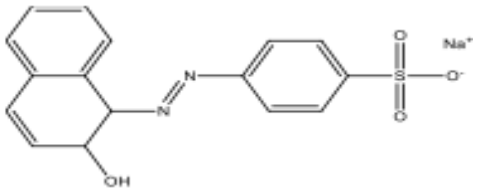	484
Phenol Red	PR	354.38	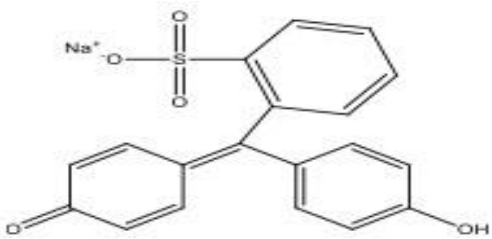	560
Acid violet 7	AV7	566.47	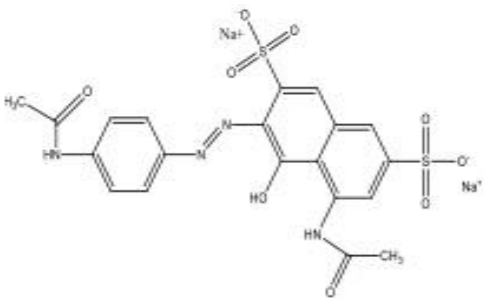	522

Dyes	Abbreviation	Molecular weight (in g/mol)	Structure	λ_{max} (in nm)
Reactive black 5	RB5	991.82	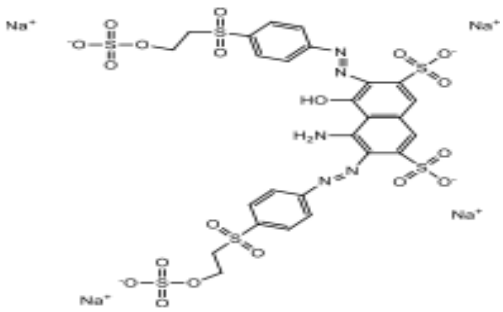	602

2.1.3 Non-ionic Dyes

2.1.3.1 Disperse dyes

Disperse dye is described as a substantially water-insoluble dye associated with one or more than one hydrophobic nature of fibers, such as polyester or cellulose acetate. Being non-ionic, it is easily volatile and vapors of dye are highly absorbed by the hydrophobic fiber. Some examples of dispersed dyes are C.I. Disperse Yellow 13 which is suitable for acetates and nylon, C.I. Disperse Violet 1 which is suitable for acetate, nylon and polyester, C.I. Disperse Blue 56 which is suitable for dyeing polyester fibers, C.I. Disperse Orange 30 is applied on acetate and triacetate, C.I. Disperse Blue 183 for dying of polyester. The chemical structure of some dispersed dyes is shown in Fig. 2.1 [8].

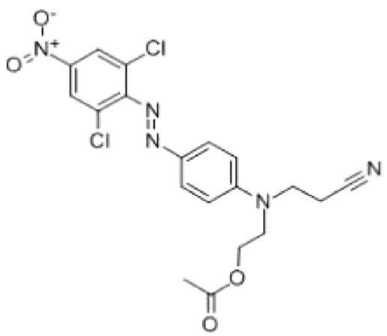

C.I. Disperse Orange 30

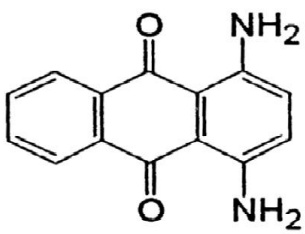

C.I. Disperse Violet 1

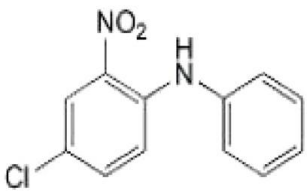

C.I. Disperse Yellow 26

Fig. 2.1: Disperse dyes

2.1.3.2 Vat dye

Vat dye is identified for better colour fastness and excellent brightness properties [9].They are mainly soluble in hot water. Some vat dyes are also soluble in sodium carbonate. The most important natural vat dye is Indigo or indigotin obtained from the plant Indigofera. Some examples of the vat dyes are C.I. Vat Blue 1, C.I. Vat Black 25, C.I. Vat Green 1. The chemical structure of some vat dyes is shown in Fig. 2.2 [10].

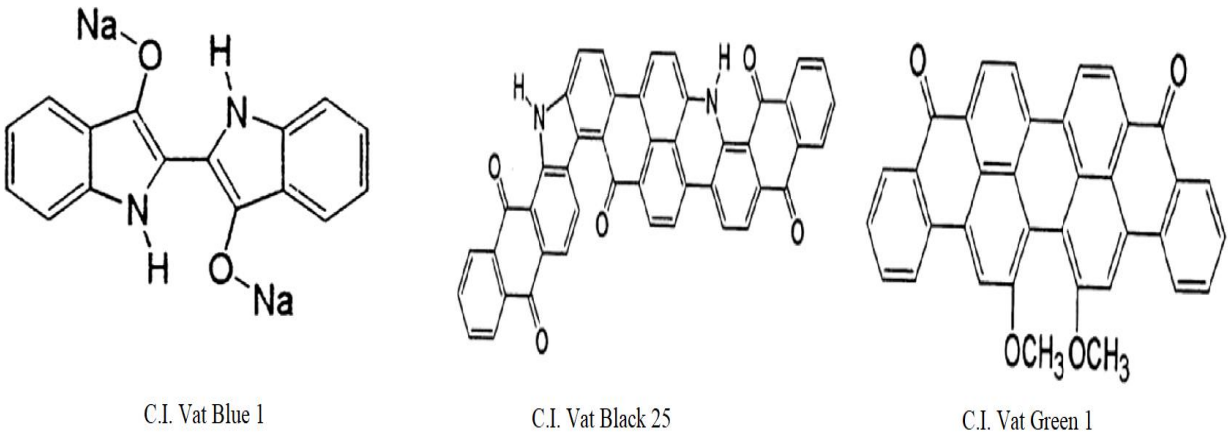

C.I. Vat Blue 1 C.I. Vat Black 25 C.I. Vat Green 1

Fig. 2.2: Vat Dyes

2.1.3.3 Sulfur dyes

Sulphur dyes are highly coloured, water insoluble compounds. They are the most commonly used dyes manufactured for cotton in terms of volume. They are predominantly black, brown, and dark blue. These dyes can be categorized into four groups such as sulfur, Leuco sulfur, solubilized and condensed sulfur dyes. Some of the sulfur dyes are C.I. Sulfur Blue 15, C.I. Leuco Sulfur Black1 and C.I. Sulfur Green 3. The chemical structure of some sulfur dyes are shown in Fig. 2.3 [10].

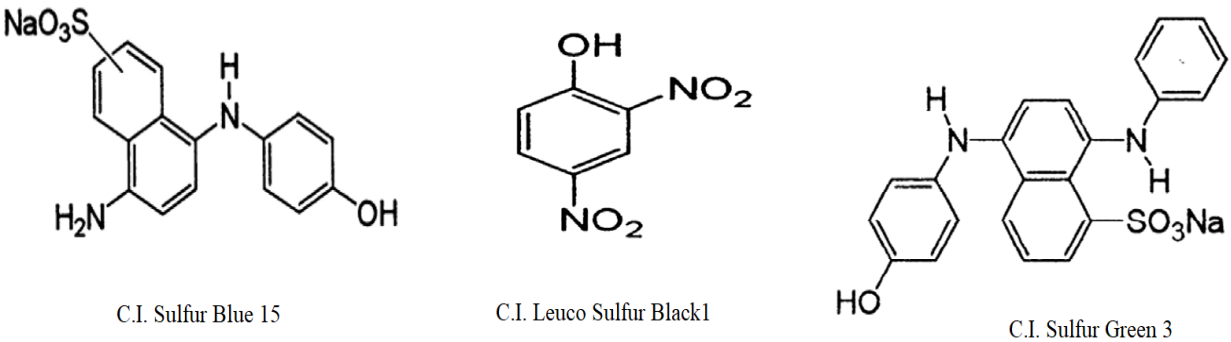

C.I. Sulfur Blue 15 C.I. Leuco Sulfur Black1 C.I. Sulfur Green 3

Fig 2.3: Sulfur dyes

Some industrial effluents containing dyes are shown in Fig. 2.4.

Fig. 2.4: Industrial effluents containing dyes.

2.2 Harmful effects of dyes

During the colouration process, a huge amount of dye does not bind to the fabric even after many cycles of fabrication. The remaining un-useful dye is discharged over the earth's surface and into natural water bodies like rivers and lakes, etc. The long exposure of the dyes can cause health hazards to the human being and they must be treated before release to the environment. Exposure of dyes can cause breathing problems due to the inhalation of the dye molecules which affect the immune system of the human. Other symptoms like itching, sore eyes, sneezing, coughing, and wheezing can also be the results of the impact of dye. On the other hand, in comparison with the other dyes, the anionic and cationic dyes can easily penetrate living body cells and can cause carcinogenic effects even at the low concentration. Rhodamine B (RhB) is widely used as a colorant in textile industries. It is also utilized in the manufacturing of numerous products such as ball pens, paints, leather, dye lasers, carbon sheets, stamp pad inks, crackers, and explosives It is a weakly basic nitrogenous molecule that is undergoing dissociation and produces a highly stable and non-biodegradable colorful cation. These colorful cations enter the surface and ground water reservoirs and cause significant alterations in the aquatic ecosystem. The widespread presence of Rhodamine B in the aquatic environment could be hazardous to both human and animal health. It causes mutagenic and oncogenic variations in living thing. It is also categorized as a neurotoxic dye in both humans and animals, causing infections of the eyes, skin, gastrointestinal tract, and respiratory tract. It's predicted No Effect Concentration (PNEC) was 14 µg/L in an aquatic organism based on ecotoxicological research. It is the lowest value for Rhodamine B's aquatic ecotoxicity that has been documented. The so-called Annual Average Quality Standard (AA-QS), the Environmental Quality Standard (EQS) for longer-term exposure, can be simply computed from these PNEC values. The AA-QS for RhB will be 14 µg/L, which is equal to the PNEC. The Maximum Acceptable Concentration (MAC-QS) for RhB is 140 µg/L. RhB is frequently employed as a systemic marker in several animals due to its high level of persistence. One study found that detectable quantities of RhB occurred in the Myocastor coypus for up to 225 days after feeding them 0.5 g /kg of the dye for three days. RhB is difficult to remove because of its persistence, which raises the possibility that it can cause several problems.[11]

Textile industries usually release a large amount of MB dyes in natural water sources, which becomes a health threat to human beings and microbes. MB dye is harmful to human health above a certain concentration due to its substantial toxicity. MB is toxic, carcinogenic, and non-biodegradable and can cause a serious threat to human health and destructive effects on the environment. MB causes several risks to human health such as respiratory distress,

abdominal disorders, blindness, and digestive and mental disorders. It also causes nausea, diarrhoea, vomiting, cyanosis, shock, gastritis, jaundice, methemoglobinemia, tissue necrosis, and increased heart rate, causing the death of premature cells in tissues and skin/eye irritations. MB contacts with skin may result in skin redness and itching. The no observed adverse effect level (NOAEL) for the MB in rats was observed to be 25 mg/kg. MB discharge into the environment is a significant threat for aesthetical and toxicological reasons. It also reduces light penetration and is a toxic supply to food chains for organisms. MB presence in water bodies, even at a very low concentration, makes highly coloured sub-products. Owing to its high molar absorption coefficient (~8.4×10^4 L/mol/cm at 664 nm), which reduces sunlight transmittance, it decreases oxygen solubility, affects the photosynthetic activity of aquatic life, and decreases the diversity and aesthetics of the biological community .[12]

Methyl orange is a carcinogenic water-soluble azo dye, and also acknowledged as an acidic or anionic dye. It can cause vomiting and diarrhea. High levels of exposure to MO can results in death. It is also metabolized into aromatic amines by intestinal microorganisms. Methyl orange is stable, shows low biodegradability and is soluble in water hence it is difficult to remove from aqueous solutions by common water purification or treatment methods.

Congo red (CR) is a diazo dye associated with benzidine which is a cancer-causing substance. Therefore, CR is also known as a human carcinogen and toxic compound for animals and plants [13]. The toxicity of Congo red is primarily connected to its intermediary metabolites, which directly disturbed DNA and produce apoptosis in HL-60 cells (human promyelocytic leukemia cell line)[14]. Apart from dyes, phenol and its derivatives are also considered toxic to the human being if long term exposed. These cause mainly diarrhea, anorexia, vertigo, progressive weight loss, excessive salivation, dark coloured urine, blood, and liver effects [15].

Knowing the bad impact of the dyes and toxic compounds on the human's life, plants, and animals, it is being crucial to eliminate the dyes from the wastewater prior to releasing into the environment.

2.3 Dye removal methods

The majorities of synthetic dyes are poisonous in nature and constitute a risk to aquatic life. To meet with tight environmental requirements, numerous traditional methods for removing colours from water and wastewater have been used. These methods are as classified in Fig. 2.5.

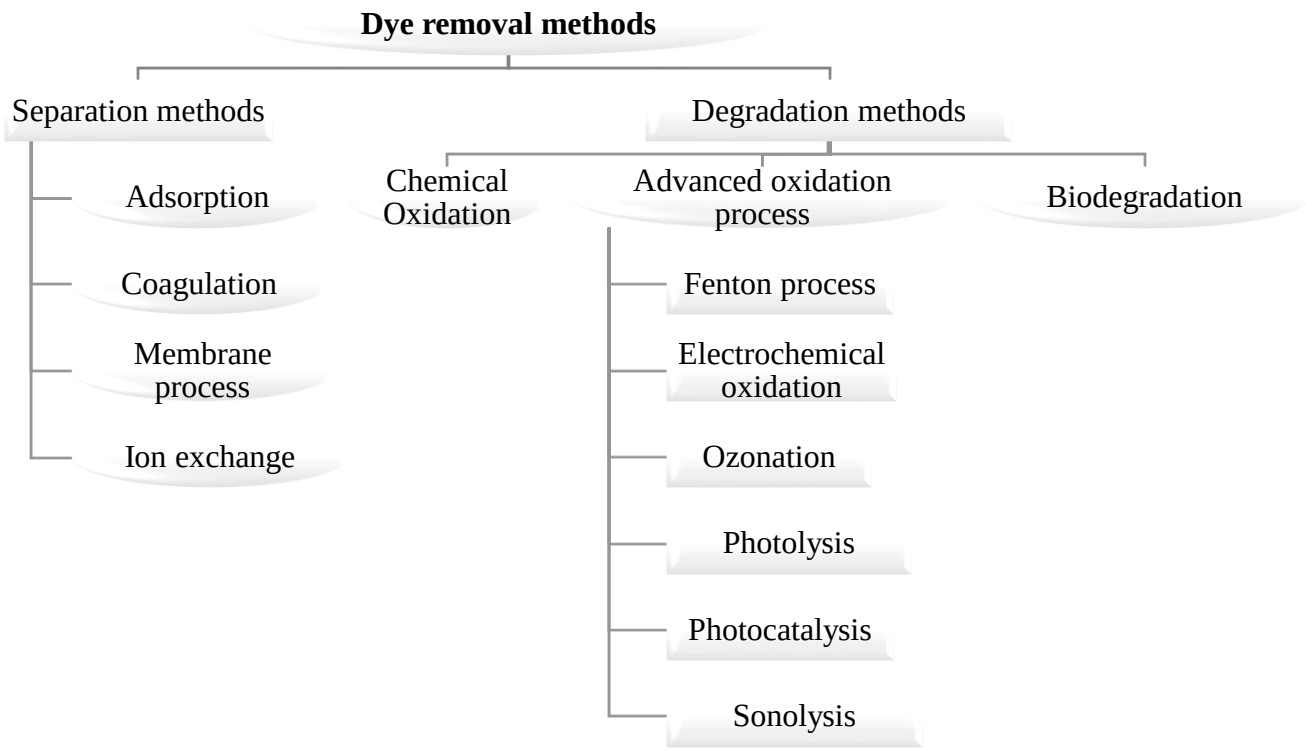

Fig 2.5: Classification of various methods for dye treatment**.**

Some of the techniques for removal of dyes are discussed in following sub-sections.

2.3.1 Chemical coagulation & flocculation

Coagulation and flocculation are commonly used as physicochemical procedures for cleaning industrial wastewater because they destabilize and create flocs, which remove colloidal particles, very small solid suspensions, and a few soluble chemicals that were previously present in the wastewater. According to several researches, the coagulation process has proven to be more effective approach compared to other processes such as anaerobic reduction, oxidation, and adsorption. It is also one of the simplest and cheapest procedures that may be easily employed in industrial settings [16]. Coagulation removes around 70 to 80 percent of the colour and reduces the concentration of organic chemicals by about the same amount. The efficacy of this procedure is determined by the qualities of raw wastewater, as well as the temperature and pH of the solution, as well as the type and dosage of coagulants used, and the mixing time. Inorganic salts like alum or ferric chloride, as well as synthetic organic polymers, are common coagulants. Although chemical coagulants are used to remove colours and

suspended particles from wastewater, they have several drawbacks, including their impact on humans by creating diseases like Alzheimer's disease, which is caused by inorganic salts, and some of them are also carcinogenic in nature.

Chemical coagulation is a complex process involving several interconnected characteristics, thus it's crucial to know how well a coagulant will perform under specific conditions. As a coagulation, alum, ferric chloride, ferric sulphate, and magnesium chloride can be employed. Destabilization is affected differently by different coagulants. The higher the counter ion's valence, the more destabilizing it is and the lower the required coagulation dose. Positively charged polymers will prevail when the pH is below the isoelectric point of metal hydroxide and colloids are precipitated by various coagulants supported by a suitable polymer. Adsorption of these positively charged polymers can destabilize negatively charged colloids by charge neutralization. Anionic polymers will predominate above the isoelectric point when particle instability may occur due to adsorption and bridge formation. When a large dose of metal ions (coagulant) is used, a sufficient degree of oversaturation occurs, resulting in the rapid precipitation of a large amount of metal hydroxide, enmeshing the colloidal particles known as sweep flocs. Monomeric and polymeric ferric species are produced when Fe (III) salts are used as coagulants, with the generation of monomeric and polymeric ferric species being pH dependent. According to several studies, the natural colour of ferric chloride solution is acidic, but successful removal can only be done when the pH is close to neutral, therefore adding a base to keep the pH stable becomes a must. Lime or sodium hydroxide (NaOH) might be used for this. Lime, on the other hand, may result in more sludge. The use of polyelectrolyte as a coagulant aid, on the other hand, often improves the coagulant's performance. As can be observed, the ideal pH for alum is close to neutral, allowing for greater colour removal efficiency. Furthermore, the inclusion of polyelectrolyte improves the colour removal performance in general. The vast amount of sludge generated by this technique, however, makes it unappealing. Magnesium chloride's optimal pH ranges from 9 to 12. When used with lime, it provides excellent colour removal. However, it produces a huge amount of sludge, which may provide a sludge disposal concern as well as additional costs. Because of the enormous volume of sludge generated and the formation of basic effluent after treatment, alum and magnesium chloride may not be regarded good coagulants. Though both ferric chloride and alum have a high efficiency, ferric chloride has lower colour removal effectiveness at low concentrations. However, when ferric chloride is combined with a little amount of cationic polymer, a considerable improvement in colour removal has been recorded.

2.3.2 Electro coagulation

The electro coagulation process is a type of colour removal from wastewater electrochemical technology. The unique properties of environmental compatibility, safety, and versatility drew a lot of attention to this technology. To meet the needs of many sectors, electrochemical technology competes with other traditional technologies such as precipitation, evaporation, ion exchange, and solvent extraction. Electrochemical technologies are superior to physicochemical and membrane technologies in general, especially when it comes to removing colour from wastewater, because they use the electron as a single reagent and do not produce solid residues. Coagulation, adsorption, precipitation, and flotation are the main methods of pollutant removal during electro coagulation. Electro coagulation provides several advantages over biological treatments, including a smaller footprint due to a shorter reaction time, lower sludge production compared to chemical coagulation, lower equipment and operation costs, and ease of use.

Coagulants are generated in situ during electro coagulation by electro oxidation of sacrificed anodes. The suspended particles or precipitates are then destabilized and aggregated by aluminum or iron hydroxide flocs, which absorb dissolved contaminants. Because aluminum and iron are inexpensive and readily available, they are commonly used in electro coagulation. Dalvand et al. investigated the effectiveness of electro coagulation with aluminum electrodes to remove Reactive Red198 (RR198) from aqueous solution [17]. Variables such as voltage variation, reaction time, inter electrode distance, initial dye concentration, electrolyte concentration, and electrode connection mode were studied to see how they affected dye removal percentage. They also investigated the best operating conditions in terms of electrical energy consumption and electrode consumption. The structure of Reactive Red198 (RR198) is made up of different groups. At 288, 373, and 518 nm, these groups have three different absorbance peaks. The benzene, naphthalene, and azo-linkage peaks could all be attributed to benzene, naphthalene rings, and azo-linkage, respectively. Depending on the type of electrode material used, dye removal during electrochemical processes could be due to dye molecules being broken down into smaller organic compounds. To assess the dye removal mechanism by electro coagulation, the absorbance of raw and treated wastewater was measured at three absorption wavelengths of 288, 373, and 518 nm. In addition, absorbance at 254 nm was measured to determine the presence of aromatic compounds in the solution caused by dye cleavage. During the electro coagulation treatment, all the absorbance peaks decreased and were almost completely gone after about 30 minutes. The decrease in absorbance peaks

indicated that dye molecule adsorption on flocs was the primary mechanism for dye removal. The removal of RR198 did not result in azo-linkage cleavage or the production of other by-products. The high COD removal rate (84.1%) confirms that the cleavage azo group plays only a minor role in dye removal. Low decomposition of dye molecules to small organic substances via electro-oxidation may explain the lower COD removal compared to dye removal.

2.3.3 Membrane process (Reverse Osmosis (RO) & Nano Filtration (NF))

Membranes are widely used in a variety of separation processes because of their ability to control materials passing through the membrane, resulting in a high degree of separation that is always achieved, making these processes widely acceptable. The membrane is a barrier that allows some substances to pass through it (permeate) while preventing others from doing so (retentate) in a very specific way. Membranes can be used to separate fluids, dissolved solids, suspended solids, and colloidal dissolved solids. The ability to remove or recover valuable or harmful components, as well as the ability to close water systems, which reduces the consumption of fresh water, are the main characteristics of membrane processes in the treatment of consumables. The use of membrane processes allows wastewater to be purified to a level that is difficult to achieve with traditional methods. Reverse Osmosis (RO) and Nano Filtration are the most widely used and significant membrane filtration techniques (NF). The operating pressure of NF is between 5 and 40 bars, and the membrane pore size is between 0.5 and 2 nm. On the one hand, it's used to separate sugars, other organic molecules, and multivalent salts from monovalent salts, ions, and water, and on the other hand, it's used to separate monovalent salts, ions, and water. In RO or hyper filtration, the membrane pore size is in the range of 0.5 nm. Operating pressures in RO are usually between 7 and 100 bars. The importance of membrane processes is demonstrated by the membrane areas installed in various industrial sectors. RO membranes are a popular choice for treating contaminated drinking water supplies because of their ability to remove both organic and inorganic compounds. Hardness, colour, a variety of bacteria and viruses, as well as organic contaminants like agricultural chemicals and trihalomethane precursors, can all be removed simultaneously using reverse osmosis. Avlonitis et al. looked at effluents from the cotton textile industry that were treated with a nanofiltration membrane to reduce the amount of water that was discarded while also allowing the treated water to be reused [18]. The results showed that NF membranes were capable of completely decolourizing the cotton dye effluent and reducing the total salt concentration by more than 72%. Even at high recoveries and low pressures, these membranes

can produce high-quality water that can be reused. Gozálvez-Zafrilla et al. looked into the treatment of secondary effluent for wastewater reuse in the textile industry [19]. They used (NF90) membrane in their research. The results showed that NF90 had the highest salt rejection and a 99 percent COD reduction (75-95%). The levels of COD removal and salt rejection were unaffected by fouling, and the permeate quality allowed for a high flux percentage to be recovered after cleaning. Abid et al. used the RO & NF process to test acid red, reactive black, and reactive blue dye [20]. They discovered that RO and NF membranes can effectively remove dye from wastewater, and that dye removal was proportional to applied pressure, pH, TDS, and dye concentration in the feed solution, but not to feed temperature.

2.3.4 Biological process

The biological process employs microorganisms such as fungi, bacteria, and algae, which are capable of biodegrading and absorbing dyes found in wastewater. The use of microorganisms to remove dyes from wastewater has several advantages, including a low cost, an environmentally friendly process that produces less secondary sludge, and nontoxic final products for complete mineralization. Many studies have been conducted that show the ability of microorganisms like Cunninghamellaelegans, Aspergillusniger, Bacillus cereus, Chlorella Spand, and Citrobactersp to remove dye from industrial wastewater. The most important factors influencing the decolourization effectiveness of microbial activity are the adaptability and activity of each microorganism. Colour is removed using biological treatment, but because most dyes are designed to resist light and oxidation degradation, they are less likely to be treated with traditional aerobic therapy. The removal of water-soluble dyes by aerobic processes is a particular problem. On wastewater sludge, some of these dyes are adsorbed. Direct biological treatment with bacteria or fungi is also possible, but the nutritional and physiological requirements of microorganisms limit the applicability of these bioremediation methods. The use of enzymes to replace traditional non-biological methods has gained popularity as a result of research into effective and environmentally friendly oxidation techniques. Biological treatment methods have proven to be effective in reducing dye house effluents, and when used properly, they are less expensive to operate than other methods. In the water treatment process which combine chemical and biological, or physical and biological, have also been found to be effective. Biological treatment of textile azo dyes has been shown to be an effective method for degrading all dye materials while also overcoming many of the disadvantages of physicochemical processes. Both aerobic and anaerobic metabolism can be

used by microbes and their enzymes to degrade dye. Several studies have been published on the degradation of environmental contaminants by different bacteria. Many bacteria have been identified as relying solely on hydrocarbons. Bacteria with hydrocarbon-degrading bacteria can degrade hydrocarbons. Because they are biodegradable and easy to maintain, these bacterial bio flocculants provide an affordable and clean alternative for replacing or supplementing current treatment processes to remove dyes from wastewater effluents. Daneshvar et al. looked into the ability of microalgae Cosmarium species to decolourize a solution containing Malachite Green, a cationic textile dye [21]. They looked at algal stability and reusability during repeated decolourization operations, as well as the relationship between kinetic properties and dye concentration and other rate-dependent environmental variables (temperature, pH, dye concentration, and algal concentration).

2.3.5 Adsorption with conventional adsorbent (activated carbon)

Adsorption is the method of choice and produces the best results among the many dye removal techniques available because it can be used to remove a variety of colouring materials. If the adsorption system is properly designed, the treated effluent will be of high quality. Depending on the nature of the forces involved, adsorption processes can be classified as either physical or chemical. Adsorbate/adsorbent interaction, adsorbent surface area and pore structure, surface chemistry, nature of the adsorbate, effect of other ions, particle size, pH, temperature, contact time, and other physico-chemical factors all influence the adsorption process. In comparison to other techniques such as coagulation, flocculation, precipitation, and activated sludge, the adsorption technique has proven to be more effective and convenient due to its low cost, simple design, easy handling, and sludge-free cleaning operations. Adsorption processes are a viable treatment option, particularly when the adsorbent is cheap and readily available. Activated carbon is the most widely used adsorbent among commercial adsorbents. The use of activated carbon as a dye removal technique has been highlighted as a viable option. Activated carbon has an extremely high affinity for many types of dyes, including basic dyes, due to its unique molecular structure. Because of its excellent adsorption ability, activated carbon is currently used as a sorbent in most commercial systems to remove dyes from wastewater. One of the best available control technologies, according to the US Environmental Protection Agency, is activated carbon adsorption. Activated carbon, on the other hand, is a preferred sorbent, but its widespread use is limited due to its high cost. Efforts have been made to find low-cost alternative adsorbents to reduce treatment costs. El Qada et al. investigated activated

carbon and compared the adsorption capacity of three different activated carbons (PAC1 and PAC2 developed at QUB for this work, and commercially available Filtrasorb 400) [22].

2.3.6 Adsorption with non-conventional adsorbents (fly ash)

Aside from traditional adsorbents like activated carbon, a variety of approaches to developing cheaper and more effective adsorbents have been investigated. Several researchers have proposed a variety of non-traditional low-cost adsorbents, including natural materials, biosorbents, and waste materials from industry and agriculture. These materials could be used to remove dyes from solutions as sorbents. Biosorbents (chitosan, peat, biomass), clay materials (bentonite, kaolinite), zeolites, siliceous materials (silica beads, alunite, perlite), agricultural wastes (bagasse pith, maize cob, rice husk, coconut shell), industrial waste products (waste carbon slurries, metal hydroxide sludge), and others have all been reported as sorbents (starch, cyclodextrin, cotton). G. Crini looked at the technical feasibility of using nontraditional low-cost adsorbents to remove dye from contaminated wastewater [23]. He believes that low-cost adsorbents have a lot of potential for commercial applications in the future. Chitosan-based sorbents have demonstrated superior dye removal capabilities when compared to activated carbon. Despite several papers on low-cost adsorbents being published, there is still a scarcity of information containing a comprehensive comparison of sorbents. Although much progress has been made in the field of low-cost sorbents, much more work is needed to predict the performance of adsorption processes for dye removal from real industrial effluents under a variety of operating conditions, (ii) better understand adsorption mechanisms, and (iii) demonstrate the use of low-cost sorbents on an industrial scale. For the removal of crystal violet and rosaniline hydrochloride (basic fuchsine) from wastewater, Mohan et al. used fly ash generated in thermal power plants as a low-cost adsorbent (Mohan et al., 2002). They discovered that as the temperature rises, the adsorption of the two dyes increases, indicating that the process is endothermic. Both the Freundlich and Langmuir models can be used to fit the data and estimate model parameters, according to the findings. Overall, the nonlinear Freundlich adsorption isotherm fits the data better. Crystal violet and basic fuchsine dyes have higher or comparable adsorption capacities on fly ash than other adsorbents used for the same or other cationic dyes. According to their findings, fly ash can be used as an effective adsorbent for dye removal.

2.3.7 Advanced oxidation process (AOP)

Traditional oxidation treatments have struggled to oxidize dyestuffs and organic compounds with complex structures at low concentrations or when they are particularly resistant to oxidants. Advanced oxidation processes (AOPs) have been developed to generate hydroxyl free radicals using various techniques to alleviate the problems mentioned. The AOPs, which combine ozone (O_3), hydrogen peroxide (H_2O_2) and UV irradiation, to treat textile wastewater, have shown the most promise. These oxidants effectively decolourized dyes but did not eliminate COD completely. Any AOP's goal is to generate and use hydroxyl free radical ($OH^{\bullet}$) as a strong oxidant to destroy compounds that cannot be oxidized by conventional oxidants. Advanced oxidation processes are defined by the production of $OH^{\bullet}$ radicals and attack selectivity, which is a useful property for an oxidant. The fact that AOP can be used in a variety of ways for $OH^{\bullet}$ adds to their versatility. Combining O_3, H_2O_2, TiO_2, UV radiation, electron-beam irradiation and ultrasound is a common way to speed up the production of $OH^{\bullet}$. The most promising are O_3/H_2O_2, O_3/UV and H_2O_2/UV for oxidizing textile wastewater. In recent decades photocatalysis has appeared as an emerging advance oxidation process.

2.4 Photocatalysis

Photocatalysis is a process to accelerate a chemical reaction using a catalyst in the presence of light sources. The main difference between photocatalytic reactions compared to other conventional catalytic reactions is that catalysts are activated by light rather than heat. Photocatalysis for water treatment was first recognized during the 1980s when photocatalytic mineralization was successfully conducted for different halogenated hydrocarbons [24]. It is an Advance Oxidation Process (AOP) where semiconductor based photocatalyst generates electron hole pairs when exposed to light irradiation, i.e., electrons are exited from the valence band to the conduction band, producing a pair of electron holes. Photo-generated electron hole pairs will migrate to the surface of semiconductor for redox reaction[25]. The hole generated in valance bond easily reacts with the H_2O and produces hydroxyls radicals ($OH^{\bullet}$) and the conduction band electron reacts with oxygen to produce superoxide radical anions ($^{\bullet}O_2^-$). The mechanism for generation of hydroxyl radicals and superoxide radical anions are shown in following equations.

$$\text{Photocatalyst} + h\upsilon \rightarrow e^-_{cb} + h^+_{vb} \quad (2.1)$$

$$H_2O + h^+_{vb} \rightarrow OH^{\bullet} + H^+ \quad (2.2)$$

$OH^- + h^+_{vb} \rightarrow OH^\bullet$ (2.3)

$OH^\bullet + OH^\bullet \rightarrow H_2O_2$ (2.4)

$H_2O_2 + h\upsilon \rightarrow 2\ OH^\bullet$ (2.5)

$O_2 + e^-_{cb} \rightarrow {}^\bullet O_2^-$ (2.6)

${}^\bullet O_2^- + H_2O_2 \rightarrow OH^\bullet + O_2 + OH^-$ (2.7)

$H_2O_2 + e^-_{cb} \rightarrow OH^\bullet + OH^-$ (2.8)

These hydroxyls radicals ($OH^\bullet$) & superoxide radical anions (${}^\bullet O_2^-$) are called Reactive Oxygen Species (ROS) which degrades the dyes and converted into CO_2, H_2O & other degradation products. The pictorial representations of dye degradation are shown in Fig. 2.6.

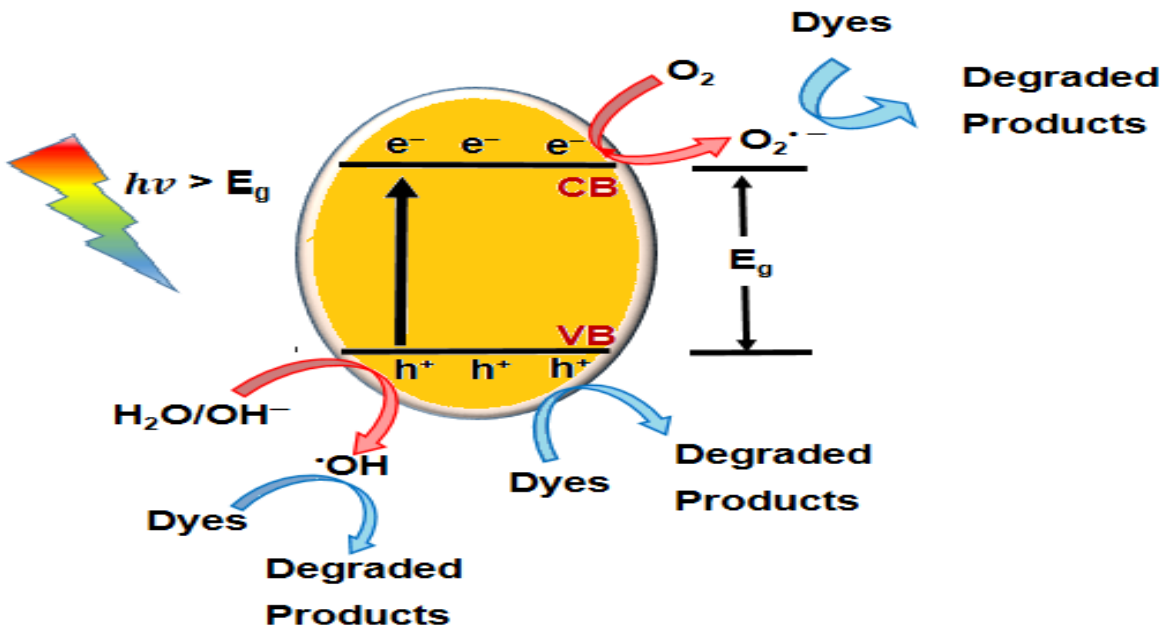

Fig. 2.6: Pictorial representation of the process taking place in the photocatalytic degradation of dyes on semiconductor surfaces

The efficacy of a photocatalyst in degrading dye is primarily determined by following three key factors:

(1) Band-gap energy (Eg): Photocatalysts with a wide bandgap are sensitive to UV light, while photocatalysts with a narrow bandgap are sensitive to visible light;

(2) Band edge potentials, i.e., the potentials of VB and CB: ROS can only be generated when the CB potential is more negative than the reduction potential of O_2 to ${}^\bullet O_2^-$ (− 0.33 eV vs. NHE) and/or VB potential is more positive than standard oxidation potential of $OH^\bullet/H_2O$

(+ 2.68 eV vs. NHE) or $OH^{\bullet}/OH^{-}$ (+ 1.99 eV vs. NHE) [26]. If this is not the case, the h^{+} in the VB reacts directly with the pollutant. The more ROS produced, the higher the semiconductor's efficiency; and

(3) Rate of $e^{-} - h^{+}$ pair recombination: Recombination of $e^{-} - h^{+}$ pairs reduces catalyst efficiency due to the strong Columbic attraction between them. Recombination causes the e^{-} to revert to the VB without undergoing the reduction reaction, resulting in the formation of $^{\bullet}O_2^{-}$ [27]. As a result, these three important factors should be considered when selecting a photocatalyst.

2.5 Different types of photocatalysts

The various types of photocatalysts are depicted in Fig. 2.7 and are described in following subsections.

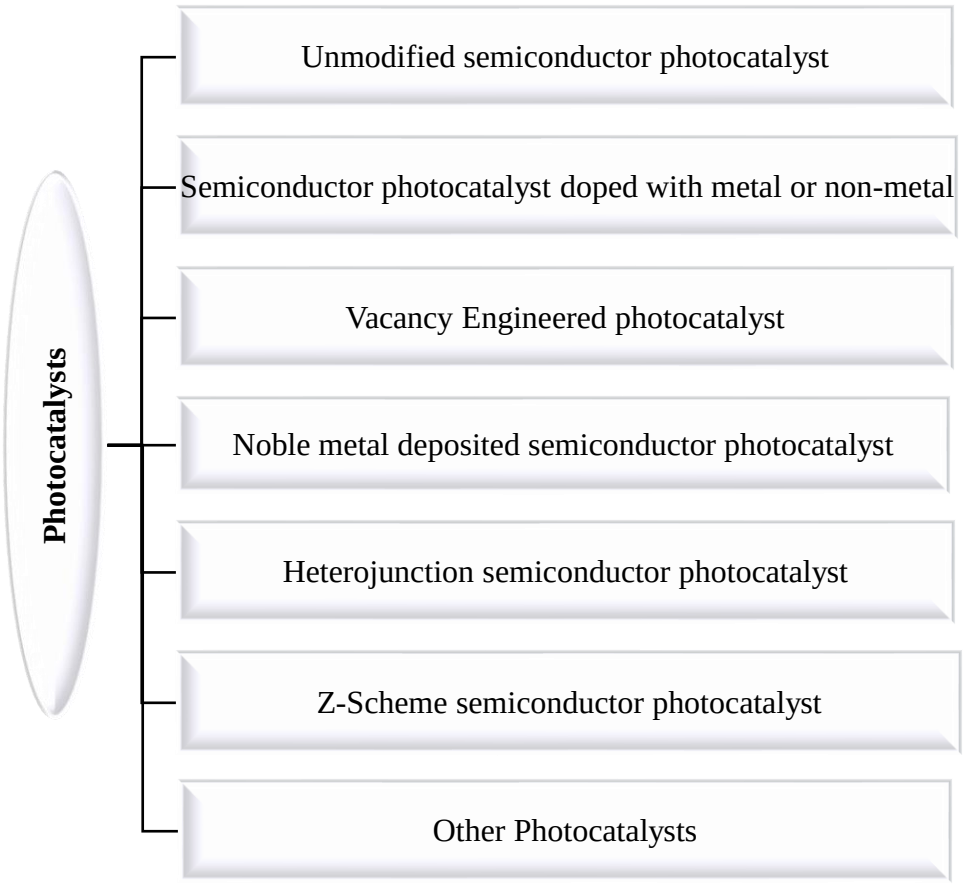

Fig. 2.7: Different types of photocatalysts

2.5.1 Unmodified semiconductor photocatalyst

Unmodified semiconductor photocatalyst is a type of photocatalyst where pure metal is used as a photocatalyst without any modification of properties by adding several impurities. Graphitic carbon nitride (g-C_3N_4), WO_3, BiOX (X = F, Br, Cl and I) and other metal-free narrow band gap (2.5-2.7 eV) semiconductors are popular visible light photocatalysts because they are easy to prepare, have high chemical stability, and have an efficient visible light response. This photocatalyst's VB potential is lower than the standard redox potentials of $OH^{\bullet}/H_2O$ and $OH^{\bullet}/OH^-$, limiting the generation of $OH^{\bullet}$. It is not possible to make a single photocatalyst that has both good visible light response and high redox ability. A major limitation of pure unmodified photocatalyst is the rapid recombination of photogenerated e^-–h^+ pairs [28]. Due to this reason nowadays, the unmodified semiconductor photocatalyst is generally not used directly for the effective removal of organic pollutant, rather than it is modified by several methods like doping, adding nanoparticles, creating vacancy etc.

2.5.2 Semiconductor photocatalyst doped with metal or non-metal

Doping wide bandgap photocatalysts with metals (Sr, Co, Ti, Bi, Fe, etc.) and nonmetals (C, N, S, B, etc.) can narrow the bandgap, allowing visible light to pass through while also improving efficiency of e^-– h^+ separation. TiO_2, ZnO, g-C_3N_4 have excellent photocatalytic activity towards the degradation of organic pollution but due to their wide bandgap they are not effective in visible range. By lowering the bandgap energy of ZnO nanoparticles by doping and introducing impurities, they became more photo-catalytically active over a wider range of wavelengths (UV to visible) [29]. For enhancing the photocatalytic oxidation of organic dyes under UV and visible light irradiation, ZnO nanoparticles have been modified with different dopants consisting of N and S atoms [30]. N-doped ZnO showed 96.22% efficiency towards the removal of Methylene Blue (MB) dye under visible light irradiation [31]. In similar way it is observed that TiO_2/g-C_3N_4 heterojunction showed 90% efficiency towards the removal of Methyl Orange (MO) dye under visible light irradiation, which is increased to 99.8% for carbon-nitrogen-sulfur hetero atom doping [32].

2.5.3 Vacancy Engineered photocatalyst

Defect engineering, particularly vacancies, has a significant impact on the modification of photocatalyst properties [33]. Vacancy induction improves the electronic structure, inhibits electron hole recombination, and can even act as a specific reaction site, improving photocatalytic performance [34]. It aids in the reduction of the band-gap energy of a semiconductor, which increases light-harvesting range the semiconductor. The creation of nitrogen vacancies in g-C_3N_4 can has been shown in recent studies to significantly improve the photocatalytic efficiency of bulk g-C_3N_4 [33], [34]. In the recent past, oxygen vacancy induced photocatalyst synthesis is becoming a research hotspot because it enriches the electron trapping and active sites, which in turn enhance the charge carrier separation, absorption and activation ability for O_2 molecules [3]. Wang et al. have reported an oxygen vacancy induced $BiO_{2-x}/Bi_2O_{2.75}$ Z-scheme heterojunction, which has shown superior photocatalytic activity [35]. Goud et al. analyzed surface oxygen vacancy facilitated Z-scheme MoS_2/Bi_2O_3 heterojunction towards the removal of Crystal Violet (CV) dye under visible light irradiation [36]. In another study by Khan et al. reported for surface oxygen vacancy CeO_2-Graphene nanostructure towards the degradation of organic dyes [37].

2.5.4 Noble metal deposited semiconductor photocatalyst

The photocatalytic performance of a semiconductor is enhanced by depositing noble metals such as Pt, Pd, Au, Ag, Cu, and others as a surface modifier. Because of the Schottky barrier at the metal– semiconductor heterojunction, photo-induced electrons in the conduction band (CB) can transfer to metal deposits, which act as electron acceptors, whereas photo-induced holes can remain on the semiconductor surface in semiconductor–metal composites. As a result, electron and hole recombination can be avoided, and the photocatalytic efficiency can be increased [38] . Pt deposited in TiO_2 showed a great removal efficiency of RhB under visible light irradiation [39]. Silver is one of the good noble metal widely used for improving photocatalytic activity of semiconductor. Mosavi et al.reported Ag deposited CdSe/Zeolite nanocomposite has about 90% efficiency towards the removal of MB dye under visible light irradiation [40]. In another study Shi et al. reported Ag/AgBr deposited Ag/Br/ZnO nanocomposite showed almost 100% efficiency for removal of RhB dye under visible light irradiation [41]. Shen et al. studied by using different noble metal Ag, Ru, Au, Pd, Pt and constructed CdS/M/TiO_2 Z-scheme photocatalyst (M = Ag, Ru, Au, Pd, and Pt) and observed

the removal efficiency of MB dye under visible light irradiation & reported their degradation potential in order of Ag >Ru>Au >Pd>Pt [42].

2.5.5 Heterojunction semiconductor photocatalyst

Heterojunction photocatalysts are now widely used, and they are more effective in separating photogenerated e^{-}– h^{+} pairs due to the combined beneficial effects of the individual semiconductors. In heterojunction semiconductor one n-type and another p-type semiconductor are combined. For type II heterojunction the VB & CB of one semiconductor is in higher level compared to the other semiconductor. A p-type and an n-type semiconductor can form a type II heterojunction, with the p-type semiconductor having higher band edge levels and work function values than the n-type. After contact, free e from the n-type semiconductor flows to the p-type semiconductor until equilibrium (EF) is reached, resulting in positively charged n-type and negatively charged p-type semiconductors at the heterojunction interface. As a result of band edge bending, an internal electric field is formed, which leads to the formation of a potential barrier. The internal electric field facilitates the transport of photogenerated e from the p-type CB to the n-type CB and photogenerated h^{+} from the n-type VB to the p-type VB with incident light, resulting in the e^{-}–h^{+} pair separation. Copper sulfides (CuS) is a p-type semiconductor with a narrow band gap of 2.0 eV, it has strong absorption potential of visible light. But pure CuS has low photocatalytic activity because of the rapid recombination of photo-induced e^{-}– h^{+} pair [43]. Bismuth tungstate (Bi_2WO_6) nanosheets have weak visible-light response and recombine readily with photogenerated carriers. But formation Bi_2WO_6/CuS p-n heterojunction showed about 99% efficiency towards the removal of RhB dye under visible light irradiation [44]. In another example we can observe that Zirconium oxide (ZrO_2) is a n-type semiconductor which has a wide band gap of (5 eV) it shows very less efficiency in visible light. Cerium oxide (CeO_2) is an-type semiconductor having a relatively narrow bandgap of 2.7. A combination of two semiconductors with different and gap level energies of type n-n junction showed exhibited better photocatalytic properties than single ones.

2.5.6 Z-Scheme semiconductor photocatalyst

The natural photosynthetic process of water splitting inspired Z-schemes [45]. Although the Z-scheme photocatalyst has the same band structure configuration as a heterojunction, the mechanism of charge carrier transfer is different. In comparison to traditional Type I and Type

heterojunctions, the Z-scheme can effectively separate electrons and holes in different semiconductors while maintaining higher oxidation and reduction potentials for holes and electrons[46] . This exaction transfer mechanism promotes recombination of photogenerated $e^- - h^+$ with weaker redox abilities, spatially separating and preserving photogenerated $e^- - h^+$ with superior redox abilities for photocatalytic reactions [47]. Additionally, narrow bandgap semiconductors can be used to construct Z-scheme systems, extending the light absorption range while maintaining the photocatalyst's high redox ability. The development of Z-scheme heterojunctions is a promising research area because it can improve light absorption and charge separation [35]. Bulk g-C_3N_4 is a good photocatalyst with bandgap 2.7 eV but the photocatalytic activity is generally restricted by its limited charge-transfer capacity. For enhancement of photocatalytic activity Z-scheme heterojunction can be made, for that it is necessary to identify the semiconductor of suitable band structure. In this regard V_2O_5 semiconductor can be used to create the Z-scheme, which has several advantages including a narrow band gap, a wide range of light response, and chemical properties that are relatively stable[48] . Hong, Jiang et al. used thermal polymerization to make a V_2O_5/g-C_3N_4 Z-scheme heterojunction composite and found that its efficiency in photocatalytic degradations of Rhodamine B (RhB) was significantly higher than that of V_2O_5 and g-C_3N_4 [49].

2.5.7 Other Photocatalysts

In recent years nanocomposite photocatalyst are mostly in use. They are basically the combination of multiple photocatalyst. These nanocomposites do not fall in the above-mentioned categories but we can get idea about their charge transfer mechanism from the above categories. These nanocomposites are very effective for degradation of synthetic dyes under visible light. For examples Ag-based semiconductors such as AgX (X = Cl, Br, I), Ag_2CrO4, Ag_2MoO_4, $AgVO_3$, Ag_3PO_4, Ag_2CO_3, Ag_2WO_4, etc., are the promising candidate for photocatalysis as they respond to visible light efficiently due to their narrow bandgap. Among them Ag_2MoO_4 nanoparticle used widely in various applications such as photo-switch devices, gas-sensing, antimicrobial agents, ion-conducting glasses etc [50], [51]. Bi_2MoO_6 is an excellent photocatalytic agent in UV region but it is less active in visible region [52]. Balasurya et al. prepared Bi_2MoO_6/Ag_2MoO_4nanocomposite which shows 91.8% efficiency towards the removal of MB dye under visible light [53]. Iqbal et al. prepared CuSe/GO nanocomposite and observed 89% efficiency towards the removal of MG dye in visible light [54]. Similarly, BPN & ZnAl-LDH nanocomposite [55]**,** TiO_2/PVA/cork nanocomposite [56]**,** are recently

discovered nanocomposites which shows great efficiency towards the removal of MB dye under visible light irradiation.

2.6 Photocatalytic degradation of dyes

Conventional treatment processes like chemical coagulation, electro coagulation, biological process, adsorption etc. are not able to remove the dyes as discussed above completely. Moreover, these processes have several disadvantages like high cost, sludge production, hard to handle etc. Due to these reasons, advance oxidation processes are used in removal of these dyes. Photocatalysis process is one of the advance oxidation processes, which can remove dye in an efficient way. Basic mechanism of photocatalysis process is already discussed above. There are various types of photocatalysis like unmodified photocatalysis, Nobel metal deposited photocatalysis, vacancy engineered photo catalysis, heterostructure photocatalysis, Z-scheme photocatalysis that also discussed in above chapter. TiO_2, ZnO, WO_3 etc are the most common semiconductor photocatalyst are used for pollution treatment but these photocatalyst have wide band gap and thus are ineffective to remove dyes in visible range. For that reason, researchers are mostly focused on preparation of nanocomposite which is the composition of different type of material with semiconductor photocatalyst with gives great removal efficiency. Some of the literatures in recent advancement regarding photocatalytic removal of dye are described below.

Ge et al., synthesized a novel visible-light-induced g-C_3N_4/Bi_2WO_6 composite photocatalysts by introducing polymeric g-C_3N_4 via a mixing and heating method. The g-C_3N_4/Bi_2WO_6 samples had a red shift and strong absorption in the visible light region and had obviously enhanced photocatalytic activities in MO degradation. The highest degradation efficiency was observed for the 70 wt% g-C_3N_4/Bi_2WO_6 sample. The synergic effect was explained and a photocatalytic mechanism was proposed as well as discussed based on energy band positions and PL spectra. The novel heterojunction materials, as highly efficient photocatalysts, may have potential applications in pollutant removal[57].

Fu et al., prepared a $BiVO_4$–graphene photocatalyst with excellent performance via a one-step hydrothermal method without the use of any surfactants. TEM observations indicate that graphene sheets are fully exfoliated and decorated with leaf-like $BiVO_4$ lamellas, due to the fact that the graphene sheets play the role of template to allow two-dimensional planar growth. The photocatalytic activity measurements demonstrate that the $BiVO_4$–graphene

photocatalysts show superior photoactivity in degradation of MB, RhB, MO and active black BL- G under visible light irradiation. The significant enhancement in photoactivity can be ascribed to the efficient separation of photo- generated carriers in the $BiVO_4$ and graphene coupling system, and the concerted effects of individual components or their integrated properties [58].

L. Shi et al. synthesized Ag/AgBr/ZnO composites using a two-step deposition precipitation method, followed by reduction under visible light irradiation to remove the RhB dye. Under visible light, Ag/AgBr/ZnO composites had significantly better photocatalytic activities for the degradation of RhB dye than pure ZnO. Synergetic effects such as increased visible light absorption, narrowed band gap, and effective separation of photogenerated electron-hole pairs are thought to be responsible for the increased photocatalytic activity. Furthermore, catalytic repetitive tests revealed that the Ag/AgBr/ZnO composite maintained good stability after 10 cycles, with activity decreasing slightly [41].

Wang et al., successfully synthesized Y-doped g-C_3N_4 visible-light-driven catalysts by a facile pyrolysis method. Y/g-C_3N_4 especially 0.25Y/g-C_3N_4 exhibits much greater photocatalytic performance than pure g-C_3N_4, which can be attributed to the slower recombination of electron–hole pairs, larger surface area, better mesoporous structure, and narrowed band gap energy of Y/g-C_3N_4. This study may inspire the rational design of high-performance g-C_3N_4 photocatalysts through the doping of rare earth elements [59].

Liu et al., successfully synthesized a novel bi-functional Z-scheme heterojunction WO_3/g-C_3N_4 with well-defined morphology by in-situ liquid phase process for the removal of MB under visible-light irradiation. It shows 95% removal efficiency in 90 min. The possible mechanism for the photocatalytic activity enhancement could be attributed to the formation of a Z-scheme heterojunction system based on the active species trapping experiments. It is observed that $^{\bullet}O_2^-$ is the main reactive species for degradation of MB [60].

Prabakaran and Pillay used a hydrothermal method to make nitrogen doped zinc oxide nanoparticles with a cabbage-like morphology (N-ZnONCBs) as a photocatalyst for photocatalytic degradation of MB under UV and visible light. Under UV and visible light irradiation for 80 minutes and 50 minutes, respectively, the N-ZnONCB photocatalyst showed efficient MB degradation (98.6 percent and 96.2 percent). In this experiment, the dye was completely mineralized. The photo-stability and reusability of the N-ZnONCB catalyst were also investigated, with a percentage degradation rate of MB (93.2%) after four cycles. Both radicals $^{\bullet}O_2^-$ and $OH^{\bullet}$ have been shown to be good oxidizing agents that readily react with the MB molecule to produce CO_2, H_2O, Cl, SO_4^{2-} and NO_3^- as degradation products [31].

Arifin et al., reported the photocatalytic decomposition of MB over titania doped copper ferrite, $CuFe_2O_4/TiO_2$ photocatalyst synthesized via sol-gel method under visible light irradiation. It showed maximum efficiency 83.7 after 3 hours of irradiation at the optimum dose of 0.5 g/L. This photocatalyst facilitates the absorption of photons and reduces the recombination of electron hole pair by effective charge separation which improves the photocatalytic activity [61].

Ghosh & Pal, reported the simple fabrication of a novel visible light active photocatalyst for the removal of MB in the presence of LED light by hydrothermally loading Bi_2O_3 nanoparticles on nitrogen vacant 2D g-C_3N_4 nanosheets. This enhanced the electron hole separation efficiency which improved the photocatalytic activity toward the degradation of MB. It shows 92% removal efficiency in 60 min [62].

El-Katori et al., synthesized an efficient and recyclable CdS/SnO_2 heterostructure for photocatalytic degradation of MB dye under UV and natural sunlight radiation. This photocatalyst enhanced the separation efficiency of the charge carrier and increased the lifetime of the reactive radicals. It is observed that the electrons in conduction band and superoxide radicals are the predominant reactive species for photocatalytic activity. This exhibits excellent photocatalytic stability and the catalyst retains 83 % of its reactivity after five consecutive cycles revealing that there is no deterioration in the catalyst structure [63].

Ferreira et al., prepared reduced graphene oxide-zinc oxide (rGO-ZnO) composite by one-step method for removal of MB under visible light irradiation. It shows 98% removal efficiency in 90 min. The photocatalytic properties of ZnO, combined with the effective adsorption capacity of rGO sheets, make the composite highly efficient for water purification applications [64].

Chaudhary et al., created novel graphene-supported ternary nanocomposites (WO_3-ZnO@rGO) for the removal of MB under visible light irradiation using simple ultrasound assisted fabrication of WO_3-ZnO binary nanostructures over 2D rGO nanosheets. The photocatalytic efficiency of WO_3-ZnO@rGO was significantly improved by impregnation of WO_3-ZnO over rGO sheets with 94 percent dye removal in 90 minutes under visible light irradiation. By effectively separating and transferring photo-induced electron-hole pairs, the WO_3-ZnO@rGO improved photocatalytic efficiency. Furthermore, even after four recycling tests, WO_3-ZnO@rGO maintained its remarkable dye degradation efficiency. It's also been discovered that ROS participate in the degradation of MB in the order $OH^{\bullet} > h^{+} > {}^{\bullet}O_2^{-}$ [65].

Lei et al., prepared Fe_3O_4@ZnO-RGO (RGO: reduced graphene oxide) composite with magnetic separation using the low-temperature hydrothermal method for removal of MB under visible light irradiation. Compared with the pure ZnO and Fe_3O_4@ZnO nanoparticles, Fe_3O_4@ZnO-RGO has a wider adsorption range for MB in visible light, and good photocatalytic activity and cyclic stability. Also, the unique structural characteristics of Fe_3O_4@ZnO-RGO enabled the separation of electron-hole pairs, which lead to its enhanced photocatalytic properties [66].

Y. Zhang et al., synthesized 2D/2D Z-scheme heterostructure photocatalyst of BiOBr/TzDa covalent organic framework (COF) (BTDC) via a facile hydrothermal method for the removal of RhB/Cr(VI) mixture. Nearly 97% of total RhB and Cr(VI) in the mixture could be removed in 20 min and 40 min, respectively. It is observed by them that h^+ and $^\bullet O_2^-$ take crucial part in the degradation of RhB while $OH^\bullet$ plays a minor role, and the function of reactive species responsible for RhB degradation decrease in the sequence of $h^+ > {}^\bullet O_2^- > OH^\bullet$ [67].

Mosavi et al., examined for the removal of MB dye by Ag@CdSe/Zeoilte photocatalyst, prepared by Response Surface Methodology (RSM). According to their findings, [MB] = 7.17 mg/L, Ag@CdSe/Zeolite dosage = 0.03 g/50 mL, pH = 8, and t = 40 minutes resulted in 89.98 percent MB removal. They also observed that in alkaline medium MB readily reacts with $OH^\bullet$and converted to CO_2 gas and effectively removed from the solution [40].

Z. Huang et al., investigated removal of MO dye by carbon-nitrogen-sulfur co-doped TiO_2/g-C_3N_4 Z-scheme heterojunction photocatalyst which was prepared via one-step hydrothermal and calcinations method sunder visible light irradiation. CNS- TiO_2/g-C_3N_4 Z-scheme heterojunction photocatalyst had excellent degradation performance (99.8%) when compared to pure TiO_2 and g-C_3N_4 under visible light irradiation. It was observed by them that $^\bullet O_2^-$ & $OH^\bullet$ played an active role in MO photocatalytic degradation process but h^+ plays a minor role [32].

X. Zhang et al., probed removal of MO dye from water by V_2O_5/P-g-C_3N_4 Z-scheme heterojunction photocatalyst under visible light irradiation. The results demonstrated that the V_2O_5/P-g-C_3N_4 Z-scheme heterostructure degraded MO 14.5 and 3.7 times faster than V_2O_5 and P-C_3N_4 when used separately. In 105 minutes, they were able to achieve 90% efficiency. They also discovered that the primary active species in the photocatalytic degradation of MO were h^+ and $^\bullet O_2^-$ [68].

Ghattavi & Nezamzadeh-Ejhieh constructed a double Z-scheme AgI/ZnO/WO_3 photocatalyst for removal of MB under visible light irradiation. This photocatalyst showed a lower

electron/hole recombination that favors the photocatalytic activity. It removes 85.2% of MB in 48.5 min. It was investigated that the photogenerated holes and hydroxyl radicals have the most essential roles in MB photodegradation by the composite [69].

Asadzadeh-Khaneghah et al., synthesized g-C_3N_4 nanosheet/carbon dot/FeOCl (denoted as C_3N_4-NS/CD/FeOCl) nanocomposites through a simple calcination procedure for photodegradation RhB dyes under visible light irradiation. The outcomes demonstrated that 250 mL of RhB solution could be successfully removed in 60 min with 0.1 g of the optimum nanocomposite. It is observed by them that h^+, $OH^\bullet$, and $^\bullet O_2^-$ all contribute in the elimination reaction [70].

Mao et al., synthesized Bi_2WO_6/CuS p-n heterojunction photocatalyst for the removal of Rhodamine B (RhB) dye under visible light irradiation. Approximately 98.8% of the RhB (10 mg/L) removed from a mixed solution within 105 min. Here photogenerated electrons/holes transferred to the surface of the Bi_2WO_6/CuS and removed the RhB directly. Bi_2WO_6/CuS can be applied over a wide pH range (2–6) with strong photocatalytic activity for removal of RhB [44].

Balasurya et al., examined for the removal of Methylene Blue (MB) dye with the help of Bi_2MoO_6-Ag_2MoO_4 nanocomposite heterojunction photocatalyst prepared via facile synthesis method under visible light irradiation. Bi_2MoO_6-Ag_2MoO_4 nanocomposite exhibited 91.8% degradation efficiency obtained after 6th cycle which was highly effective than individual Ag_2MoO_4 (54.66%) and Bi_2MoO_6 (58.6%). It is also reported by them that this heterojunction can prevent the recombination of e^-/h^+ pair and enhance the photocatalytic degradation process. $OH^\bullet$ plays the major role in photocatalytic degradation of MB dye[53].

Ahmad et al., synthesized a recoverable and stable binary nanocomposite that has received keen attention for its effectiveness in treatment of wastewater. The degradation efficiency of the 30% CNO/g-CN nanocomposite was 99.6%, 98.5%, 99%, and 92.8% for RhB, MB, MO, and the photo- reduction of Cr (VI), while that of bare g-CN was only 71.70%, 53.3%,19.29% and 22.24%, and that of bare CNO was 49.50%, 28.80%, 8% and 33.33% for the same pollutants, respectively under visible light over a period of 150 min. So, the 30% CNO/g-CN binary nanocomposite exhibited excellent photocatalytic degradation of organic dyes and Cr (VI) reduction, by decreasing the bandgap as compared to bare CNO and g-CN. Based on electrochemical experiments, it was confirmed that electrons and holes are involved in the degrading of different pollutants. Radical trapping experiments showed that $\bullet O_2 -$ and h^+ play a dominant role in the photocatalytic degradation process. The enhanced photocatalytic activity is mainly due to heterojunction formation between g-C_3N_4 and $CuNb_2O_6$, accelerating the

separation efficiency of photo- induced electron-hole pairs. The photocatalytic efficiency of the nano- composite was highly dependent on the effectiveness of charge separation and electron transfer. The bare g-C_3N_4 itself did not possess the high redox ability required to produce OH• radicals but when it was connected with $CuNb_2O_6$, the formation of ºOH radicals occurred through a series of reactions involving $•O_2^-$ [71].

Karpuraranjith et al., fabricated highly efficient g-C_3N_4@TiO_2/MoS_2 nano-architectures by solvothermal approach. The g-C_3N_4@TiO_2/MoS_2 nanohybrids exhibited improved MB dye degradation performance (97.5%) under visible light irradiant. The kinetic rate constant value of nanohybrids was obtained in $3.18 * 10^{-2}$ min^{-1}, which is higher than g-CN@TiO_2 ($1.20 * 10^{-2}$ /min). The results concluded that MoS_2 nanobox embedded on g-C_3N_4@ TiO_2 nano-architectures could greatly promote their environmental remediation and possibly used for industrial practical applications [72].

Lu et al., prepared Bi_2WO_6 nanosheets decorated TiO_2 nanotube arrays (BWO/TNTAs) to degrade pollutants under visible light irradiation. The photocatalytic degradation performance of TC and RhB with Bi_2WO_6 decorated TNTAs were found to be higher than that of pristine TNTAs. Especially, 0.2 BWO/TNTAs displayed the optimal photocatalytic degradation of TC with an efficiency of 92.2% in 180 min and RhB with an efficiency of 97.9% in 120 min under visible light. This catalyst possessed good recyclability and stability for five cycles. The introduction of Bi_2WO_6 extended visible light absorption and inhibited the charge recombination, which was conducive to improving the photocatalytic performance. Furthermore, •OH as the photocatalytic dominant species directly attacked the TC molecules. The possible decomposition pathway mechanism was proposed. This work demonstrated recyclable TiO_2-based nanotube arrays for the removal of organic pollutants with potential in large-scale water treatment [73].

Kenfoud et al., synthesized $BaFe_2O_4$ spinel by the sol-gel route. The XRD analysis confirmed the formation of a BFO orthorhombic phase with nano crystallites (~ 33 nm). FTIR and XPS were also performed to characterize the catalyst. The morphology was investigated using SEM analysis. The optical properties showed its potential for photocatalytic applications. A bandgap of 2.10 eV allows the conversion of more than half of the solar radiation. Photoluminescence (PL) demonstrated the potential to improve BFO by adding ZnO nanoparticles to separate and prevent electron-hole recombination and this is reflected in the augmentation of the photoactivity. The charge carrier dynamics were elucidated by using the Electrochemical Impedance Spectroscopy, which confirmed the semiconducting behavior of BFO. The electrochemical characterization showed promising outcomes in the generation of hydrogen

under visible light. The photocatalytic activity of the spinel BFO was tested for the RhB dye and enhanced by ZnO. RhB was effectively oxidized and removed on the hetero junction (BFO/ZnO) with an efficiency much more than BFO alone under visible light, showing the synergy effect. After 180 min, 93% degradation efficiency was achieved under optimal conditions: at pH ~6.12 and 26^{o}C. The removal kinetic of RhB was found to obey a first order model with a half photocatalytic life of 49 min. The scavenger tests illustrated that both $^{\bullet}O_2^-$ and $^{\bullet}OH$ were the main reactive species dominant in the photodegradation of RhB dye. As per the results, BFO/ZnO heterojunction could be a promising alternative for applications in water treatment and energy supply for hydrogen production due to its interesting opto-electrochemical properties [74].

Iqbal et al., fabricated $LaNiO_3$ with gadolinium and iron doped NPs and investigated the effects of doping on catalytic and antimicrobial activities. The structural analysis of as-synthesized material annealed at 950°C depicted the single-phase distorted rhombohedral geometry with effective doping of Gd and Fe metal ions on the octahedral and tetrahedral sites of $LaNiO_3$. The decline in the PL intensity on doping revealed that the doped materials possessed more electronic states to stabilize the charge carrier species which inhibited electron-hole recombination. Energy band gap was found to decrease on Gd and Fe doping. The photocatalytic activity of as-fabricated $LaNiO_3$ with Gd and Fe doped NPs were examined by degrading RhB under sunlight. It was found that the doped photocatalyst material had a faster rate of degradation (89.3%) of RhB dye as compared with the undoped material. The doping also affected the antimicrobial properties, tested against bacterial and fungal strains in comparison to ampicillin and ciprofloxacin drugs. In view of the efficient photocatalytic and promising antimicrobial activity, the Gd and Fe doped nanoparticles could be employed as active antimicrobial agent as well as photocatalyst for dye removal in effluents under visible light irradiation [75].

Pan et al., prepared a series of g-C_3N_4/MnO_2/Pt photocatalysts having photocatalytic activity for H_2 evolution by modifying MnO_2 and Pt nanoparticles on the surface of g-C_3N_4. Compared with the single cocatalyst constructed on g-C_3N_4, the design of dual cocatalyst significantly improved the photocatalytic performance of H_2 evolution. For MnO_2 to Pt ratio of 1:1, the H_2 production of 12.5 g-C_3N_4/ MnO_2/Pt was as high as 17.1 mmol /g/ h. g-C_3N_4/ MnO_2/Pt can not only provide abundant double active sites but also produce synergistic effect and improve carrier separation efficiency as compared with pure g-C_3N_4,. Further, g-C_3N_4/MnO_2/Pt had excellent degradation performance. In the presence of light irradiation and PMS, the removal rates of phenol, sulfadiazine, bisphenol A, Rhodamine B and methyl orange for 12.5-g-C_3N_4/

MnO_2/Pt were 57, 68, 97, 99, and 100%, respectively. The novel g-C_3N_4/M MnO_2/Pt catalyst was expected to become a practical and efficient catalyst of visible light and a candidate for high performance photocatalyst of H_2 evolution and pollutants remediation [76].

Srinivasan alias Arunsankar et al investigated C–ZnO/V_2O_5 nanocomposite for decomposition of organic compound under visible light irradiation. The XRD results exhibited the formation of heterojunction nanocomposites by the presence of diffraction peaks of both V_2O_5 and ZnO. The presence of V_2O_5 in the composite acted as a sensitizer to absorb the visible light. It was found that enhancement of the light absorption and charge separation ability of ZnO can be achieved through nanocomposite. Photocatalytic degradation experiments were performed over the MB dye under visible light irradiation. The nanocomposite 50 wt% V_2O_5 loaded ZnO (CZV3) had superior photocatalytic degradation activity for MB dye compared with other samples. The enhanced photocatalytic activity of the photocatalyst CZV3 could be due to its lower PL intensity, which indicated the suppression of electron–hole recombination compared to that of other photocatalysts. V_2O_5 had significant role of in improving the catalytic performance of CZV3 by the charge segregation through the interfacial contact of C–ZnO. The doping of cationic element (carbon) and the formation of heterostructure composites with (V_2O_5) played a critical role in overcoming the limitations of bare ZnO [77].

Chauhan et al. successfully decorated V_2O_5 nanowires with rGO sheets and used for photodegradation of RhB dyes. The addition of rGO sheet with V_2O_5 nanowires enhanced the visible light absorption and reduced the band gap of the photocatalyst from 3 eV to 2.86 eV. V_2O_5-rGO nanocomposite was found to degrade the RhB dye entirely in 50 min under solar radiation. The existence of rGO is attributed to the increase in photon energy absorbing capacity, reduction in recombination losses, therefore raising the electron & hole participation in the photocatalytic activity. This fast dye degradation capacity of V_2O_5-rGO nanocomposite is partially supported by the dye adsorption property of the rGO nanosheet. At pH 9, fastest removal of RhB was found. This study suggested utilization of V_2O_5-rGO nanocomposite in the dye degradation in textile effluent in controlled pH conditions, which mainly comprise of alkaline dyes such as textile wastewater. The photocatalyst was found to be reusable for 6 no. of cycles[78].

Bashir et al. synthesized Sodium doped-V_2O_5 nanorods for visible light photocatalytic degradation of RhB dye. The pure V_2O_5 and Na-doped V_2O_5 photocatalysts were synthesized by one-step hydrothermal method. The Na-doped V_2O_5 nanorods were synthesized in three

different concentrations and studied in comparision to pure V_2O_5. All the doped and un-doped photocatalysts were characterized. The photocatalytic performance of these synthesized photocatalysts were studied on RhB dye under visible light irradiation. The photodegradation efficiency was found to have improved in all the samples. $Na.V_2O_5$ (5 wt%) exhibited the maximum degradation performance of 88.9% for RhB dye in 100 min. The rate constant value (0.01619 min^{-1}) of the $Na.V_2O_5$ (5 wt%) photocatalyst was found to be higher than that of other photocatalysts. Hence, the $Na.V_2O_5$ (5 wt%) nanorods sample is considered to be the best photocatalyst having highest degradation.[79]

Hou et al. prepared a ternary Bi_2O_3–CuO–$CuBi_2O_4$ hybrid photocatalysts with the nanosheet microstructure using one-pot solvothermal method, and the Cu/Bi concentration ratio was altered to adjust the morphology, optical absorption, photoelectric and photocatalytic performances. The Bi_2O_3–CuO (5%) photocatalyst had highly outstanding photocatalytic activity toward RhB/MB degradation under no solar and visible light irradiation. Radical scavenging experiment showed $^{\bullet}O_2^-$ and •OH radicals are the active species for the dye degradation. A double Z-scheme heterojunction construction at the Bi_2O_3- –CuO–$CuBi_2O_4$ surface was proposed to explain the photocatalytic performance. Further, the Bi_2O_3–CuO (5%) photoelectrode exhibited outstanding photoelectric conversion, the high photocurrent (2.16 μA/cm^2)/photovoltage (−0.068 V) were produced under visible light irradiation, and the strong visible light absorption and low interface resistance were the main reasons for the photoelectrochemical performance.[80]

Fang et al. synthesized 15CuIn heterojunctions by growing $CuBi_2O_4$ nanosheets on the outer surface of flower like In_2O_3 to realize outstanding decolorization of MB under visible light. The heterojunctions contributed to the separation and transfer of photogenerated charge carriers, providing a large surface area for adsorption of MB, exposing an abundance of active sites for surface catalysis, and extending the visible light response range. The photodegradation efficiency for MB by 15CuIn can reach 97% within 80 min. Further, the 15CuIn material retained good catalytic properties for the decolorization of MB after four cycles. The radical scavenging experiment revealed the main active species of 15CuIn were $\cdot O_2^-$ and ·OH. In addition, free radical trapping and theoretical analysis verify the rationality of the Z-scheme mechanism. This study presented a novel and fully solid-state Z-scheme heterojunction photocatalyst and provided design ideas for constructing efficient 2D/3D In_2O_3-based photocatalysts.[81]

Jenifer & Sriram synthesized pristine and Zn doped V_2O_5 nanoparticles by a sol–gel method. The prepared samples were orthorhombic in nature and had bandgap in the visible region ranging from 2.14 eV to 2.19 eV. Other characteristics like M−S analysis, VB-XPS, TRPL and EIS analysis were performed to analyze the band formation and charge carrier lifetime. From the characteristics, it was found that the sample V5 exhibited profound charge carrier lifetime with decrease in charge transfer resistance. The photocatalytic tests were performed on MB, MG and MV. More than 90 % of efficiencies were observed for all the samples within the range of 105 to 120 min. However, 90 % efficiency was achieved for MG in 30 min. The reusability test of the prepared samples was performed for three times and the results show the consistency of the samples. To understand the mechanism underlying the photocatalytic activity, scavengers test was performed and the results showed the major role of hydroxide radicals in the degradation of the dyes tested. From the obtained results, it is evident that the photocatalytic activity of V_2O_5 nanoparticles can be improved by appropriate doping.[82]
The results of above literatures are summarized in Table 2.3.

Table 2.3: Performance of various photocatalyst for degradation of Dyes in various conditions

Photocatalyst	**Photocatalyst Type**	**Target Pollutant**	**Light**	**Operating Condition**	**Degradation Efficiency & Time**	**References**
g-C_3N_4/ Bi_2WO_6	Composite	MO	500 W Xe lamp with 420 nm cutoff filter	MO: 10 mg/L, Photocatalyst: 3 g/L	99.9% in 3 hr.	[57]
$BiVO_4$–graphene	Doped	MB	500W xenon lamp through UV cut-off filter	Dye:20 mg/L, Photocatalyst: 0.5 g/L	89% in 180min; 99% in 300 min	[58]
		MO			94% in 180 min;99%, 300 min	

Photocatalyst	Photocatalyst Type	Target Pollutant	Light	Operating Condition	Degradation Efficiency & Time	References
		RhB			95% in 180 min; 99%, 300 min	
Ag/AgBr/ZnO	Noble metal Deposited nanocomposite	RhB	300 W iodine tungsten lamp	RhB: 5 mg/L Photocatalyst: 1 g/L	100%, 3 hr	[41]
0.25Y/g-C_3N_4	Doped	RhB	500-W xenon lamp light irradiation with a 420 nm filter	RhB: 5mg/L Photocatalyst: 0.6 mg/L	100%, 110 min	[59]
WO_3/g-C_3N_4	Z-Scheme	MB	300 W Xenon lamp with a UV cut off filter	MB: 50 mg/L Photocatalyst: 0.5 g/L	95%, 90 min	[60]
N-ZnONCBs	Doped	MB	250 W high pressure visible lamp	MB: 15 ppm Photocatalyst: 0.25 g/L pH: 9-11	96.22%, 50 Min	[31]
$CuFe_2O_4/TiO_2$	Doped	MB	500 W Xenon	MB: 20 ppm	83.7%, 3 hr	[61]

Photocatalyst	Photocatalyst Type	Target Pollutant	Light	Operating Condition	Degradation Efficiency & Time	References
			lamp	Photocatalyst: 0.5 g/L pH: 2.2		
Bi_2O_3 /g-C_3N_4	Nitrogen vacancy – Z scheme	MB	18 W LED (14mW/cm2)	MB: 10 mg/L Photocatalyst: 2 g/L	92%, 60 min	[62]
CdS/SnO_2	Heterojunction	MB	Sunlight (1200-1450 W/m2)	MB: 2 x 10-5 (M) Photocatalyst: 1 g/L	95%, 180 min	[63]
Reduced (r)GO-ZnO	Nanocomposite	MB	Visible light (250C) (370-900 nm)	MB: 5 x 10-4 (M) Photocatalyst: 0.25 g/L	98%, 90 min	[64]
WO_3-ZnO@rGO	Nanocomposite	MB	200 W tungsten filament Lamp with ultraviolet cut-off filter (.>420 nm)	MB: 5 ppm Photocatalyst: 0.2 g/L	94%, 90 min	[65]

Photocatalyst	**Photocatalyst Type**	**Target Pollutant**	**Light**	**Operating Condition**	**Degradation Efficiency & Time**	**References**
Fe_3O_4@ZnO-RGO	Nanocomposite	MB	Visible light (250C) (200-800 nm)	MB: 20 mg/L Photocatalyst: 0.25g/L	100%, 180 Min	[66]
BiOBr/TzDa COF (BTDC)	Direct Z-scheme	RhB	Visible (300 W Xe Lamp with a filter to cut-off UV light)	RhB: 10 ppm Photocatalyst: 0.2 g/L pH: 2.1-8.1	97%, 20 min	[67]
Ag@CdSe /Zeoilte	Noble metal Deposited Nanocomposite	MB	Visible (300 W tungsten-halogen lamp with UV cutoff filter	MB: 7.17 mg/L, Photocatalyst: 0.6 g/L pH: 8	89.98%, 40 min	[40]
TiO_2/g-C_3N_4	Hetero atom doping Z-scheme	MO	300 W xenon lamp with a 420 nm cut-off filter	MO: 20 mg/L Photocatalyst: 0.4 g/L	99.8%, 90 Min	[32]
V_2O_5/P-g-C_3N_4	Z-scheme	MO	500 W Xenon lamp with a 420 nm filter	MO: 10 mg/L	90%, 105 min	[68]

Photocatalyst	Photocatalyst Type	Target Pollutant	Light	Operating Condition	Degradation Efficiency & Time	References
				Photocatalyst: 1 g/L		
AgI/ZnO/WO_3	Double Z-scheme	MB	100 W tungsten lamp	MB: 7 mg/L Photocatalyst: 3.8 g/L pH: 4	85.2%, 48.5 Min	[69]
C_3N_4 - NS/CD/FeOCl	Z-Scheme Nanocomposite	RhB	50 W LED lamp	RhB: 1 x 10^{-5} M Photocatalyst: 0.4 g/L	100%, 60 min	[70]
Bi_2WO_6/CuS	Heterojunction	RhB	500 W Xe Lamp with a filter to cut-off UV light	RhB: 10 mg/L Photocatalyst: 1 g/L pH: 2-6	98.8%, 105 Min	[44]
Bi_2MoO_6-Ag_2MoO_4	Nanocomposite	MB	500 W tungsten lamp & UV–visible absorption Spectrophotometer (ƛ max = 660 nm).	MB: 10 mg/L Photocatalyst: 3 mg	91.8%, 216 min	[53]
	Nanocomposite	MB	500 W Xenon lamp with a	MB: 10 ppm,	98.5%, 150 min	[71]

Photocatalyst	**Photocatalyst Type**	**Target Pollutant**	**Light**	**Operating Condition**	**Degradation Efficiency & Time**	**References**
30% $CuNb_2O_6$/g-C_3N_4			visible filter of 470-780 nm	Photocatalyst: 0.2g/L		
		MO		MO: 10 ppm, Photocatalyst: 0.2g/L	99%, 15 min	
		RhB		RhB: 10 ppm, Photocatalyst: 0.2g/L	99.6%, 150 min	
g-C_3N_4@TiO_2/MoS_2		MB	Vis-light irradiated by a 350 W Xe lamp	MB: 10 ppm Photocatalyst: 0.6 g/L	97.5%, 60 min	[72]
0.2 Bi_2WO_6/TiO_2 NTAS	Nanocomposite	RhB	visible-light irradiation (λ>420 nm)	RhB: 2.5 mg/L	97.9%, 120 min	[73]
$BaFe_2O_4$/ZnO	Nanocomposite	RhB	Visible light irradiation by tungsten lamp (200 W)	RhB: 15 mg/L, Photocatalyst: 1 g/L, pH ~ 6.12	93% in 3 hr	[74]
Gd and Fe doped $LaNiO_3$	Doped	RhB	Sunlight	Dye: 50 mg/L, Photocatalyst: 5 mg	89.3%, 90 min	[75]

Photocatalyst	**Photocatalyst Type**	**Target Pollutant**	**Light**	**Operating Condition**	**Degradation Efficiency & Time**	**References**
12.5-g-C_3N_4/MnO_2/Pt + PMS	Modified with dual Co-catalyst	RhB	300 W Xe lamp (AM 1.5 air quality filter)	Dye: 20 mg/L, Photocatalyst: 0.5 g/L PMS	99%, 30 min	[76]
		MO			100%, 30 min	
C–ZnO/V_2O_5	Nanocomposite	MB	500 W halogen lamp	Dye: 10 mg/L Photocatalyst: 0.75 g/L	96.74 % in 75 min	[77]
V_2O_5-rGO	Nanocomposite	RhB	Sunlight	Dye: 20 mg/L Photocatalyst: 1 g/L	97% in 50 min	[78]
Na.V_2O_5	Doped	RhB	200 W bulb having tungsten filament	Dye: 5 mg/L Photocatalyst: 0.1 g/L	88.9 % in 100 min.	[79]
Bi_2O_3–$CuBi_2O_4$–CuO	Double Z-scheme	RhB	Visible light	Photocatalyst: 1 g/L	93.15% in 160 min	[80]
		MB			100 in 70 min	
Bi2O4/In2O3	Z-scheme	MB	Simulated light source with a cutoff	Dye: 10 mg/L	97 % in 80 min.	[81]

Photocatalyst	**Photocatalyst Type**	**Target Pollutant**	**Light**	**Operating Condition**	**Degradation Efficiency & Time**	**References**
			filter (λ > 400 nm)	Photocatalyst: 1 g/L		
Zn doped V_2O_5	Doped	MB	Xe arc lamp (300 W)	Appropriate amount of photocatalyst in 60 mL dye solution	99 % in 90 min	[82]
		MV			99 % in 105 min	
		MG			96 % in 30 min	

2.7 Kinetics of Photocatalytic degradation of dye

The literature so far studied it is observed that the photocatalytic degradation of dye follows the pseudo first order kinetics equation. Let us consider the initial concentration (t=0) of dye is "C_0" after time "t" the concentration changes to C_t which can be determined by equation 2.9.

$$ln\frac{C_0}{C_t} = kt \quad (2.9)$$

Where "k" is the reaction rate constant of the dye degradation. Here, slope will be calculated from pseudo first order kinetic graph. The removal percentage of dye can be calculated by equation 2.10.

$$R(\%) = \frac{C_0 - C_t}{C_t} \times 100 \quad (2.10)$$

Where "R" is the percentage removed at the time "t".

2.8 Factors controlling Photocatalytic degradation of dyes

Performance of photocatalytic degradation of dyes depends on several parameters such as pH, light intensity, the ratio of catalyst to dye, and the presence of interfering compounds (e.g., bromides, anti-scaling agents, bicarbonates, phosphates, and radical scavengers. The effects of these factors on the dye degradation performance as described by Anwer et al. are discussed below [83].

2.8.1 Effect of pH

The pH of wastewater containing dye determines the electrostatic interaction between catalyst surfaces, substrates, and radicals during the degradation process. Surface charge and aggregation of the catalysts are associated with wastewater pH.

2.8.2 Pollutant/photocatalyst adsorption

The adsorption of dyes on the photocatalyst surface is dependent on the electrostatic interactions and binding affinity between the dye molecule and the catalyst surface. Moderate adsorption of dye molecules on the photocatalyst surface is beneficial for degradation performance based on the synergy between adsorption and photocatalysis. The adsorption of dye molecules onto the catalyst surface is an essential step for effective degradation. Composite materials with good adsorption properties utilize this synergy principle for simultaneous adsorption and degradation of dye molecules. Although adsorption of dye on the surface is important for photocatalytic dye degradation, it may also be disadvantageous beyond a certain limit. A very high adsorption of dye molecules on the catalyst surface suppresses the number

of photons reaching surface-active sites. In addition, dye molecules may also act as sensitizers that can absorb electrons and scatter them in undesirable directions.

2.8.3 Effect of light intensity

Photocatalytic phenomena rely on the energy supplied by light quanta. Electron–hole pairs are generated in the CB and VB of a photocatalytic material when they receive photons with energy equal to or greater than the band gap of the material. The light intensity plays a critical role in photocatalytic dye removal.

2.8.4 Effect of photocatalyst loading

The mass of photocatalyst in a wastewater suspension has a significant effect on the reaction rate and total dye degradation capability.

2.8.5 Effect of dye loading

The interaction between a photocatalyst substrate and a dye molecule is related to the nature of the functional groups of the dye molecules as well as their abundance in the reactor. The optimal concentration of dye molecules for a photocatalytic reaction is highly dependent on the kind of dye. In general, as the initial dye pollutant concentration increases, the photocatalytic degradation efficiency decreases because more dye molecules compete for limited active sites. Increasing photocatalyst loading leads to increased turbidity. Furthermore, a high dye concentration makes the dye itself absorb more light than a photocatalyst, thereby deteriorating photocatalytic degradation performance.

In addition to the factors discussed above, the presence of inorganic metal ions in dye-contaminated solution can also affect the photocatalyst's performance. In this regard, depending upon the ionic nature of dye molecules, the metal ions may either accelerate or decelerate the dye degradation. Generally, metal ions are adsorbed on to the photocatalyst's surface to make the catalyst electro-neutral or slightly positively charge. As this effect reduces the electrostatic repulsion for anionic dyes, they can be adsorbed and degraded readily in the presence of metal ions. On the contrary, a retarding effect can also be observed for cationic dyes due to the decrease in attraction between positively charged dye molecules and neutral/ slightly positive catalyst surface.

2.9 Critical review of literature

Recently, water contamination by dye discharged from various industries (e.g., paper making, textile dyeing, cosmetics, paints, food processing, etc.) has attracted significant attention due to hazards to public health and ecosystems. Treatment processes like coagulation, flocculation, reverse osmosis etc. are unable to effectively remove the dyes due to their complex structure and produces a huge amount of sludge. As a result, the Advance oxidation process is used to remove dyes from wastewater efficiently. Photocatalytic degradation of dye is one of the emerging processes for removing dye in a highly efficient manner without producing sludge. Researches are done in using Sunlight as a source of energy for the photocatalytic degradation. Sunlight has only 4% UV light and the majority is visible light (56%). If UV light source is used in industries, it will make the system highly energy intensive. Hence visible light assisted photocatalysis is a better alternative than UV light assisted photocatalysis. From the above literature survey, it is seen that many researchers are working on it in and they have synthesized different types of material by using different methods and tested for removal efficiency of synthetic dyes. Among the different types of photocatalyst nanocomposite heterojunction is the mostly used photocatalyst in recent days which improves the removal efficiency in a significant way as compared to pristine photocatalyst materials. Some researchers have used noble-metals like platinum, silver etc. as raw materials for photocatalyst synthesis to increase the photocatalytic efficiencies by reducing the electron-hole recombination rates, but these are costly materials.

Nano sized metal oxides have been proven as good photocatalytic materials with larger surface area and efficient recyclability, some reported catalysts are Bi_2WO_6, α-Fe_2O_3, CuO and Cu_2O, ZnO, TiO2, Cr_2O_3, WO_3 and V_2O_5 nano particles. V_2O_5 is a transition metal oxide (TMO) semiconductor material used in photocatalytic degradation applications due to its narrow band gap, non-toxicity, good chemical, electrical and photo stability, low cost, ease in synthesis, large abundancy and high visible light absorption. Compared to the various other photocatalysts often used (ZnO (3.3 eV) or TiO_2 (3.2 eV)), the spectral range of absorption in V_2O_5 is broader due to its small bandgap (2.2–2.5 eV, λ = 564 nm). This allows the photocatalytic activity to be extended to much of the visible spectrum, up to 560 nm. Still, there is scope for improvement by lowering the bandgap and delaying the recombination of electrons and holes to increase the photocatalytic activity in the entire visible range.

The copper bismuth oxide ($CuBi_2O_4$), on the other hand, is a ternary metal oxide with p-type semiconductor characteristics which presents interesting and attractive photocatalytic properties, including an absorption window throughout the entire visible spectrum (<800 nm)

due to its band gap of ~1.8 eV. However, as with other single photocatalysts, $CuBi_2O_4$ exhibits some disadvantages including mismatched band positions, excessive recombination of photogenerated charge carriers and insufficient quantum yields.

The band edges of V_2O_5 (E_{CB}= 0.47 eV, E_{VB}= 2.73 eV) matches well with $CuBi_2O_4$ (E_{CB}=−0.74 eV, E_{VB}=0.92 eV) to form a Z-scheme photocatalytic system. If that can be accomplished, the photoexcited electron in conduction band (CB) of $CuBi_2O_4$ will show the strong reducibility and the photoexcited hole on valence band (VB) of V_2O_5 will exhibit the strong oxidizability, respectively. Further, it will lead to delaying of recombination of electrons and holes resulting in increase in the photocatalytic activity in the entire visible range. The composite of $CuBi_2O_4$ and V_2O_5 could be an efficient visible light photocatalyst for degradation of organic pollutants. However, no such study was found in literature.

Chapter 3

OBJECTIVE AND SCOPE OF WORK

3.1 Objective

The objective of the present work is to synthesize a $CuBi_2O_4$ and V_2O_5 composite suitable for efficient photocatalytic degradation of dyes under visible-light irradiation.

3.2 Scope of Work

- Synthesis of $CuBi_2O_4$ and V_2O_5 composite in various ratios.
- Characterization of as-synthesized material.
- Perform batch-mode studies for the photocatalytic degradation of dyes.
- Optimization of important process parameters such as catalyst dose, pH, concentration of the dye, etc.
- Determine the reaction kinetics and photocatalysis mechanism of the synthesized material.
- Determine the COD removal efficiency by the photocatalyst towards dye removal.

Chapter 4

MATERIALS AND METHODS

4.1Materials

Copper Nitrate ($Cu(NO_3)_2.3H_2O$), Bismuth Nitrate ($Bi(NO_3)_3.5H_2O$), Potassium Nitrate (KNO_3), Sodium Nitrite ($NaNO_2$) were procured from Merck. Ammonium Metavandate (NH_4VO_3) was acquired from Loba Chemie. The dyes Rhodamine B, Methylene Blue and Methyl Orange were procured from Loba Chemie, Qualigens and Ranbaxy respectively. Double distilled water was used throughout this study.

4.2 Photocatalyst synthesis

4.2.1 Synthesis of V_2O_5

V_2O_5 was synthesized by hydrothermal method following a recent report [77] with minor variations. A 0.2 M ammonium metavanadate (NH_4VO_3) precursor solution was prepared in distilled water by adding the required amount of diluted sulfuric acid (H_2SO_4) to adjust the pH to 2. The mixture solution was magnetically stirred for 30 min, and the hydrothermal synthesis was done for 3 h at 150 °C. The product obtained was washed with distilled water and dried at 65°C followed by annealing at 600 °C for 1 h. The schematic diagram of preparation of V_2O_5 is shown in Fig. 4.1

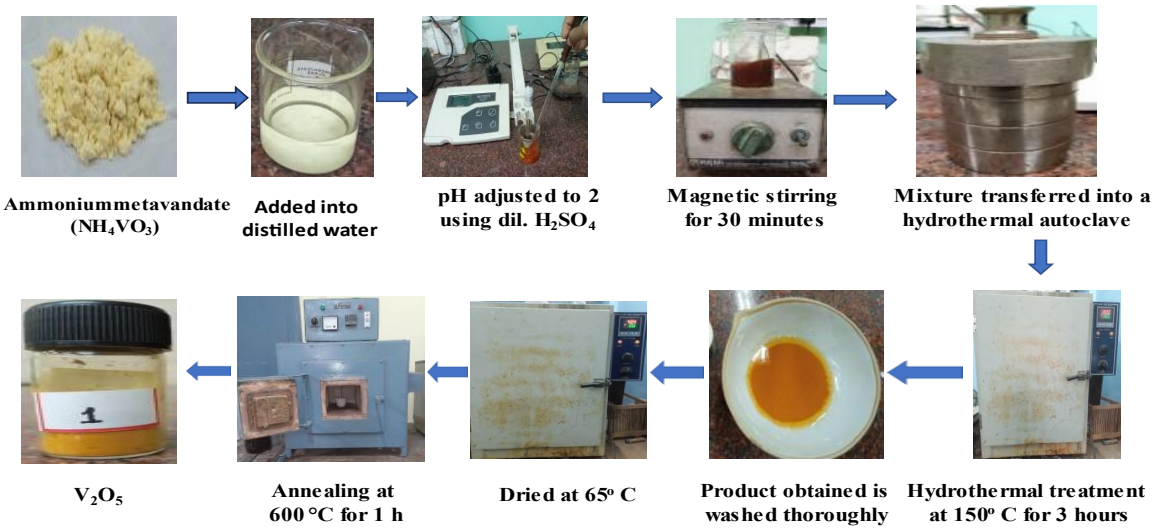

Fig 4.1: Schematic diagram of preparation of V_2O_5

4.2.2 Synthesis of $CuBi_2O_4$

The molten salt method was used to synthesize $CuBi_2O_4$. 4 g of $Bi(NO_3)_3.5H_2O$ and 1 g of $Cu(NO_3)_2.3H_2O$ were used for maintaining the molar ratio of Bi:Cu = 2:1 as the precursors and grinded for about 15 mins in an agate mortar. Subsequently, KNO_3 and $NaNO_2$ salt mixtures with a weight ratio of KNO_3: $NaNO_2$ = 1:1 were taken as the co-solvent. Molten salt each of 20 g is taken and a total weight of raw material and molten salt of 45 g is made so that the weight ratio of raw material to molten salt becomes 1:8. After being grinded for over 30 mins, the mixture including raw materials and molten salts was placed in an alumina crucible and then calcined at a temperature of 400°C in a muffle furnace for duration of 8 h. After the molten salt reaction, the as-obtained catalyst was washed repeatedly with distilled water to remove the molten salts and the resultant product was dried at 65°C. The product obtained was grinded and stored for further experiments. The schematic diagram of preparation of $CuBi_2O_4$ is shown in Fig. 4.2.

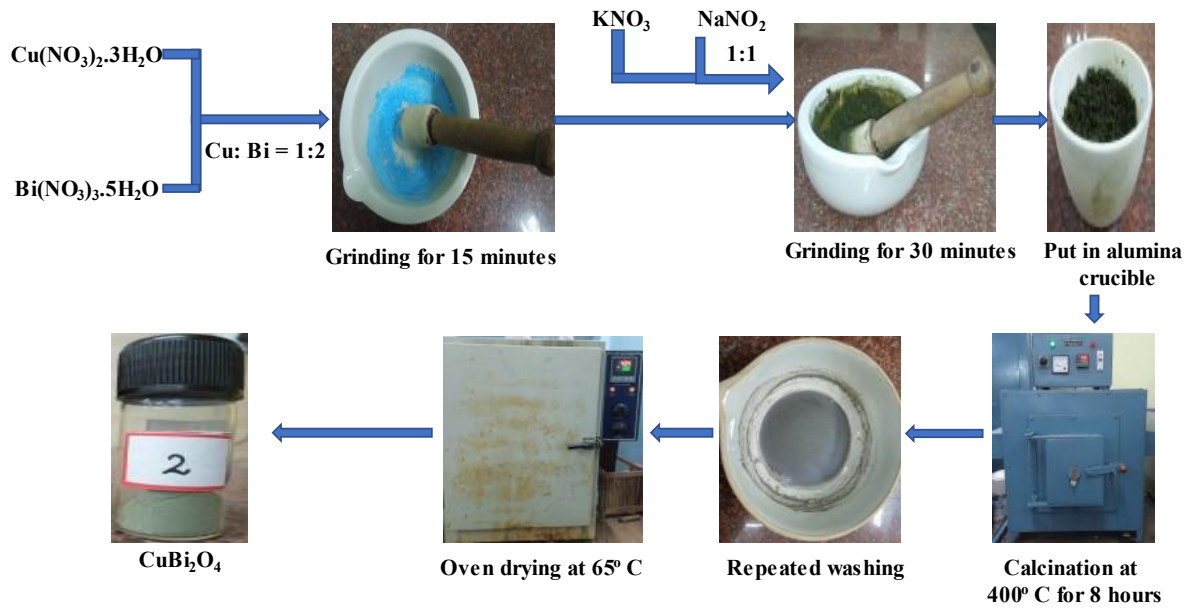

Fig. 4.2: Schematic diagram of preparation of $CuBi_2O_4$

4.2.3 Synthesis of nanocomposite materials

The hydrothermal method was used to make the nanocomposite. Initially, 100 mg of V_2O_5 and a specific amount of $CuBi_2O_4$ were added to 40 mL deionized water, followed by 2 hours of magnetic stirring. The resulting mixtures were then transferred to a 50 mL Teflon-lined

hydrothermal autoclave and treated for 20 hours at 150°C. The products were thoroughly washed and dried at 65°C. The final product was obtained on grinding. The schematic diagram of preparation of $CuBi_2O_4/V_2O_5$ nanocomposite is shown in Fig. 4.3. Different nanocomposites were synthesized by taking the amount of $CuBi_2O_4$ as 10, 20, 30 and 40 mg and the nanocomposites so obtained were designated as 10-$CuBi_2O_4/V_2O_5$, 20-$CuBi_2O_4/V_2O_5$, 30-$CuBi_2O_4/V_2O_5$ and 40-$CuBi_2O_4/V_2O_5$ respectively. In a similar way 10-$V_2O_5/CuBi_2O_4$, 20-$V_2O_5/CuBi_2O_4$, 30-$V_2O_5/CuBi_2O_4$ and 40-$V_2O_5/CuBi_2O_4$ were also synthesized by taking 100 mg $CuBi_2O_4$ and 10, 20, 30 and 40 mg of V_2O_5.

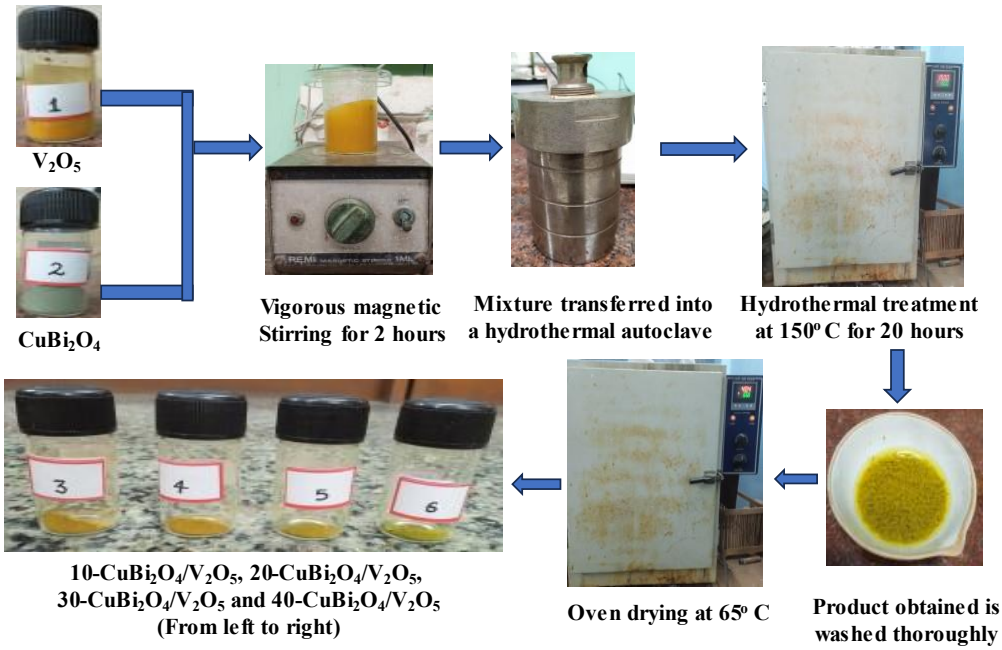

Fig. 4.3: Schematic diagram of preparation of nanocomposites

4.3 Characterization

The X-ray diffraction pattern was recorded using Rigaku X-ray diffractometer equipped with Cu Kα (λ = 1.54 Å) radiation source operating at 40 kV with 30 mA. The X-ray diffraction patterns were recorded for 16 min with the continual scanning rate of 5° min^{-1} in the wide range of 2θ = 5–85°. A Hitachi SU3800 scanning electron microscope used to observe the surface morphology of the photocatalyst. The optical properties were determined by UV–visible spectrophotometer in the wavelength range λ=200–1200 nm.

4.4 Photocatalytic experiment

The photocatalytic efficiency of the as synthesized photocatalysts were evaluated by degrading dyes under visible LED light (20 W, Philips, India) irradiation. Typically, 10 mL of dye was

taken in a 100 mL glass beaker and a certain amount of photocatalyst was added to it. A magnetic stirrer was used to stir the mixture at 500 rpm for 30 minutes in the dark to achieve adsorption–desorption equilibrium between the catalyst and the dye. It was followed by photocatalytic reaction under visible light irradiation. The supernatant was filtered using a 0.22 mm syringe filter after the photocatalytic reaction was completed, and the dye concentration was determined using a UV/Visible spectrophotometer (Perkin Elmer-Lambda 25). The dye removal efficiency was determined using the equation 4.1.

$$R\% = \frac{C_0 - C_t}{C_0} \times 100 \qquad (4.1)$$

Where "R" is the percentage removed of dye at the time "t". C_0 and Ct are the initial and final dye concentrations respectively.

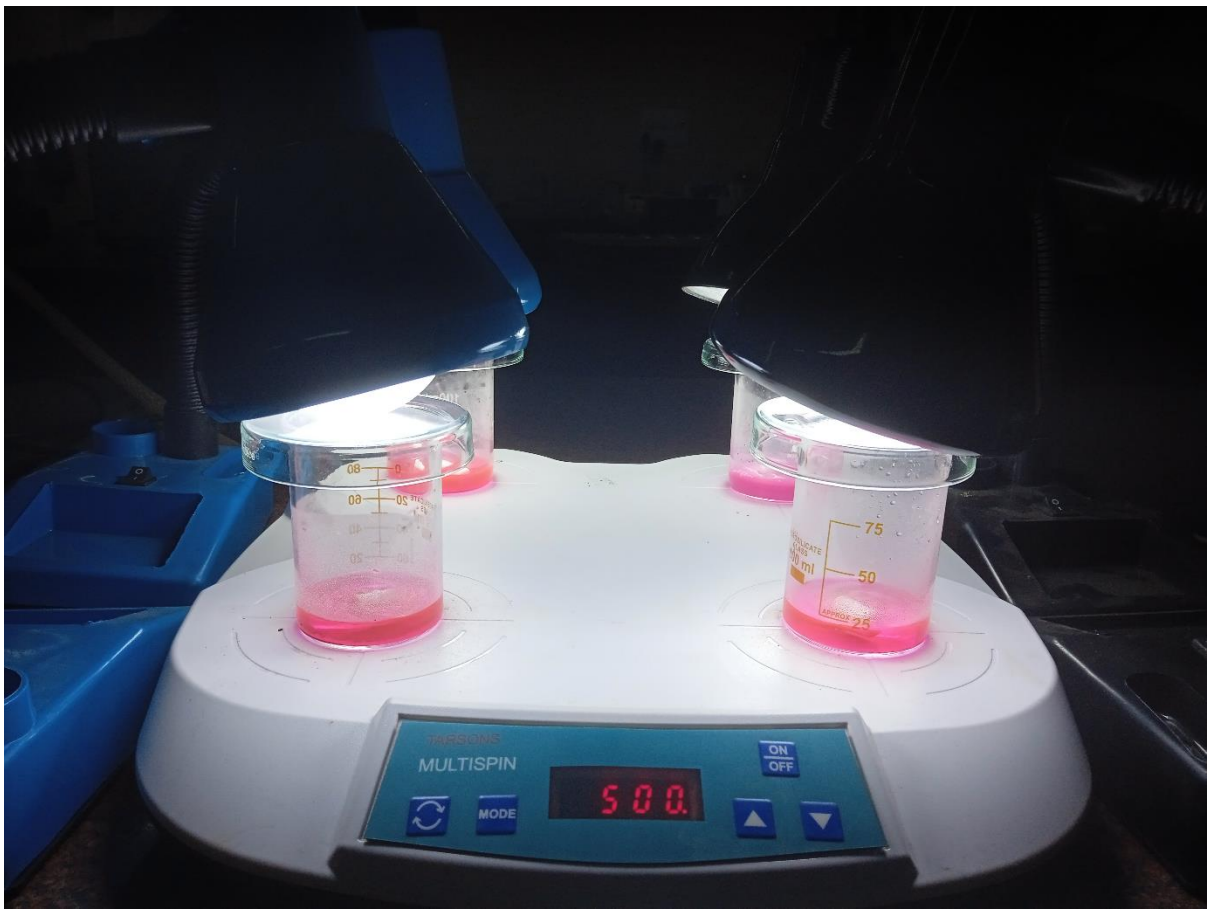

Fig. 4.4: Batch experiment for removal of dye using as synthesized photocatalyst under 20W LED light irradiation

Fig. 4.5: UV-Visible spectrophotometer

4.5 Radical Scavenging Experiment

To scavenge superoxide radicals ($^{\bullet}O_2^-$), holes (h^+) and, hydroxyl radicals ($OH^{\bullet}$), radical scavengers such as p-Benzoquinone (p-BQ), Ethylenediamine tetra acetic acid disodium salt (EDTA-2Na), and Isopropanol (IPA) were used. The concentrations of BQ, EDTA-2Na, and IPA were 0.25 mM, 1 mM, and 1 mM, respectively. Photocatalytic degradation experiments were carried out in the same way as before, but with the addition of scavengers to the suspensions beforehand.

4.6 Chemical oxygen demand (COD) determination experiment

COD determination experiment was done by closed reflux colourimetric method. In this method firstly the standard absorbance curve of COD was determined using the spectrophotometer. For determination of standard COD curve the standard solutions of KHP (Potassium Hydrogen Phthalate) of different concentrations, $K_2Cr_2O_7$ and Ag_2SO_4 were prepared. 2.5 ml of KHP solution of different concentration along with 1.5 ml of $K_2Cr_2O_7$ solution and 3.5 ml of Ag_2SO_4 solution is mixed and heated at 150°C for 2 h in closed reflux. Then the sample is cooled and measured the absorbance value with respect to the different concentration of KHP. Following the creation of the standard curve, the dye sample is used in place of KHP, and the respective COD is determined.

COD removal efficiency can be determined by the equation 4.2.

$$E\ (\%) = \frac{COD_i - COD_f}{COD_i} \times 100 \qquad (4.2)$$

Here “E” is the COD removal efficiency. COD_i & COD_f is the initial COD of RhB solution before application of photocatalyst and final COD of dye solution after photocatalysis experiment.

Fig. 4.6: Closed reflux setup for determination of COD

Chapter 5

RESULTS AND DISCUSSION

5.1 Characterization of Materials

5.1.1 XRD

The X-ray diffraction pattern of 30-$CuBi_2O_4/V_2O_5$ is shown in Fig. 5.1. The diffraction peaks observed at 2θ= 21.725, 25.653, 26.114, 33.339, 34.315, 41.299, 47.342, 48.864, 51.244, 55.662, 58.087, 59.049, 62.104, 64.705, 68.352, 68.904 and 71.867 are correspond to (101), (201), (110), (111), (310), (002), (600), (012), (020), (021), (221), (412), (710), (800), (122), (303) and (702) crystal planes respectively matches with V_2O_5. The diffraction peaks observed at 2θ= 37.477 and 78.309 are correspond to (202) and (622) crystal planes respectively matches with $CuBi_2O_4$.

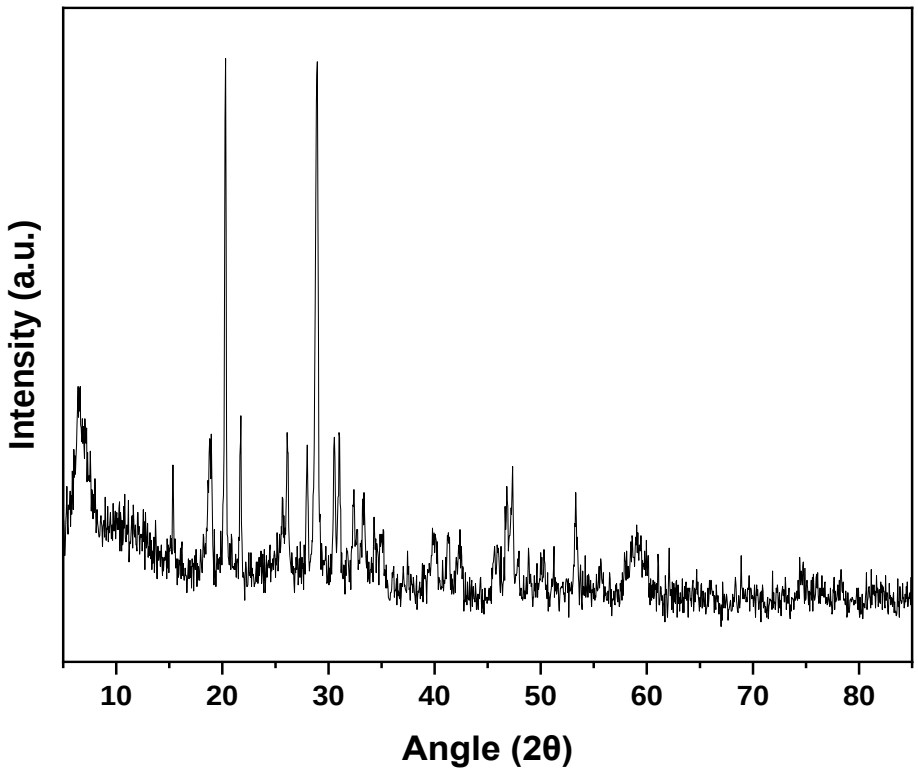

Fig. 5.1 X-ray diffraction pattern of 30-$CuBi_2O_4/V_2O_5$

5.1.2 SEM

SEM images of 30-$CuBi_2O_4/V_2O_5$ is illustrated in Fig. 5.2. It signifies nanosheet-like structures. Generally, nanosheet structures attracted more consideration because of their greater surface area, more active sites on the surface, outstanding electron movement, and a good platform for separating charge carriers [84].

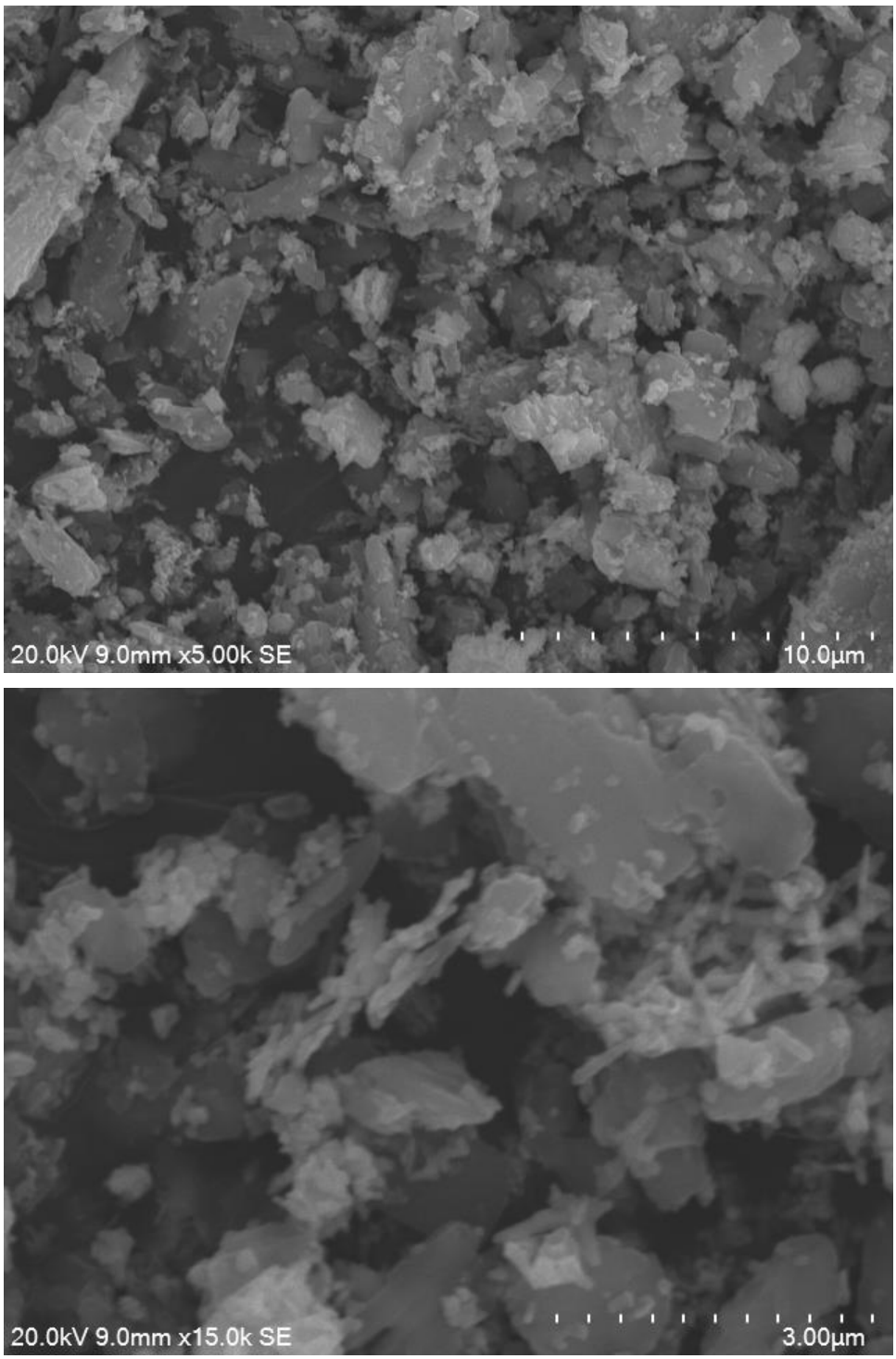

Fig. 5.2: SEM image of 30-$CuBi_2O_4/V_2O_5$

5.1.3 UV-Vis DRS

The optical property of the synthesized photocatalysts were probed by UV–Vis diffuse reflectance spectra (UV–vis DRS) and the spectrum is shown in Fig.5.3. According to the DRS, the absorption edges of $V_2O_5$and $CuBi_2O_4$ are found to be around 577 nm and 1008 nm respectively while that of the composite materials 10-$CuBi_2O_4$,20-$CuBi_2O_4$, 30-$CuBi_2O_4$, and 40-$CuBi_2O_4$ are found to be 600 nm, 596nm, 661 nm and 630 nm respectively. Kubelka-Munk theory is utilized to evaluate the energy bandgap of the synthesized material shown in the plot of $[h\nu F(R\infty)]^2$ vs hν in Fig. 5.4 . The bandgap energies (Eg) of $V_2O_5$and $CuBi_2O_4$ are evaluated to be 2.29 eV and 1.64 eV respectively.

Thus, the increased absorption in the visible light range, and thus the increased photocatalytic efficiency of 30-$CuBi_2O_4/V_2O_5$, could be attributed to the synergistic effect of $CuBi_2O_4$and V_2O_5. The band edge positions of the valence band (VB) and conduction band (CB) potentials of V_2O_5 and $CuBi_2O_4$ were calculated applying the equations reported in the literature [85]:

$$E_{VB} = X - E^e + 0.5\, E_g \qquad (5.1)$$

$$E_{CB} = E_{VB} - E_g \qquad (5.2)$$

where X is the electronegativity of semiconductors, which is the geometric average of the absolute electronegativity of the constituent atoms. The value of X for V_2O_5 and $CuBi_2O_4$ are 6.10 eV and 4.59 eV respectively.

E^e is the energy of free electrons on the hydrogen scale (4.5 eV) and

E_g is the band gap energy the semiconductors.

Through the calculation, the VB and CB potentials of V_2O_5 are around 2.745 eV and 0.455 eV respectively while that of $CuBi_2O_4$ are 0.91 eV and -0.73 eV respectively. The result is summarized in table 5.1.

Table 5.1: Absolute electronegativity, estimated band gap, energy levels of calculated conduction band edge, and valence band for V_2O_5, $CuBi_2O_4$

Sample	**X (eV)**	**E_g (eV)**	**E_{VB} (eV)**	**E_{CB} (eV)**
V_2O_5	6.1	2.29	2.745	0.455
$CuBi_2O_4$	4.59	1.64	0.91	-0.73

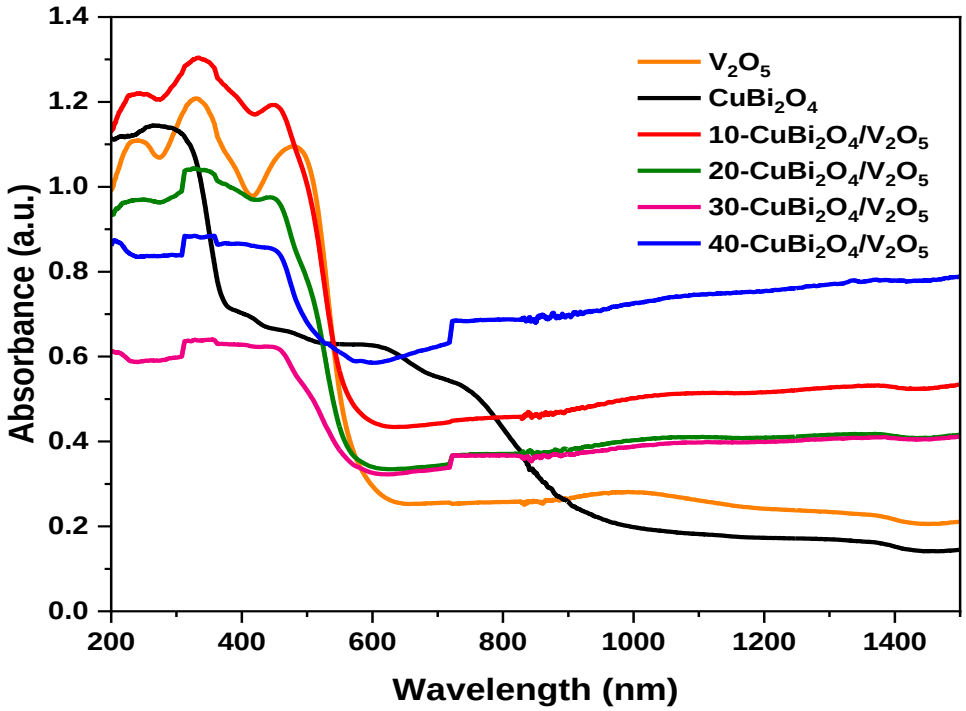

Fig. 5.3: UV–visible absorbance spectra

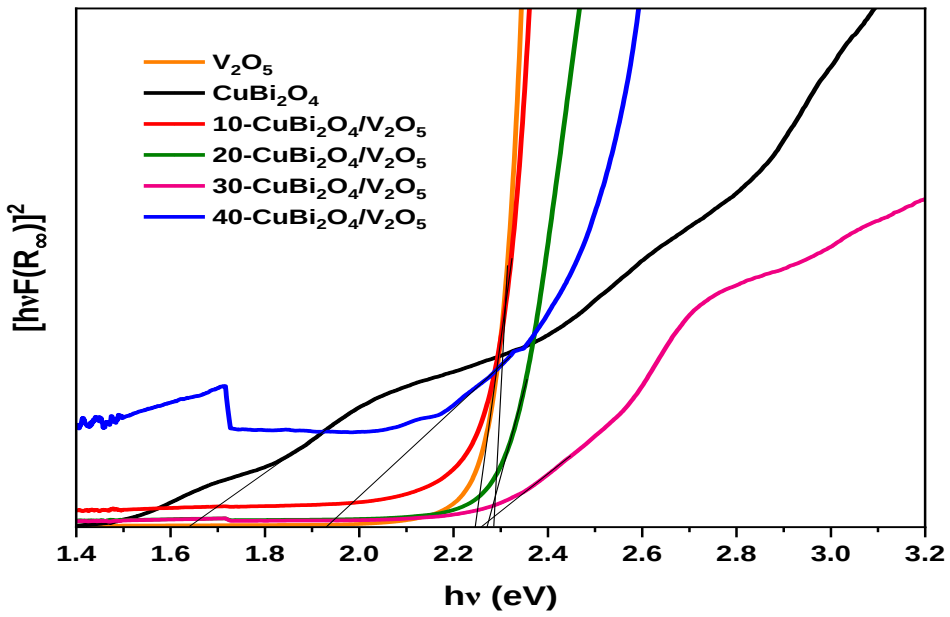

Fig. 5.4: Tauc plot of V_2O_5, $CuBi_2O_4$, and $CuBi_2O_4/V_2O_5$ nanocomposites

5.2 PHOTOCATALYTIC ACTIVITY

The photocatalytic activity of all the catalysts for initial RhB concentration 20 mg/L and photocatalyst dose 1 g/L under 20 W LED illumination is depicted in Fig. 5.5. During the photolysis experiment in the absence of catalysts, no significant change in the RhB concentration was observed over time, indicating that RhB is relatively stable under visible light irradiation. V_2O_5 and $CuBi_2O_4$ degraded only 20.7% and 7% of RhB within 60 min, respectively. However, significant enhancement of photocatalytic efficiency for the degradation of RhB was observed by the nanocomposites of the two. The nanocomposites 10-$CuBi_2O_4/V_2O_5$, 20-$CuBi_2O_4/V_2O_5$, 30-$CuBi_2O_4/V_2O_5$ and 40-$CuBi_2O_4/V_2O_5$ have removal efficiency of 55.9 %, 56.1 %, 73.8% and 60.8% respectively towards RhB in 60 min. The degradation efficiency with 10-$V_2O_5/CuBi_2O_4$, 20-$V_2O_5/CuBi_2O_4$, 30-$V_2O_5/CuBi_2O_4$ and 40-$V_2O_5/CuBi_2O_4$ nanocomposites was very less in 60 minutes.

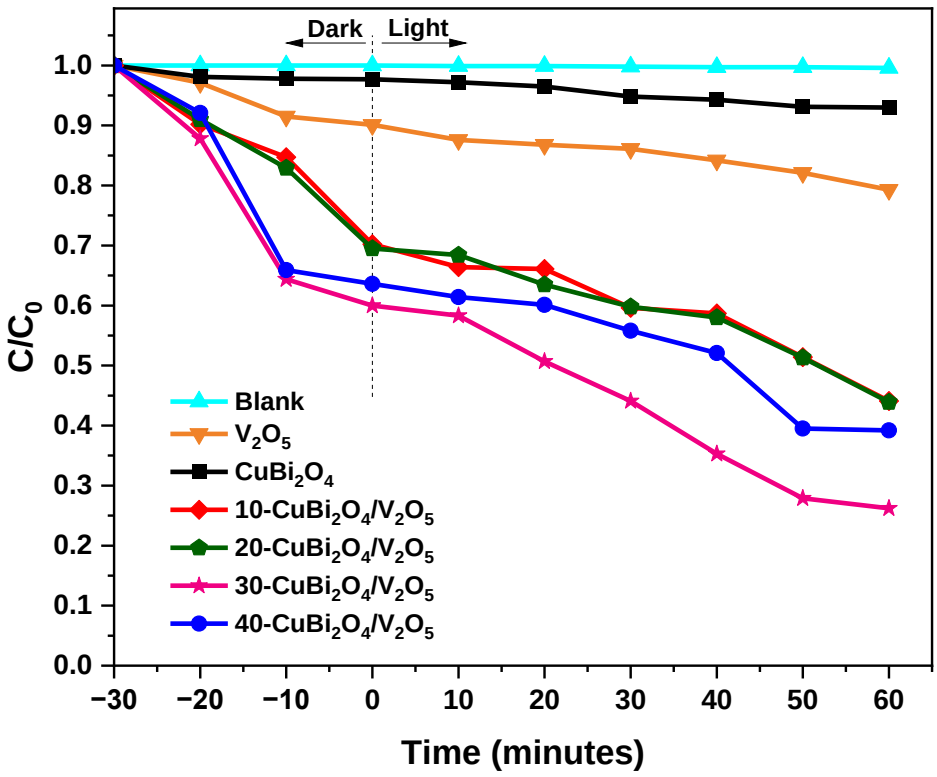

Fig. 5.5: Photocatalytic degradation efficiency with respect to time using different photocatalysts

The degradation kinetics plots between ln(C/C$_0$) and time revealed that first order degradation kinetics is being followed. Moreover, the apparent rate coefficients of the photocatalysts were determined from Fig. 5.6. The apparent rate constants of RhB degradation using V_2O_5 and $CuBi_2O_4$ sample was observed as 0.00194 and 0.00092 $min^{-1,}$ respectively. Thus, it can be comprehended that the 30-$CuBi_2O_4/V_2O_5$ possesses 8 times degradation efficiency than that of V_2O_5 and 16.8 times degradation efficiency of $CuBi_2O_4$.

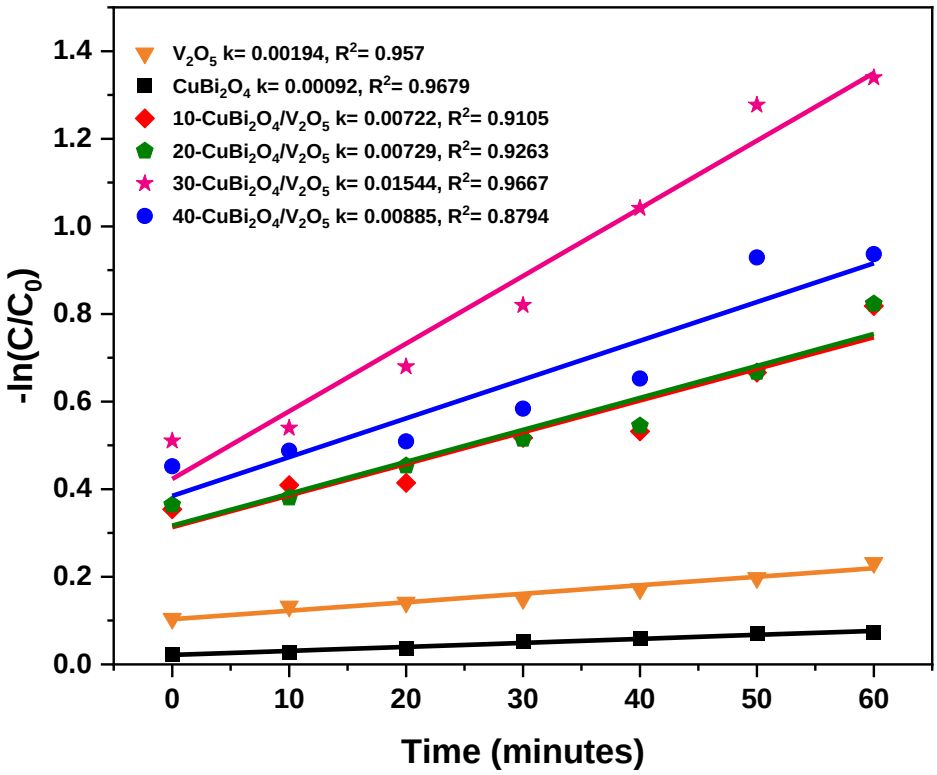

Fig. 5.6: Pseudo first order reaction kinetics of different nanocomposites towards RhB (20 mg/L) degradation.

5.3 Effect of various factors on Photocatalytic degradation

5.3.1 Effect of Photocatalyst Load

To evaluate the impact of the photocatalyst dosage on the degradation process, experimentations were conducted using various catalyst dosage (0.5–1.5 g/L) using 30-$CuBi_2O_4/V_2O_5$ on RhB (20mg/L). The observations are described in Fig. 5.7. For 0.5 g/L dose, only 28.5 percent of removal was achieved in 60 minutes which is very less in contrast to 73.8

% for 1 g/L dosage. This phenomenon could be ascribed to the increased quantity of active reaction spots with the increase in dosage. On further increasing dosage to 1.5 g/L, only minor increase in removal efficiency of 76.3% was obtained. Therefore, the optimum dosage of 1 g/L was used for further experiments.

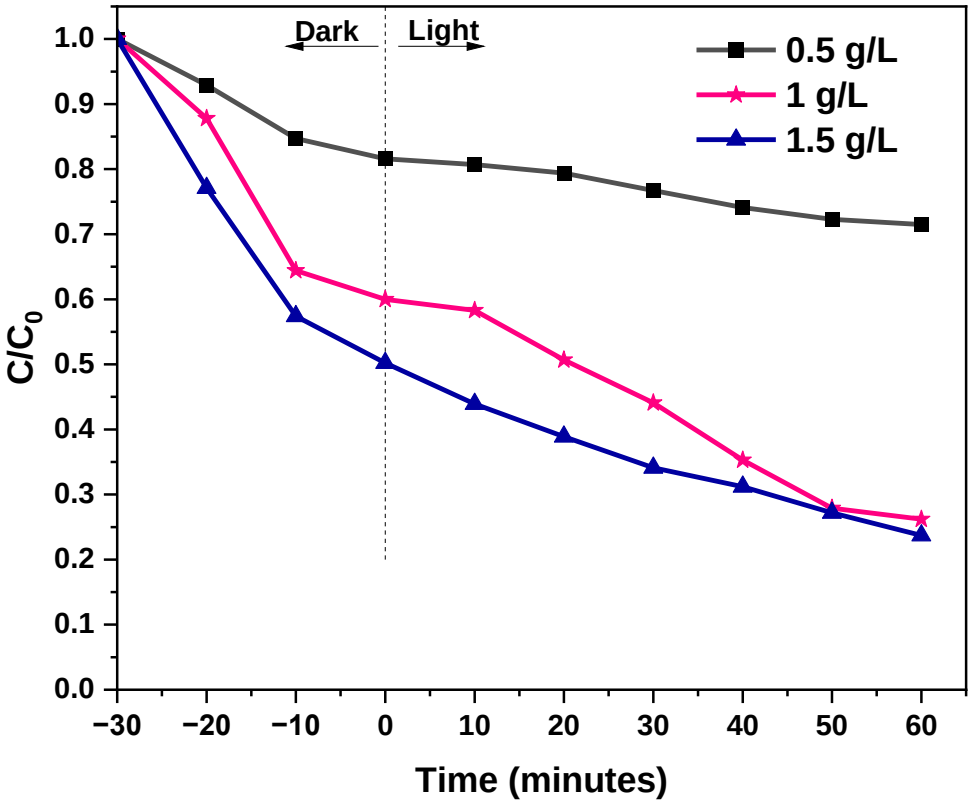

Fig. 5.7: Dose variation of 30-$CuBi_2O_4/V_2O_5$ nanocomposite for determining the optimum dose towards RhB (20 mg/L) degradation

5.3.2 Effect of initial pH

The effects of pH on degradation of dyes are particularly deleterious, as the hydrogen ion concentration directly plays a major role in the formation of the hydroxyl free radicals. Therefore, the impact of pH on the degradation process was assessed by fluctuating the solution pH in the stretch of 2–12, keeping all other parameters constant (i.e., initial RhB concentration: 20 mg/L; dosage: 1 g/L and time: 60 min). The outcomes are demonstrated in Fig.5.8. The

solution pH was regulated with 0.1 N NaOH or 0.1 N HCl. Adsorption efficiency increased at lower pH and vice-versa. Adsorption efficiency at pH 2, 3, 7, 10 and 12 was found to be 93.8 %., 62.9 %, 40%, 6.8 % and 2.1 % respectively. With increase in pH, degradation decreased. Degradation after 60 minutes of photocatalysis at pH 2, 3, 7, 10 and 12 was found to be 97.6 %, 81.4%, 73.8%, 27.7% and 14.3% respectively.

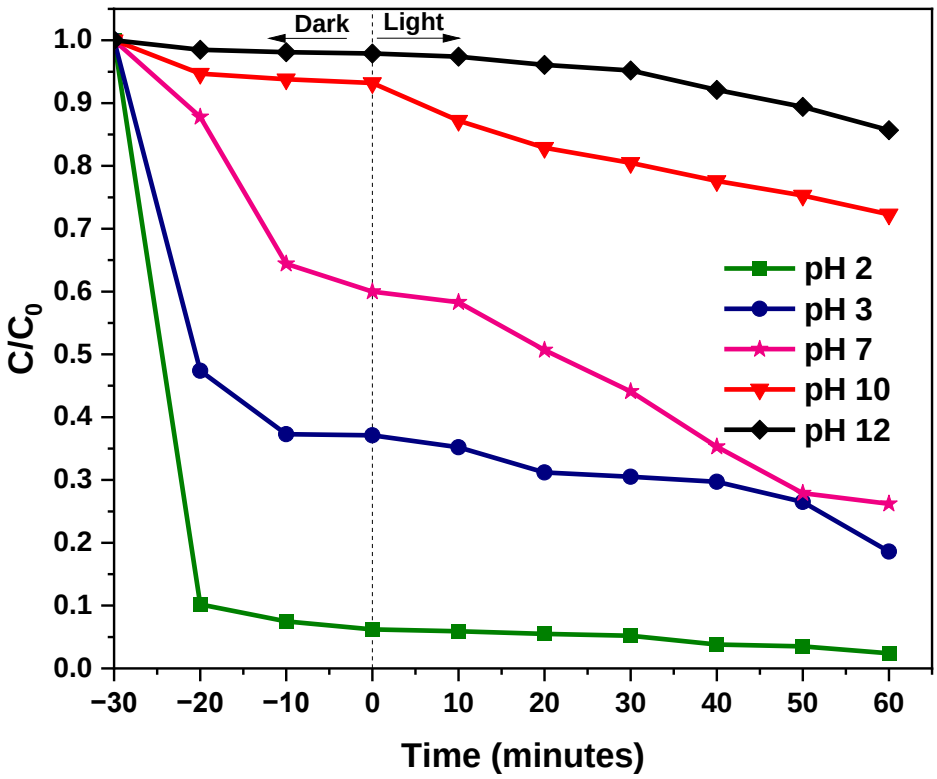

Fig. 5.8: Effect of pH on degradation efficiency using 30-$CuBi_2O_4/V_2O_5$ nanocomposite towards RhB (20 mg/L)

5.3.3 Effect of Initial Dye Concentration

For practical application, it is essential to investigate the impact of initial RhB concentration on the degradation process. Therefore, tests were performed in the initial RhB concentrations range of 10−40 mg/L, keeping all other parameters unchanged. The outcomes are presented in Fig.5.9. After 60 minutes of photocatalysis the degradation efficiency for initial dye concentrations 10 mg/L, 20 mg/L, 30 mg/L and 40 mg/L was found to be 79.7 %, 73.8 %, 57 % and 54.9 % respectively which shows a decreasing trend. The active surface on the catalyst available for the reaction is critical for the degradation to take place. As the dye concentration

is increased keeping the catalyst amount constant, fewer active sites become available for the reaction. Furthermore high concentration makes the dye itself absorb more light than a photocatalyst, thereby deteriorating photocatalytic degradation performance.

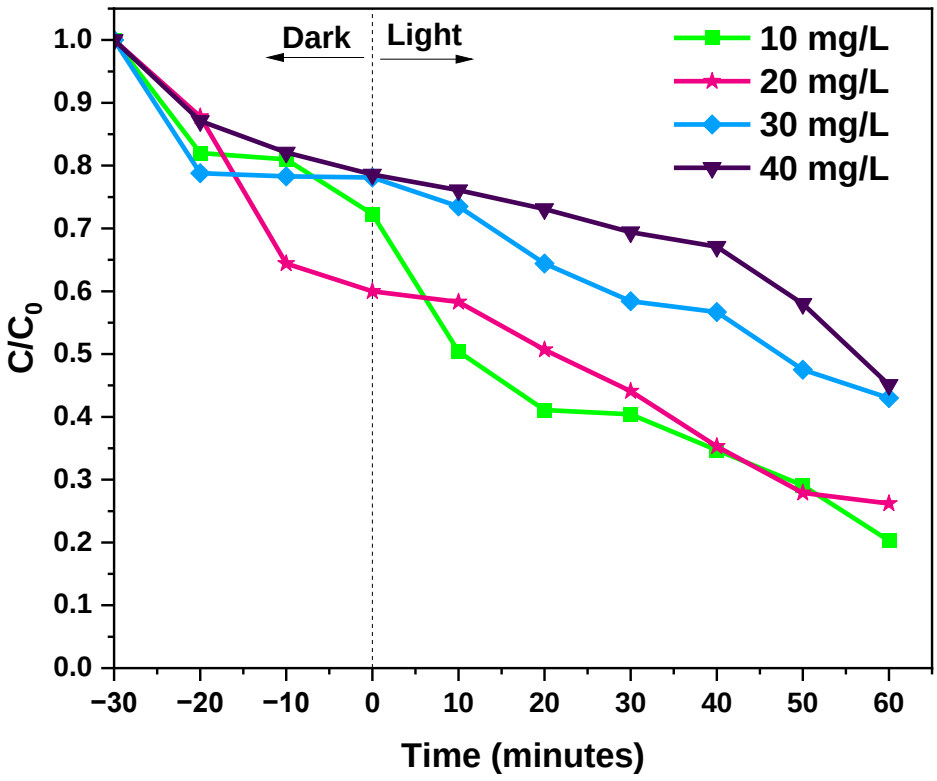

Fig. 5.9: Effect initial RhB concentration on degradation efficiency using 30-$CuBi_2O_4/V_2O_5$ nanocomposite dosage 1 g/L

5.3.4 Effect of Stirring speed

The physical state (solid, liquid, or gas) of a catalyst and dye substrate also influence the photocatalytic degradation rate of dye. When reactants are in the same phase in aqueous solution, thermal motion brings them into contact. However, when they are in different phases, the reaction is limited to the interface between the reactants. Reaction can only occur at the area of contact. Vigorous shaking and stirring may be needed to bring the reaction to completion. This means that the more finely divided a solid or liquid reactant, the greater its surface area per unit volume and the more contact it makes with the other reactant, thus faster would be the reaction. The effect of stirring on photocatalytic degradation rate of RhB dye in

aqueous solution was studied by changing stirring speed to 1000 rpm from 500 rpm at initial RhB concentrations 10 mg/L and 20 mg/Land the result is plotted in Fig.5.10 and Fig. 5.11. The increase in stirring speed increases the solution flow along the photocatalysts surfaces and also increases homogeneity of photocatalysts in the solution.

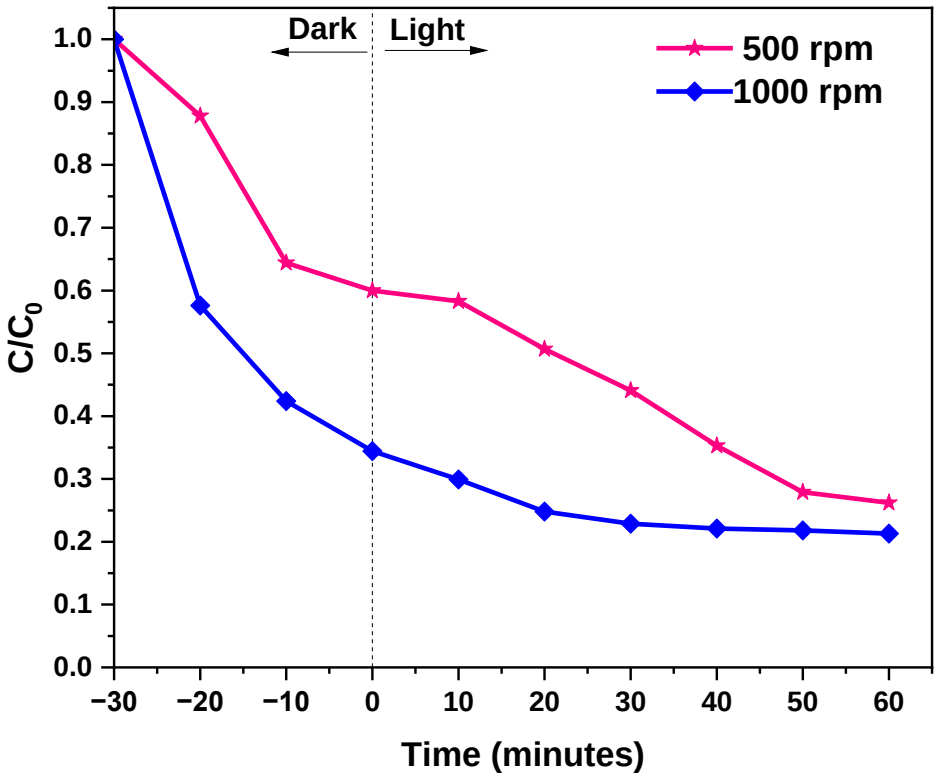

Fig. 5.10: Effect of magnetic stirring speed on degradation efficiency of RhB (20mg/L) using 30-$CuBi_2O_4/V_2O_5$, dosage 1g/L

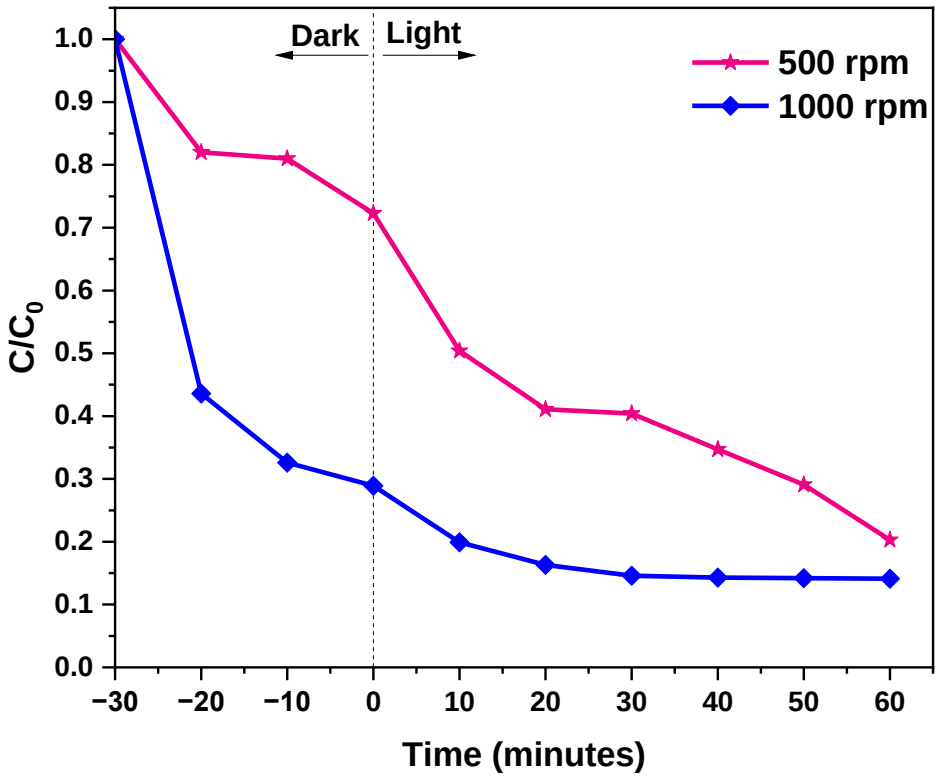

Fig. 5.11: Effect of magnetic stirring speed on degradation efficiency of RhB(10 mg/L) using 30-$CuBi_2O_4/V_2O_5$, dosage 1g/L

5.4 Photocatalysis of different dyes

The efficacy of 30-$CuBi_2O_4/V_2O_5$ on Methylene Blue and Methyl Orange has also been tested for initial dye concentration 20 mg/L, dosage 1g/L. and a comparison is shown in Fig.5.12. It removed only 52 % of MO in 60 minutes of photocatalysis. It has very high adsorption capacity for MB dye with 95 % adsorption capacity in 30 minutes in dark.

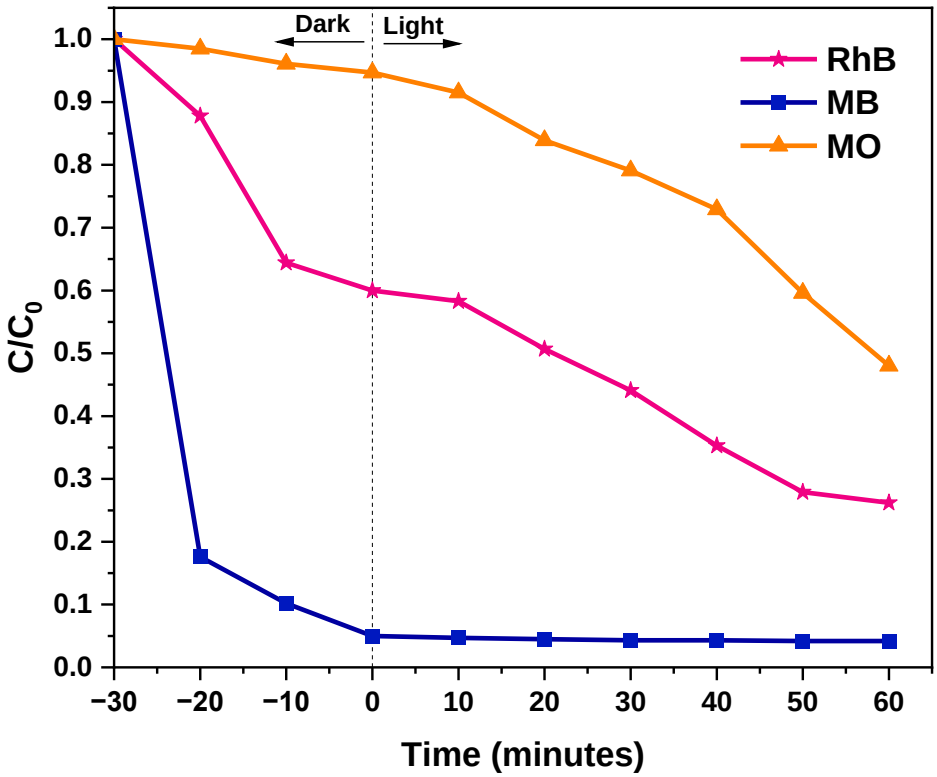

Fig. 5.12: Photocatalysis of different dyes (C_0: 20mg/L) using 30-$CuBi_2O_4/V_2O_5$

5.5 Comparison of result with recent literature

A comparison of result obtained in this study with that in some recent literatures is given in Table 5.2.The 30-$CuBi_2O_4/V_2O_5$ is found good photocatalyst for degradation of dye under low power utility.

Table 5.2: Summary of some recent literatures on degradation of dyes

Photocatalyst	Photocatalyst doses (g/l)	Dye	Dye Concentration (mg/l)	Light Source	% Degradation, time	TON ($*10^{-5}$)	TOF ($*10^{-7}$)	TOF/Power ($*10^{-9}$)	Reference
AgI/ZnO/WO_3	3.8	MB	7	100 W tungsten filament lamp	85.2%, 48.5 min	0.491	1.012	1.012	[69]
$CuFe_2O_4/TiO_2$	0.5	MB	20	500 W Xenon lamp	83.7%, 180 min	**10.467**	5.815	1.163	[86]
Ag@CdSe / Zeoilte	0.6	MB	7.17	300 W tungsten halogen lamp	89.98%, 40 min	3.362	8.404	2.801	[40]
CuBi2O4/In2O3	1	MB	10	300 W xenon lamp	97 %, 80 min	3.033	3.791	1.264	[81]
$BaFe_2O_4$/ZnO	1	RhB	15	200 W tungsten lamp	93 %, 180 min	2.912	1.618	0.809	[74]
V_2O_5/P-g-C_3N_4	1	MO	10	500 W xenon lamp	90 %, 105 min	2.750	2.619	0.524	[68]
C-ZnO/V2O5	0.75	MB	10	500 W halogen lamp	96.74 % in 75 min	4.033	5.377	1.075	[77]`
Na. V_2O_5	0.1	RhB	5	200 W tungsten	88.9 % in 100 min	9.280	**9.280**	4.640	[79]
$CuBi_2O_4/V_2O_5$	1	RhB	20	20W LED bulb	73.8 %, 60 min	3.081	5.136	**25.678**	**This study**
		MB	20		95 %, (Adsorption)				
		MO	20		52 %, 60 min	3.177	5.295	**26.477**	

TON = Moles of pollutant degraded per unit mass of catalyst, (moles/g).

TOF = TON/time, (moles/g/min).

TOF/Power, mole/g/min/W

5.6 RADICAL SCAVENGING EXPERIMENT

To observe the primary reactive species causing dye degradation, radical scavenging study was carried out using 30-$CuBi_2O_4/V_2O_5$ dosage 1 g/L on RhB(C_0: 20 mg/L). The study results is depicted in Fig. 5.13. The radical scavengers EDTA-2Na, p-BQ and IPA decreased the removal percentage to 60%, 41.7% and 45.2% respectively which was 73.8% without any radical scavengers. Therefore, the reactive oxygen species contribute in the order ($^{\bullet}O_2^-$> $OH^{\bullet}$>h^+) to the degradation of RhB.

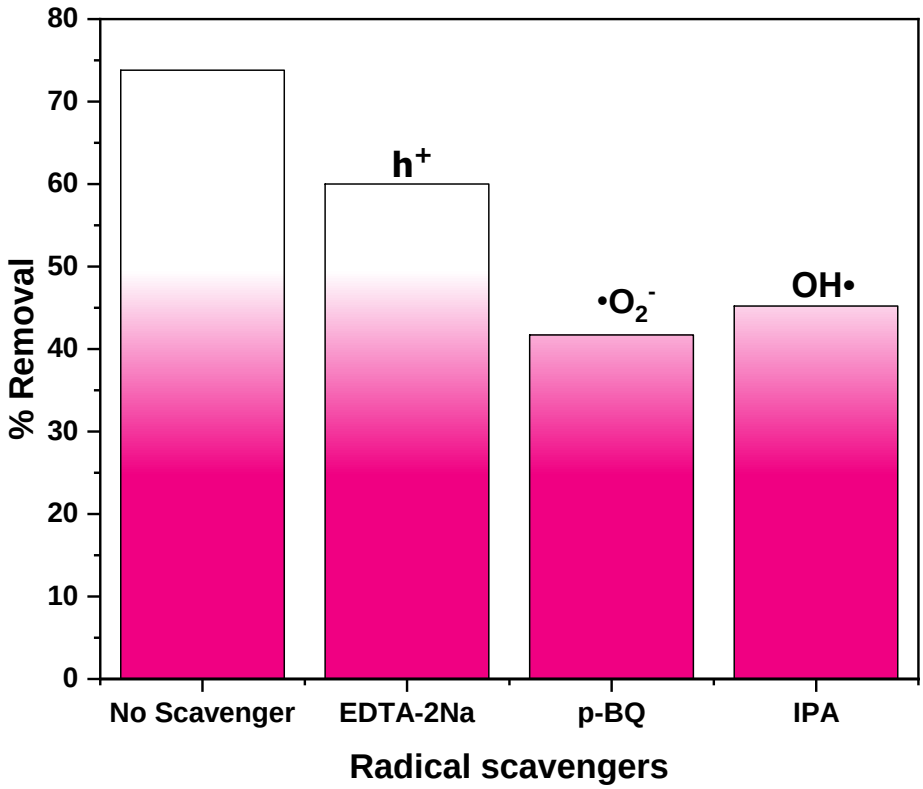

Fig. 5.13: Photocatalytic degradation efficiency of 30-$CuBi_2O_4/V_2O_5$ nanocomposite towards RhB (C_0: 20 mg/L) influenced by radical scavengers

5.7 PHOTOCATALYSIS MECHANISM

A tentatively probable mechanism for visible light photocatalytic decomposition efficiency of the heterojunction is proposed based on the band positions result (Fig. 5.14). Photo-induced charge carriers are produced by both the semiconductors of $CuBi_2O_4$ and V_2O_5 under visible light irradiation. When $CuBi_2O_4$ and V_2O_5 form a conventional electron–hole separation process, the electrons accumulated in the CB of $CuBi_2O_4$ tend to excite the CB of V_2O_5, because the CB position of $CuBi_2O_4$ is more negative than V_2O_5. Meanwhile, under simulated visible light, the holes in the VB of V_2O_5 will migrate to the VB of $CuBi_2O_4$, because the VB position of V_2O_5 is more positive than the $CuBi_2O_4$ sheet. The heterojunction then forms a type-II staggered band alignment, which aids in the separation and transfer of photo induced electrons and holes. However, because the photo induced electrons on the CB of V_2O_5 are less negative than the potential required for O_2 generation ($O_2/^{\bullet}O_2^-$ = -0.33 eV vs NHE), they are unable to convert O_2 into superoxide ($^{\bullet}O_2^-$) radical anion. Furthermore, the VB potential of 0.91 eV for $CuBi_2O_4$ is lower than the $H_2O/OH^{\bullet}$ redox potential (2.68 eV vs. NHE), indicating that the photo-induced holes accumulated on the VB of $CuBi_2O_4$ are unable to oxidize the adsorbed water molecules to form an $OH^{\bullet}$ radical. As a result, if the photogenerated electrons and holes in the $CuBi_2O_4/V_2O_5$ heterostructures are separated and transferred using the conventional hetero-junction process, the formation of $OH^{\bullet}$ and $^{\bullet}O_2^-$ ROS is not favourable, resulting in lower photo activity for pollutant degradation. As a result, the photo degradation activity of the $CuBi_2O_4/V_2O_5$ heterojunction was lower. Based on the foregoing discussion, it is suggested that the Z-scheme charge transfer system used by the $CuBi_2O_4/V_2O_5$ heterostructures be used instead of the conventional system to account for the heterostructures' improved photocatalytic performance (Fig. 5.15).The photo induced electrons in the V_2O_5conduction band migrate to the valence band of the $CuBi_2O_4$ in the direct Z-scheme charge transfer mechanism. The surrounding water molecules can be oxidized into $OH^{\bullet}$ radicals by the more positive VB potential of V_2O_5 (2.745eV) compared to the $H_2O/OH^{\bullet}$ potential. In addition, O_2 can be reduced to produce the reactive $^{\bullet}O_2^-$ radical anion due to the $CuBi_2O_4$ CB potential, which is more negative (-0.73 eV) than the $O_2/^{\bullet}O_2^-$ potential. When compared to isolated V_2O_5 photocatalysts, heterostructures may exhibit higher reduction/oxidation ability due to higher levels of $^{\bullet}O_2^-$and $OH^{\bullet}$ radical generation. This will enhance photocatalytic activity. As a result, the degradation of the pollutant is caused by $^{\bullet}O_2^-$ and $OH^{\bullet}$ radicals. This implies that, as shown in equations below. Several pollutants in the water matrices can be degraded by reactive $^{\bullet}O_2^-$ and $OH^{\bullet}$ radicals with high activity.

$$CuBi_2O_4 + V_2O_5 + h\nu \rightarrow CuBi_2O_4\ (e^-) + V_2O_5\ (h^+) \quad (5.1)$$

$$CuBi_2O_4\ (e^-) + O_2 \rightarrow {}^{\bullet}O_2^- \quad (5.2)$$

$$V_2O_5\ (h^+) + H_2O \rightarrow OH^{\bullet} + H+ \quad (5.3)$$

$$OH^{\bullet}, {}^{\bullet}O_2^- + \text{pollutant} \rightarrow CO_2 + H_2O + \text{by products} \quad (5.4)$$

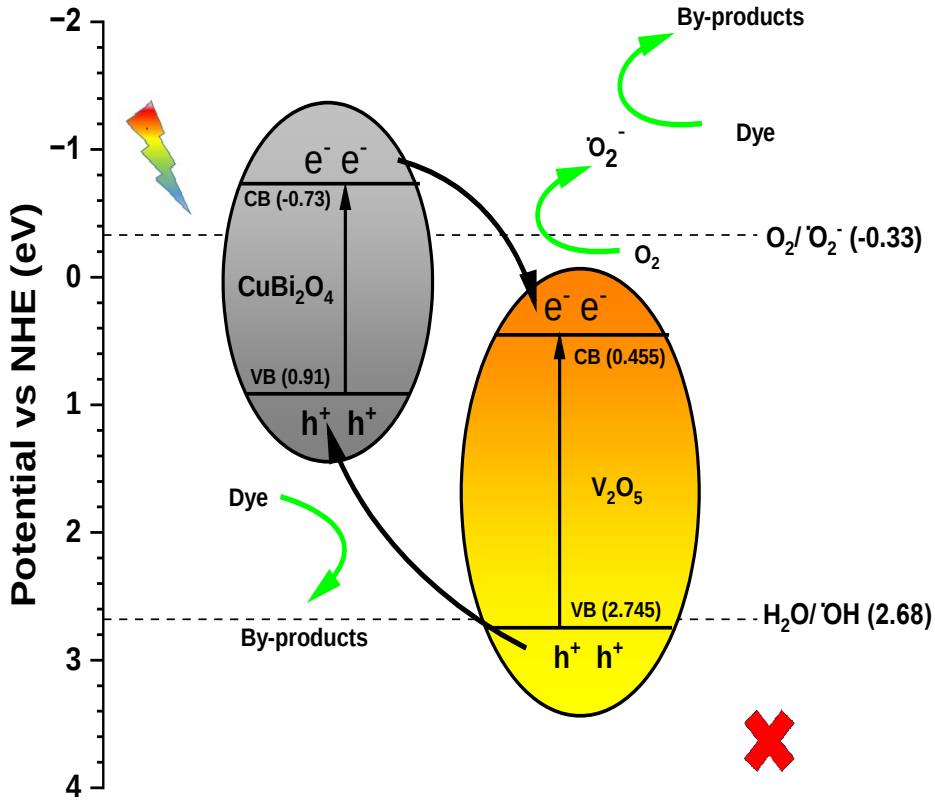

Fig. 5.14: Photocatalytic Proposed hetero-junction charge transfer mechanism for the photocatalytic activity over 30-$CuBi_2O_4/V_2O_5$ nanocomposite.

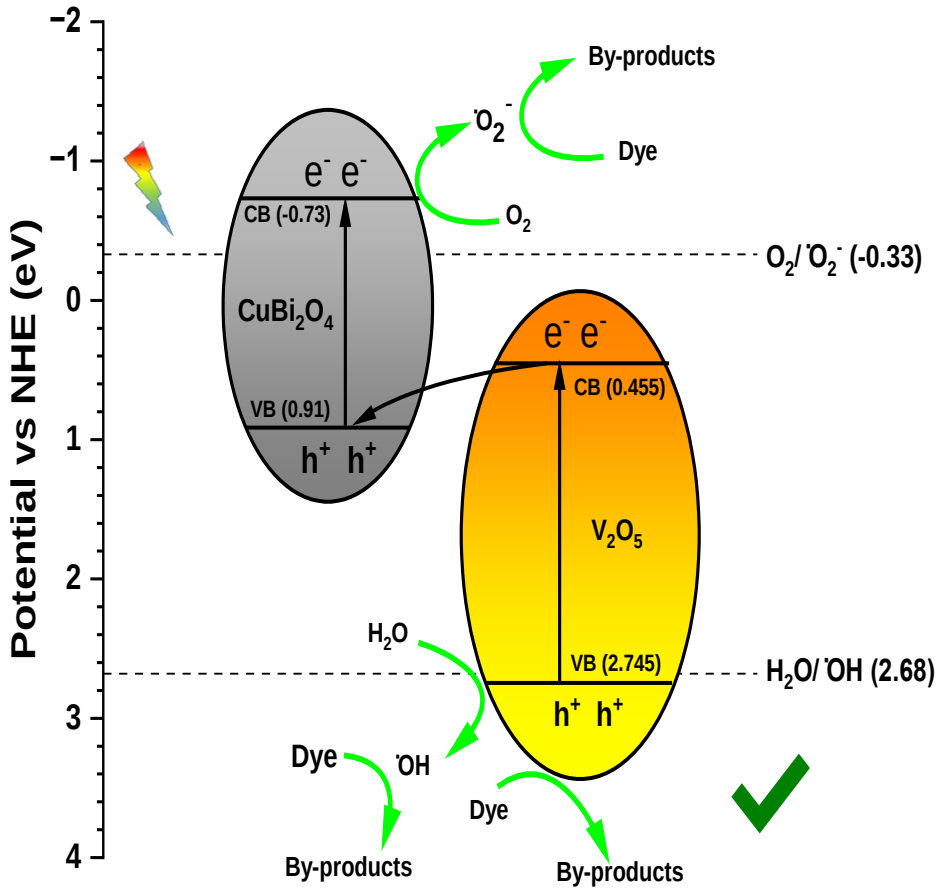

Fig. 5.15: Proposed Z-scheme charge transfer mechanism for the enhanced photocatalytic performance over 30-$CuBi_2O_4/V_2O_5$nanocomposite**.**

5.8 DETERMINATION OF CHEMICAL OXYGEN DEMAND (COD)

The chemical oxygen demand test is widely used as an effective technique to measure the organic strength of wastewater. The COD is used as a measure of the oxygen equivalent of the organic content in a sample that is susceptible to oxidation to CO_2 and H_2O by a strong oxidant. The COD of the dye solution before and after the treatment was estimated. The Initial COD of 20 mg/L RhB solution was found to be 43 mg/L. The COD of the sample obtained after 60 minutes of photocatalytic degradation of RhB (C_0: 20 mg/L) by 30-$CuBi_2O_4/V_2O_5$ (dosage: 1g/L) was found to be 9 mg/L. Thus we get COD removal efficiency of 79%.

Chapter 6

CONCLUSION AND SCOPE FOR THE FUTURE WORK

6.1 CONCLUSION

$CuBi_2O_4/V_2O_5$ nanocomposite was successfully synthesized by hydrothermal approach. Its photocatalytic effectiveness for degradation of RhB, MB and MO dyes under visible LED light irradiation has been reported. The 30-$CuBi_2O_4/V_2O_5$ nanocomposite has a removal efficiency of 73.8 % on RhB (20 mg/L) solution for 60 minutes of photocatalysis while the pristine materials V_2O_5 and $CuBi_2O_4$ has the removal efficiency of 20.7 % and 7 % under the given reactor setup condition. The nanocomposite showed excellent adsorption capacity on MB (20 mg/L) with 95% adsorption capacity in 30 minutes. The effect of photocatalyst dose, initial solution pH, initial dye concentration and stirring has been reported. Furthermore, the radical scavenging experiments proved that the main reactive species that cause RhB to degrade over the 30-$CuBi_2O_4/V_2O_5$ nanocomposite are $^{\bullet}O_2^-$ & $OH^{\bullet}$. Based on radical scavenging experiments and energy band structures, a Z-scheme heterojunction photocatalytic mechanism has been suggested. During the photocatalytic degradation of RhB, the as-prepared 30-$CuBi_2O_4/V_2O_5$ nanocomposite also displays a 79 % COD removal efficiency. As a result, the current study illustrates the synthesis of a novel and effective photocatalyst for the low-cost, energy-efficient, visible light-assisted treatment of dye pollutants, which will encourage the synthesis of additional photocatalysts of a like nature for environmental remediation.

6.2 SCOPE FOR THE FUTURE WORK

For utilizing sunlight as a source of energy for photocatalysis, the efficacy of as synthesized photocatalysts in sunlight can be analyzed in various daylight conditions.

All the experiments were conducted on the dye solution prepared with no other interferences. The efficacy of the as-synthesized material need to be ascertained on the effluents of dyeing related industries for utility in actual field. Furthermore, the study is limited in commercial applications due to the lack of suitable large-scale reactor or treatment plant. For commercialization and development of photocatalytic application in the treatment of wastewater a well-designed suitable large-scale reactor is suggested to achieve a realistic and practically feasible alternative to conventional degradation techniques within reasonable time.

References

[1] M. Saeed, M. Muneer, A. ul Haq, and N. Akram, 'Photocatalysis: an effective tool for photodegradation of dyes—a review', *Environ. Sci. Pollut. Res.*, vol. 29, no. 1, pp. 293–311, 2022, doi: 10.1007/s11356-021-16389-7.

[2] H. Anwer, A. Mahmood, J. Lee, K. H. Kim, J. W. Park, and A. C. K. Yip, 'Photocatalysts for degradation of dyes in industrial effluents: Opportunities and challenges', *Nano Res.*, vol. 12, no. 5, pp. 955–972, 2019, doi: 10.1007/s12274-019-2287-0.

[3] B. B. Garcia, G. Lourinho, P. Romano, and P. S. D. Brito, 'Photocatalytic degradation of swine wastewater on aqueous TiO2 suspensions: optimization and modeling via Box-Behnken design', *Heliyon*, vol. 6, no. 1, p. e03293, Jan. 2020, doi: 10.1016/j.heliyon.2020.e03293.

[4] A. Mishra *et al.*, 'Rapid photodegradation of methylene blue dye by rGO- V2O5 nano composite', *J. Alloys Compd.*, vol. 842, p. 155746, 2020, doi: 10.1016/j.jallcom.2020.155746.

[5] Y. Hong *et al.*, 'In-situ synthesis of direct solid-state Z-scheme V2O5/g-C3N4 heterojunctions with enhanced visible light efficiency in photocatalytic degradation of pollutants', *Appl. Catal. B Environ.*, vol. 180, pp. 663–673, 2016, doi: 10.1016/j.apcatb.2015.06.057.

[6] F. M. Sanakousar, C. Vidyasagar, V. M. Jiménez-Pérez, and K. Prakash, 'Recent progress on visible-light-driven metal and non-metal doped ZnO nanostructures for photocatalytic degradation of organic pollutants', *Mater. Sci. Semicond. Process.*, vol. 140, no. December 2021, 2022, doi: 10.1016/j.mssp.2021.106390.

[7] Z. Carmen and S. Daniela, 'Characteristics , Polluting Effects and Separation / Elimination Procedures from Industrial Effluents – A Critical Overview', *Text. Org. Dye*, pp. 55–86, 2010.

[8] M. Clark, *Handbook of textile and industrial dyeing*. Woodhead Publishing Limited, 2011. doi: 10.1533/9780857094919.

[9] S. M. Burkinshaw and Y.-A. Son, 'The dyeing of supermicrofibre nylon with acid and vat dyes', *Dye. Pigment.*, vol. 87, no. 2, pp. 132–138, Oct. 2010, doi: 10.1016/j.dyepig.2010.03.009.

[10] J. Sharma, S. Sharma, and V. Soni, ‘Classification and impact of synthetic textile dyes on Aquatic Flora: A review’, *Reg. Stud. Mar. Sci.*, vol. 45, p. 101802, Jun. 2021, doi: 10.1016/j.rsma.2021.101802.

[11] J. Sharma, S. Sharma, U. Bhatt, and V. Soni, ‘Toxic effects of Rhodamine B on antioxidant system and photosynthesis of Hydrilla verticillata’, *J. Hazard. Mater. Lett.*, vol. 3, no. August, p. 100069, 2022, doi: 10.1016/j.hazl.2022.100069.

[12] A. K. Sarkar Phyllis, G. Tortora, and I. Johnson, ‘Photodegradation’, *Fairchild Books Dict. Text.*, 2022, doi: 10.5040/9781501365072.12105.

[13] R. S. de Farias, H. L. de B. Buarque, M. R. da Cruz, L. M. F. Cardoso, T. de A. Gondim, and V. R. de Paulo, ‘Adsorption of congo red dye from aqueous solution onto amino-functionalized silica gel’, *Eng. Sanit. e Ambient.*, vol. 23, no. 6, pp. 1053–1060, Dec. 2018, doi: 10.1590/s1413-41522018172982.

[14] M. Hernández-Zamora, F. Martínez-Jerónimo, E. Cristiani-Urbina, and R. O. Cañizares-Villanueva, ‘Congo red dye affects survival and reproduction in the cladoceran Ceriodaphnia dubia. Effects of direct and dietary exposure’, *Ecotoxicology*, vol. 25, no. 10, pp. 1832–1840, Dec. 2016, doi: 10.1007/s10646-016-1731-x.

[15] I. C. McCall, A. Betanzos, D. A. Weber, P. Nava, G. W. Miller, and C. A. Parkos, ‘Effects of phenol on barrier function of a human intestinal epithelial cell line correlate with altered tight junction protein localization’, *Toxicol. Appl. Pharmacol.*, vol. 241, no. 1, pp. 61–70, Nov. 2009, doi: 10.1016/j.taap.2009.08.002.

[16] L. Kos, ‘Use of Chitosan for Textile Wastewater Decolourization’, *Fibres Text. East. Eur.*, vol. 24, no. 3(117), pp. 130–135, Apr. 2016, doi: 10.5604/12303666.1196623.

[17] A. Dalvand, M. Gholami, A. Joneidi, and N. M. Mahmoodi, ‘Dye Removal, Energy Consumption and Operating Cost of Electrocoagulation of Textile Wastewater as a Clean Process’, *CLEAN - Soil, Air, Water*, vol. 39, no. 7, pp. 665–672, Jul. 2011, doi: 10.1002/clen.201000233.

[18] S. A. Avlonitis, I. Poulios, D. Sotiriou, M. Pappas, and K. Moutesidis, ‘Simulated cotton dye effluents treatment and reuse by nanofiltration’, *Desalination*, vol. 221, no. 1–3, pp. 259–267, Mar. 2008, doi: 10.1016/j.desal.2007.01.082.

[19] J. M. Gozálvez-Zafrilla, D. Sanz-Escribano, J. Lora-García, and M. C. León Hidalgo,

‘Nanofiltration of secondary effluent for wastewater reuse in the textile industry’, *Desalination*, vol. 222, no. 1–3, pp. 272–279, Mar. 2008, doi: 10.1016/j.desal.2007.01.173.

[20] M. F. Abid, M. A. Zablouk, and A. M. Abid-Alameer, ‘Experimental study of dye removal from industrial wastewater by membrane technologies of reverse osmosis and nanofiltration’, *J. Environ. Heal. Sci. Eng.*, vol. 9, no. 1, pp. 1–9, 2012.

[21] N. Daneshvar, M. Ayazloo, A. R. Khataee, and M. Pourhassan, ‘Biological decolorization of dye solution containing Malachite Green by microalgae Cosmarium sp.’, *Bioresour. Technol.*, vol. 98, no. 6, pp. 1176–1182, Apr. 2007, doi: 10.1016/j.biortech.2006.05.025.

[22] E. N. El Qada, S. J. Allen, and G. M. Walker, ‘Adsorption of basic dyes from aqueous solution onto activated carbons’, *Chem. Eng. J.*, vol. 135, no. 3, pp. 174–184, Feb. 2008, doi: 10.1016/j.cej.2007.02.023.

[23] G. CRINI, ‘Non-conventional low-cost adsorbents for dye removal: A review’, *Bioresour. Technol.*, vol. 97, no. 9, pp. 1061–1085, Jun. 2006, doi: 10.1016/j.biortech.2005.05.001.

[24] A. PRUDEN, ‘Photoassisted heterogeneous catalysis: The degradation of trichloroethylene in water’, *J. Catal.*, vol. 82, no. 2, pp. 404–417, Aug. 1983, doi: 10.1016/0021-9517(83)90207-5.

[25] R. M. Mohamed, D. L. McKinney, and W. M. Sigmund, ‘Enhanced nanocatalysts’, *Mater. Sci. Eng. R Reports*, vol. 73, no. 1, pp. 1–13, Jan. 2012, doi: 10.1016/j.mser.2011.09.001.

[26] S. Panneri *et al.*, ‘Photoregenerable, Bifunctional Granules of Carbon-Doped g-C 3 N 4 as Adsorptive Photocatalyst for the Efficient Removal of Tetracycline Antibiotic’, *ACS Sustain. Chem. Eng.*, vol. 5, no. 2, pp. 1610–1618, Feb. 2017, doi: 10.1021/acssuschemeng.6b02383.

[27] M. Pelaez *et al.*, ‘A review on the visible light active titanium dioxide photocatalysts for environmental applications’, *Appl. Catal. B Environ.*, vol. 125, pp. 331–349, Aug. 2012, doi: 10.1016/j.apcatb.2012.05.036.

[28] J. Xue, S. Ma, Y. Zhou, Z. Zhang, and M. He, ‘Facile Photochemical Synthesis of

Au/Pt/g-C 3 N 4 with Plasmon-Enhanced Photocatalytic Activity for Antibiotic Degradation', *ACS Appl. Mater. Interfaces*, vol. 7, no. 18, pp. 9630–9637, May 2015, doi: 10.1021/acsami.5b01212.

[29] S. Sun, X. Chang, X. Li, and Z. Li, 'Synthesis of N-doped ZnO nanoparticles with improved photocatalytical activity', *Ceram. Int.*, vol. 39, no. 5, pp. 5197–5203, Jul. 2013, doi: 10.1016/j.ceramint.2012.12.018.

[30] S. S. Shinde, C. H. Bhosale, and K. Y. Rajpure, 'Photocatalytic degradation of toluene using sprayed N-doped ZnO thin films in aqueous suspension', *J. Photochem. Photobiol. B Biol.*, vol. 113, pp. 70–77, Aug. 2012, doi: 10.1016/j.jphotobiol.2012.05.008.

[31] E. Prabakaran and K. Pillay, 'Synthesis of N-doped ZnO nanoparticles with cabbage morphology as a catalyst for the efficient photocatalytic degradation of methylene blue under UV and visible light', *RSC Adv.*, vol. 9, no. 13, pp. 7509–7535, 2019, doi: 10.1039/C8RA09962F.

[32] Z. Huang, S. Jia, J. Wei, and Z. Shao, 'A visible light active, carbon–nitrogen–sulfur co-doped TiO 2 /g-C 3 N 4 Z-scheme heterojunction as an effective photocatalyst to remove dye pollutants', *RSC Adv.*, vol. 11, no. 27, pp. 16747–16754, 2021, doi: 10.1039/D1RA01890F.

[33] P. Niu, M. Qiao, Y. Li, L. Huang, and T. Zhai, 'Distinctive defects engineering in graphitic carbon nitride for greatly extended visible light photocatalytic hydrogen evolution', *Nano Energy*, vol. 44, pp. 73–81, Feb. 2018, doi: 10.1016/j.nanoen.2017.11.059.

[34] J. Ding *et al.*, 'Nitrogen vacancy engineered graphitic C3N4-based polymers for photocatalytic oxidation of aromatic alcohols to aldehydes', *Appl. Catal. B Environ.*, vol. 221, pp. 626–634, Feb. 2018, doi: 10.1016/j.apcatb.2017.09.048.

[35] M. Wang *et al.*, 'Defect-mediated Z-scheme BiO2-x/Bi2O2.75 photocatalyst for full spectrum solar-driven organic dyes degradation', *Appl. Catal. B Environ.*, vol. 254, pp. 98–112, Oct. 2019, doi: 10.1016/j.apcatb.2019.04.044.

[36] B. S. Goud *et al.*, 'Surface oxygen vacancy facilitated Z-scheme MoS2/Bi2O3 heterojunction for enhanced visible-light driven photocatalysis-pollutant degradation

and hydrogen production', *Int. J. Hydrogen Energy*, vol. 45, no. 38, pp. 18961–18975, Jul. 2020, doi: 10.1016/j.ijhydene.2020.05.073.

[37] M. E. Khan, M. M. Khan, and M. H. Cho, 'Ce3+-ion, Surface Oxygen Vacancy, and Visible Light-induced Photocatalytic Dye Degradation and Photocapacitive Performance of CeO2-Graphene Nanostructures', *Sci. Rep.*, vol. 7, no. 1, p. 5928, Jul. 2017, doi: 10.1038/s41598-017-06139-6.

[38] J. Sá, M. Fernández-García, and J. A. Anderson, 'Photoformed electron transfer from TiO2 to metal clusters', *Catal. Commun.*, vol. 9, no. 10, pp. 1991–1995, Jun. 2008, doi: 10.1016/j.catcom.2008.03.041.

[39] D. Zhang, 'Visible light-induced photocatalysis through surface plasmon excitation of platinum-metallized titania for photocatalytic bleaching of rhodamine B', *Monatshefte für Chemie - Chem. Mon.*, vol. 143, no. 5, pp. 729–738, May 2012, doi: 10.1007/s00706-011-0631-2.

[40] S. A. Mosavi, A. Ghadi, P. Gharbani, and A. Mehrizad, 'Photocatalytic removal of Methylene Blue using Ag@CdSe/Zeoilte nanocomposite under visible light irradiation by Response Surface Methodology', *Mater. Chem. Phys.*, vol. 267, p. 124696, Jul. 2021, doi: 10.1016/j.matchemphys.2021.124696.

[41] L. Shi *et al.*, 'Highly efficient visible light-driven Ag/AgBr/ZnO composite photocatalyst for degrading Rhodamine B', *Ceram. Int.*, vol. 40, no. 2, pp. 3495–3502, Mar. 2014, doi: 10.1016/j.ceramint.2013.09.080.

[42] S. Shen, L. Guo, X. Chen, F. Ren, C. X. Kronawitter, and S. S. Mao, 'Effect of Noble Metal in CdS/M/TiO 2 for Photocatalytic Degradation of Methylene Blue under Visible Light', *Int. J. Green Nanotechnol. Mater. Sci. Eng.*, vol. 1, no. 2, pp. M94–M104, May 2010, doi: 10.1080/19430841003684823.

[43] L. Gao, J. Du, and T. Ma, 'Cysteine-assisted synthesis of CuS-TiO 2 composites with enhanced photocatalytic activity', *Ceram. Int.*, vol. 43, no. 12, pp. 9559–9563, Aug. 2017, doi: 10.1016/j.ceramint.2017.04.093.

[44] W. Mao, L. Zhang, T. Wang, Y. Bai, and Y. Guan, 'Fabrication of highly efficient Bi2WO6/CuS composite for visible-light photocatalytic removal of organic pollutants and Cr(VI) from wastewater', *Front. Environ. Sci. Eng.*, vol. 15, no. 4, p. 52, Aug. 2021,

doi: 10.1007/s11783-020-1344-8.

[45] T. S. Natarajan, K. R. Thampi, and R. J. Tayade, 'Visible light driven redox-mediator-free dual semiconductor photocatalytic systems for pollutant degradation and the ambiguity in applying Z-scheme concept', *Appl. Catal. B Environ.*, vol. 227, pp. 296–311, Jul. 2018, doi: 10.1016/j.apcatb.2018.01.015.

[46] H. Li, Y. Zhou, W. Tu, J. Ye, and Z. Zou, 'State-of-the-Art Progress in Diverse Heterostructured Photocatalysts toward Promoting Photocatalytic Performance', *Adv. Funct. Mater.*, vol. 25, no. 7, pp. 998–1013, Feb. 2015, doi: 10.1002/adfm.201401636.

[47] Q. Xu, L. Zhang, J. Yu, S. Wageh, A. A. Al-Ghamdi, and M. Jaroniec, 'Direct Z-scheme photocatalysts: Principles, synthesis, and applications', *Mater. Today*, vol. 21, no. 10, pp. 1042–1063, Dec. 2018, doi: 10.1016/j.mattod.2018.04.008.

[48] C. Yan and L. Liu, 'Sn-doped V2O5 nanoparticles as catalyst for fast removal of ammonia in air via PEC and PEC-MFC', *Chem. Eng. J.*, vol. 392, p. 123738, Jul. 2020, doi: 10.1016/j.cej.2019.123738.

[49] Y. Hong *et al.*, 'In-situ synthesis of direct solid-state Z-scheme V2O5/g-C3N4 heterojunctions with enhanced visible light efficiency in photocatalytic degradation of pollutants', *Appl. Catal. B Environ.*, vol. 180, pp. 663–673, Jan. 2016, doi: 10.1016/j.apcatb.2015.06.057.

[50] A. F. Gouveia *et al.*, 'Experimental and Theoretical Investigations of Electronic Structure and Photoluminescence Properties of β-Ag 2 MoO 4 Microcrystals', *Inorg. Chem.*, vol. 53, no. 11, pp. 5589–5599, Jun. 2014, doi: 10.1021/ic500335x.

[51] B. Deb and A. Ghosh, 'Silver Ion Dynamics in Ag 2 S-Doped Silver Molybdate–Glass Nanocomposites: Correlation of Conductivity and Scaling with Structure', *J. Phys. Chem. C*, vol. 115, no. 29, pp. 14141–14147, Jul. 2011, doi: 10.1021/jp204474n.

[52] Z. Zhang, C. Zhao, S. Lin, H. Li, Y. Feng, and X. Gao, 'Oxygen vacancy modified Bi2MoO6/WO3 electrode with enhanced photoelectrocatalytic degradation activity toward RhB', *Fuel*, vol. 285, p. 119171, Feb. 2021, doi: 10.1016/j.fuel.2020.119171.

[53] S. Balasurya, A. Das, A. A. Alyousef, A. Alqasim, N. Almutairi, and S. Sudheer Khan, 'Facile synthesis of Bi2MoO6-Ag2MoO4 nanocomposite for the enhanced visible light photocatalytic removal of methylene blue and its antimicrobial application', *J. Mol. Liq.*,

vol. 337, p. 116350, Sep. 2021, doi: 10.1016/j.molliq.2021.116350.

[54] M. Iqbal *et al.*, 'Graphene oxide nanocomposite with CuSe and photocatalytic removal of methyl green dye under visible light irradiation', *Diam. Relat. Mater.*, vol. 113, p. 108254, Mar. 2021, doi: 10.1016/j.diamond.2021.108254.

[55] J. Yang *et al.*, 'Black phosphorus nanosheets and ZnAl-LDH nanocomposite as environmental-friendly photocatalysts for the degradation of Methylene blue under visible light irradiation', *Appl. Clay Sci.*, vol. 200, p. 105902, Jan. 2021, doi: 10.1016/j.clay.2020.105902.

[56] N. H. Mohamad Idris *et al.*, 'Titanium Dioxide/Polyvinyl Alcohol/Cork Nanocomposite: A Floating Photocatalyst for the Degradation of Methylene Blue under Irradiation of a Visible Light Source', *ACS Omega*, vol. 6, no. 22, pp. 14493–14503, Jun. 2021, doi: 10.1021/acsomega.1c01458.

[57] L. Ge, C. Han, and J. Liu, 'Novel visible light-induced g-C3N4/Bi2WO6 composite photocatalysts for efficient degradation of methyl orange', *Appl. Catal. B Environ.*, vol. 108–109, pp. 100–107, Oct. 2011, doi: 10.1016/j.apcatb.2011.08.014.

[58] Y. Fu, X. Sun, and X. Wang, 'BiVO4–graphene catalyst and its high photocatalytic performance under visible light irradiation', *Mater. Chem. Phys.*, vol. 131, no. 1–2, pp. 325–330, Dec. 2011, doi: 10.1016/j.matchemphys.2011.09.049.

[59] Y. Wang *et al.*, 'Facile synthesis of Y-doped graphitic carbon nitride with enhanced photocatalytic performance', *Catal. Commun.*, vol. 84, pp. 179–182, Sep. 2016, doi: 10.1016/j.catcom.2016.06.020.

[60] X. Liu *et al.*, 'Synergy of adsorption and visible-light photocatalytic degradation of methylene blue by a bifunctional Z-scheme heterojunction of WO3/g-C3N4', *Appl. Surf. Sci.*, vol. 405, pp. 359–371, May 2017, doi: 10.1016/j.apsusc.2017.02.025.

[61] M. N. Arifin, K. M. R. Karim, H. Abdullah, and M. R. Khan, 'Synthesis of Titania Doped Copper Ferrite Photocatalyst and Its Photoactivity towards Methylene Blue Degradation under Visible Light Irradiation', *Bull. Chem. React. Eng. Catal.*, vol. 14, no. 1, p. 219, Apr. 2019, doi: 10.9767/bcrec.14.1.3616.219-227.

[62] U. Ghosh and A. Pal, 'Fabrication of a novel Bi2O3 nanoparticle impregnated nitrogen vacant 2D g-C3N4 nanosheet Z scheme photocatalyst for improved degradation of

methylene blue dye under LED light illumination', *Appl. Surf. Sci.*, vol. 507, p. 144965, Mar. 2020, doi: 10.1016/j.apsusc.2019.144965.

[63] E. E. El-Katori, M. A. Ahmed, A. A. El-Bindary, and A. M. Oraby, 'Impact of CdS/SnO2 heterostructured nanoparticle as visible light active photocatalyst for the removal methylene blue dye', *J. Photochem. Photobiol. A Chem.*, vol. 392, p. 112403, Apr. 2020, doi: 10.1016/j.jphotochem.2020.112403.

[64] W. H. Ferreira, L. G. A. Silva, B. C. S. Pereira, R. F. Gouvêa, and C. T. Andrade, 'Adsorption and visible-light photocatalytic performance of a graphene derivative for methylene blue degradation', *Environ. Nanotechnology, Monit. Manag.*, vol. 14, p. 100373, Dec. 2020, doi: 10.1016/j.enmm.2020.100373.

[65] K. Chaudhary *et al.*, 'Binary WO3-ZnO nanostructures supported rGO ternary nanocomposite for visible light driven photocatalytic degradation of methylene blue', *Synth. Met.*, vol. 269, p. 116526, Nov. 2020, doi: 10.1016/j.synthmet.2020.116526.

[66] Y. Lei, J. Ding, P. Yu, G. He, Y. Chen, and H. Chen, 'Low-temperature preparation of magnetically separable Fe3O4@ZnO-RGO for high-performance removal of methylene blue in visible light', *J. Alloys Compd.*, vol. 821, p. 153366, Apr. 2020, doi: 10.1016/j.jallcom.2019.153366.

[67] Y. Zhang *et al.*, 'A direct Z-scheme BiOBr/TzDa COF heterojunction photocatalyst with enhanced performance on visible-light driven removal of organic dye and Cr(VI)', *Sep. Purif. Technol.*, vol. 275, p. 119216, Nov. 2021, doi: 10.1016/j.seppur.2021.119216.

[68] X. Zhang *et al.*, 'V2O5/P-g-C3N4 Z-scheme enhanced heterogeneous photocatalytic removal of methyl orange from water under visible light irradiation', *Colloids Surfaces A Physicochem. Eng. Asp.*, vol. 608, p. 125580, Jan. 2021, doi: 10.1016/j.colsurfa.2020.125580.

[69] S. Ghattavi and A. Nezamzadeh-Ejhieh, 'A double-Z-scheme ZnO/AgI/WO3 photocatalyst with high visible light activity: Experimental design and mechanism pathway in the degradation of methylene blue', *J. Mol. Liq.*, vol. 322, p. 114563, Jan. 2021, doi: 10.1016/j.molliq.2020.114563.

[70] S. Asadzadeh-Khaneghah, A. Habibi-Yangjeh, D. Seifzadeh, H. Chand, and V. Krishnan, 'Visible-light-activated g-C3N4 nanosheet/carbon dot/FeOCl

nanocomposites: Photodegradation of dye pollutants and tetracycline hydrochloride', *Colloids Surfaces A Physicochem. Eng. Asp.*, vol. 617, p. 126424, May 2021, doi: 10.1016/j.colsurfa.2021.126424.

[71] N. Ahmad, C.-F. J. Kuo, and M. Mustaqeem, 'Synthesis of novel CuNb2O6/g-C3N4 binary photocatalyst towards efficient visible light reduction of Cr (VI) and dyes degradation for environmental remediation', *Chemosphere*, vol. 298, p. 134153, Jul. 2022, doi: 10.1016/j.chemosphere.2022.134153.

[72] M. Karpuraranjith *et al.*, 'Three-dimensional porous MoS2 nanobox embedded g-C3N4@TiO2 architecture for highly efficient photocatalytic degradation of organic pollutant', *J. Colloid Interface Sci.*, vol. 605, pp. 613–623, Jan. 2022, doi: 10.1016/j.jcis.2021.07.133.

[73] Q. Lu *et al.*, 'Rational fabrication of Bi2WO6 decorated TiO2 nanotube arrays for photocatalytic degradation of organic pollutants', *Mater. Res. Bull.*, vol. 145, p. 111563, Jan. 2022, doi: 10.1016/j.materresbull.2021.111563.

[74] H. Kenfoud, N. Nasrallah, O. Baaloudj, C. Belabed, T. Chaabane, and M. Trari, 'Opto-electrochemical characteristics of synthesized BaFe2O4 nanocomposites: Photocatalytic degradation and hydrogen generation investigation', *Int. J. Hydrogen Energy*, vol. 47, no. 24, pp. 12039–12051, Mar. 2022, doi: 10.1016/j.ijhydene.2022.01.232.

[75] S. Iqbal, I. Bibi, F. Majid, S. Kamal, N. Alwadai, and M. Iqbal, 'Band gap tuning by Gd and Fe doping of LaNiO3 to boost solar light harvesting for photocatalytic application: A mechanistic approach', *Opt. Mater. (Amst).*, vol. 124, p. 111962, Feb. 2022, doi: 10.1016/j.optmat.2021.111962.

[76] X. Pan, F. Kong, and M. Xing, 'Spatial separation of photo-generated carriers in g-C3N4/MnO2/Pt with enhanced H2 evolution and organic pollutant control', *Res. Chem. Intermed.*, vol. 48, no. 7, pp. 2837–2855, Jul. 2022, doi: 10.1007/s11164-022-04748-z.

[77] N. Srinivasan alias Arunsankar, M. Anbuchezhiyan, and S. Harish, 'Investigation of C–ZnO/V2O5 nanocomposite for organic compound decomposition under visible light', *J. Mater. Sci. Mater. Electron.*, vol. 33, no. 12, pp. 9743–9754, 2022, doi: 10.1007/s10854-022-07818-5.

[78] P. S. Chauhan, K. Kumar, K. Singh, and S. Bhattacharya, ‘Fast decolorization of rhodamine-B dye using novel V2O5-rGO photocatalyst under solar irradiation’, *Synth. Met.*, vol. 283, no. September 2021, p. 116981, 2022, doi: 10.1016/j.synthmet.2021.116981.

[79] N. Bashir *et al.*, ‘Sodium doped-V2O5 nanorods for visible light irradiated photocatalytic performance for the degradation of Rh-dye’, *Ceram. Int.*, vol. 48, no. 8, pp. 10932–10940, 2022, doi: 10.1016/j.ceramint.2021.12.312.

[80] J. Hou, Y. Xie, Y. Sun, Y. Kuang, Z. Jiao, and Q. Wang, ‘Construction of a double Z-scheme Bi2O3–CuBi2O4–CuO composite photocatalyst for the enhanced photocatalytic activity’, *Ceram. Int.*, vol. 48, no. 14, pp. 20648–20657, 2022, doi: 10.1016/j.ceramint.2022.04.034.

[81] C. Fang, H. Su, M. Hu, Z. Jiang, L. Xu, and C. Liu, ‘Construction and performance of a novel CuBi2O4/In2O3 Z-scheme heterojunction photocatalyst’, *Mater. Sci. Semicond. Process.*, vol. 160, no. March, p. 107464, 2023, doi: 10.1016/j.mssp.2023.107464.

[82] A. Jenifer and S. Sriram, ‘Enhanced photocatalytic organic dye degradation activities of pristine and Zn-doped V2O5 nanoparticles’, *Appl. Surf. Sci.*, vol. 611, no. PA, p. 155629, 2023, doi: 10.1016/j.apsusc.2022.155629.

[83] H. Anwer, A. Mahmood, J. Lee, K.-H. Kim, J.-W. Park, and A. C. K. Yip, ‘Photocatalysts for degradation of dyes in industrial effluents: Opportunities and challenges’, *Nano Res.*, vol. 12, no. 5, pp. 955–972, May 2019, doi: 10.1007/s12274-019-2287-0.

[84] D. Huang *et al.*, ‘Megamerger in photocatalytic field: 2D g-C3N4 nanosheets serve as support of 0D nanomaterials for improving photocatalytic performance’, *Appl. Catal. B Environ.*, vol. 240, pp. 153–173, Jan. 2019, doi: 10.1016/j.apcatb.2018.08.071.

[85] W. Shi, F. Guo, and S. Yuan, ‘In situ synthesis of Z-scheme Ag3PO4/CuBi2O4 photocatalysts and enhanced photocatalytic performance for the degradation of tetracycline under visible light irradiation’, *Appl. Catal. B Environ.*, vol. 209, pp. 720–728, 2017, doi: 10.1016/j.apcatb.2017.03.048.

[86] M. N. Arifin, K. M. Rezaul Karim, H. Abdullah, and M. R. Khan, ‘Synthesis of titania doped copper ferrite photocatalyst and its photoactivity towards methylene blue

degradation under visible light irradiation', *Bull. Chem. React. Eng. & Catal.*, vol. 14, no. 1, pp. 219–227, 2019, doi: 10.9767/bcrec.14.1.3616.219-227.